THERMODYNAMIC LINKAGE AND NONLINEAR REGRESSION ANALYSIS: A MOLECULAR BASIS FOR MODELING BIOMACROMOLECULAR PROCESSES

I. INTRODUCTION

Historically, throughout the scientific community there has been much interest in finding a molecular basis for quantifying the variation of biomacromolecular processes with added low-molecular-weight cosolutes. In

the biochemical area, the variation of enzyme kinetics with substrates, cofactors, mono and divalent salts, as well as various inhibitors and activators has been used as a model for *in vitro* studies of metabolic pathways. However, in many instances, these compete with one another for activation or inhibition sites on the enzyme and may also form complexes with each other. In some cases, cosolutes must complex before activation of the enzyme can occur. Hence, a complex and cumbersome network of cooperative interactions exists in biologically active processes. These interactions must be quantified by the biochemist before relevant changes in the enzyme structure, through genetic engineering, or by the addition of other cosolutes such as drugs can be successfully accomplished. What is clearly needed is a mathematical methodology with a sound molecular foundation for quantification of these interacting processes.

In the food science area, functionality is an operational description of the behavior of a component under defined environmental conditions. Some examples of the functional properties of proteins are solubility, colloid stability, and gelation of proteins. A major limitation to this field of study may be our scientific approach. In attempting to define any one property accurately, we may lose sight of the objective, which is to use these functional tests in a predictive fashion. Thus, in studying just one aspect of one protein the interactions which occur in a real food system may be overlooked. These interactions can render a one-dimensional functional test inaccurate.

Many functional tests have been developed for proteins under a variety of conditions, yet the predictive value of these tests is often low for real processing situations. Rather than devising new and perhaps "ultimate" functional property tests, research perhaps should focus on the basis for the behavior of proteins in these tests. More in-depth understanding of the basic chemical and physical properties which contribute to functionality is needed. There must also be a good interface between this basic work and its ultimate application in food systems, otherwise the applicable questions may never be asked or answered. Whey protein isolate (WPI) can form heat-induced stable gels. For this model it may not be important to conduct research to find the ultimate test conditions for gelation of WPI, but rather to uncover the molecular basis for its ability to form gels and to be able to quantitate changes in such behavior with environmental changes. Such information could allow us to understand why soy or plant proteins fail to function in the same way, and could suggest further modifications to increase their utilization.

With these problems in mind, it is the purpose of this article to provide a general mathematical methodology with a sound molecular basis which allows investigators to quantify the variation of selected biomacromolecu-

lar processes with added cosolutes. It will also be shown how one can use this methodology when a variety of competing cosolutes are used. The methodology is based on Wyman's Theory of Thermodynamic Linkage, which is well-tested, theoretically sound, and provides a molecular as well as thermodynamic basis. What is new is the quantitative extension of this theory to systems with multiphasic behavior through use of nonlinear regression analysis. This article reviews how biochemical processes, such as enzyme kinetics of homogeneous and heterogeneous preparations, as well as functional properties of proteins such as solubility, colloidal stability, and gelation, can be thermodynamically linked to the addition of various cosolutes. The quantitation of this linkage process yields equilibrium constants for the interaction of these cosolutes with the biomacromolecular property via nonlinear regression analysis.

II. PROTEIN SALT-INDUCED SOLUBILITY PROFILES

A. SOY PROTEIN ISOLATE

1. Overview

Shen (1981) has shown that the salt-dependent variation in the solubility of native and denatured soybean isolates cannot be explained by the theory of Melander and Horvath (1977a,b). This latter theory predicts that at low salt concentration the solubility of a protein should increase because of an electrostatic contribution to the free energy. At higher salt concentrations a salting-out free energy should predominate because of the increase of surface tension of the salt solution altering the exposed hydrophobic surface area of the protein. However, for both native and heat-denatured soybean isolates the opposite phenomenon occurs, i.e., the protein solubility decreases to a minimum value with added salt and then increases to a constant value at salt concentrations of approximately 1 *M* (Shen, 1981). In addition, the shape of this salt-induced solubility profile is the same for both the native and denatured forms of the isolate when sodium or ammonium chloride, ammonium bromide, ammonium nitrate, and sodium iodide are used. Moreover, the limiting values of solubility at high salt concentrations appear to follow the usual lyotropic or Höffmeister series. It has been suggested that these results could be explained by an increase in the hydrophobic surface area of the protein leading to protein self-association with added salt, followed by a salting-in caused by an increase in the dipole moment of the protein due to a nonspecific solvation effect

at higher salt concentrations. The possibility that ion binding causes the net charge of the protein to be zero, resulting in salting-out, while further salt binding causes salting-in was discounted. The rationale for this decision was that the binding of either NH_4^+ or Na^+ to soy proteins is negligible. Other investigators (Steinhardt and Reynolds, 1969) have shown sodium and ammonium salts bind significantly to proteins. Therefore, using the concept of Ockham's Razor, this ion-binding model appears to be more plausible than the other more cumbersome, qualitative description. For this reason, a reevaluation of these results using equations adapted from Wyman's Theory of Linked Functions (Wyman, 1964) is presented.

The solubility of a protein is thermodynamically linked to its salt-binding capacity. Solubility profiles are fitted by these derived equations using nonlinear regression analysis. The stoichiometry, with corresponding binding constant, and as salting-out and salting-in parameters are obtained.

2. *Theory*

Based on the assumption that there are essentially two classes of binding sites for ligands responsible for the sequential salting-out and salting-in processes, the concept of Wyman's (1964) linked functions can be used to treat these processes according to the following reaction.

$$\underset{(S_0)}{P} + nX \overset{k_1^n}{\rightleftharpoons} \underset{(S_1)}{PX_n} + mX \overset{k_2^m}{\rightleftharpoons} \underset{(S_2)}{PX_nX_m} \tag{1}$$

where P is the unbound protein, X is the free salt, n and m are the number of X moles bound to species PX_n and PX_nX_m, and S_0, S_1, and S_2 are the solubilities of the species indicated. For this study, S_1 and S_2 are relative to S_0. The mathematical relationship representing the above sequential stoichiometry can be represented according to the following:

$$S_{app} = S_0 f(P) + S_1[f(PX_n) - f(PX_nX_m)] + S_2 f(PX_nX_m) \tag{2}$$

where S_{app} is the apparent protein solubility at a given salt concentration, (X_T), $f(i)$ are the protein fractional component of species i, and the Ss are as previously defined. Incorporation of the salt-binding equilibrium constants as defined by Eqs. (1) and (2) yields the following:

$$S_{app} = \frac{S_0 p}{p + k_1^n pX^n} + \frac{S_1 k_1^n pX^n}{p + k_1^n pX^n} + \frac{(S_2 - S_1)k_2^m pX^m}{p + k_2^m pX^m} \tag{3}$$

where p is the concentration in percent of the unbound protein and X is the concentration of unbound salt. Cancellation of common terms yields

$$S_{app} = \frac{S_0}{1 + k_1^n X^n} + \frac{S_1 k_1^n X^n}{1 + k_1^n X^n} + \frac{(S_2 - S_1) k_2^m X^m}{1 + k_2^m X^m} \tag{4}$$

It should be stressed here that Eq. (4) is valid for sequential binding, i.e., $k_1 > k_2$ and n sites saturate prior to the binding of m sites on the protein. Also, for n or m greater than one, note that k_1 and k_2 represent an average value for each of the n or m binding sites. In reality, n or m moles of salt will bind with only one equilibrium constant (K_1), i.e., $K_1 = k_1^n$ and $K_2 = k_2^m$.

Now, since the total salt concentration, X_T, is the sum of the free salt concentration, X, and the concentration of the bound salt of both species PX_n and PX_nX_m, it can be shown that

$$X_T = X\left(1 + \frac{n k_1^n P_T X^{n-1}}{1 + k_1^n X^n} + \frac{m k_2^m P_T X^{m-1}}{1 + k_2^m X^m}\right) \tag{5}$$

where P_T is the total concentration of protein. From Eq. (5) $X_T = X$ when P_T is small relative to X. For these experiments, this assumption is reasonable because of the concentration range of the total salt used and the large molecular weight of the soy protein isolate. Therefore, since the total salt concentration instead of the free concentration can be used in Eq. (4), i.e., replace all values of X with X_T, the salt-induced solubility profiles can be directly analyzed using a Gauss–Newton nonlinear regression analysis program developed at this laboratory. All solubility profiles were analyzed by fixing the values of n and m and calculating the best least-squares fit for the optimum evaluated k_1 and k_2 values. The n and m values were then fixed to new values and the whole procedure repeated. The n and m values which yielded the minimum root-mean-square value for the analysis were then reported.

3. *Analysis of Data*

The salt-induced solubility data of Shen (1981) were analyzed according to Eq. (4) using nonlinear regression analysis for the native soy isolate at

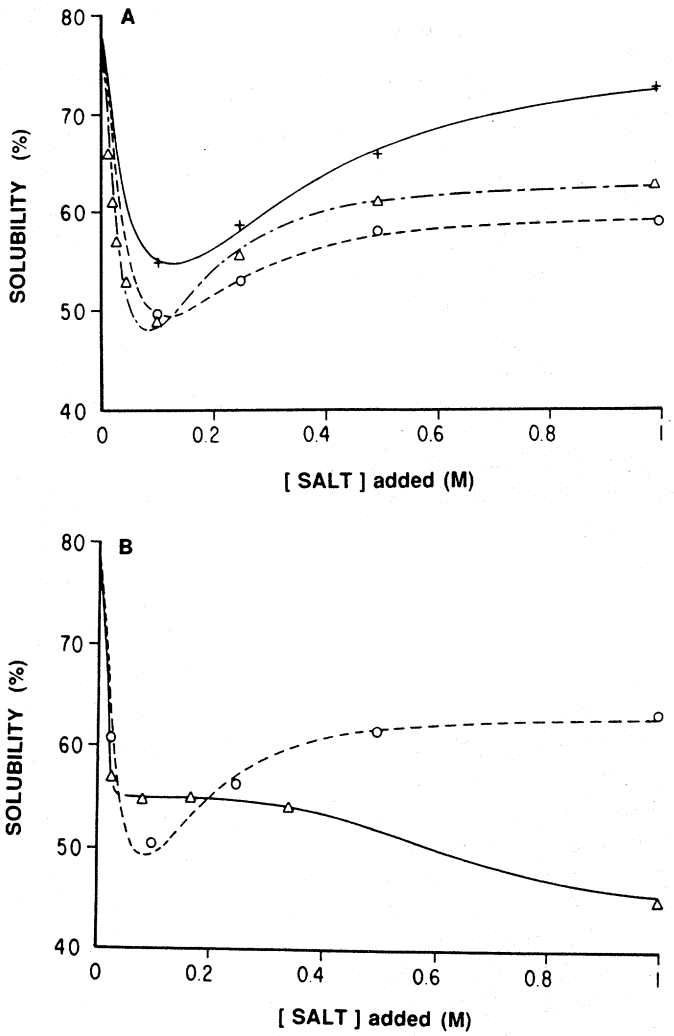

FIG. 1. Salt-induced solubility profile of native soy isolate. (A) ○, Solubility data for NaCl or NH_4; ---, theoretical curve for NaCl or NH_4 data; △, solubility data for NH_4Br; —·—, theoretical curve for NH_4Br data; +, solubility data for NaI; ——, theoretical curve for NaI data.(B) ○, Solubility data for NH_4NO_3; ---, theoretical curve for NH_4NO_3 data; △, solubility data for $(NH_4)_2SO_4$ or Na_2SO_4; ——, theoretical curve for $(NH_4)_2SO_4$ or Na_2SO_4 data.

neutral pH. The results are shown in Fig. 1A for NaCl or NH_4Cl, and NH_4Br and NaI, and Fig. 1B for NH_4NO_3 and $(NH_4)_2SO_4$ or Na_2SO_4. The best fits for denatured soy isolate at neutral pH with the same salts as in Fig. 1A and B are shown in Fig. 2A and B. The resulting theoretical curves

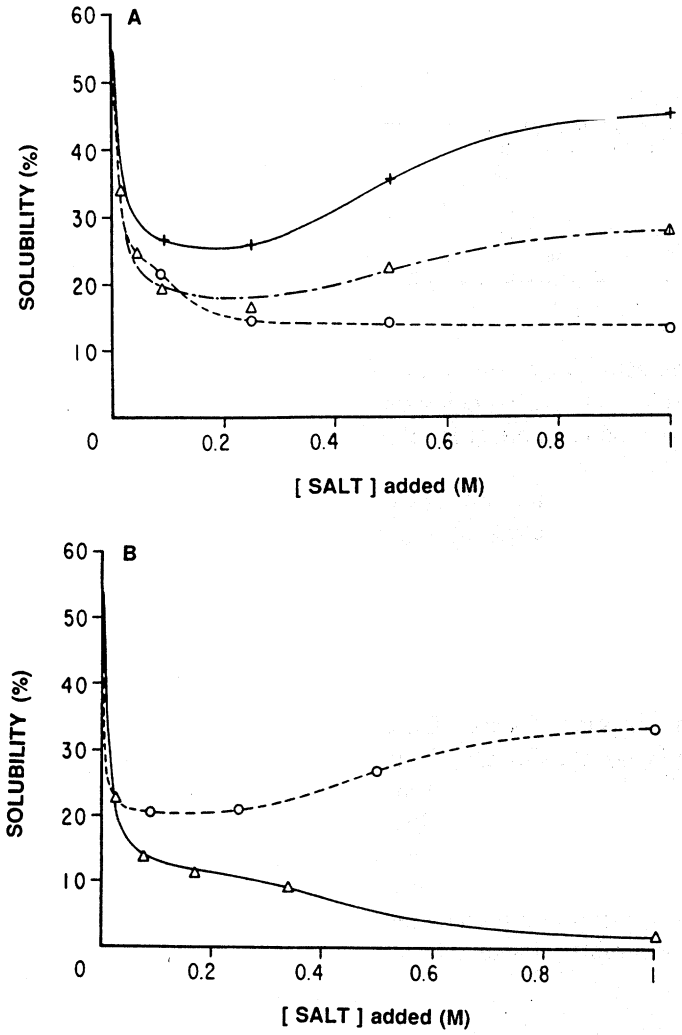

FIG. 2. Salt-induced solubility profile of denatured soy isolate. Details for A and B are the same as in Fig. 1A and B, respectively.

for the profiles in Figs. 1 and 2 are in excellent agreement with all the solubility data. The curves which represent the nonlinear regression best fit for the lowest root-mean-square values for fixed values of n and m, are all within a relative standard deviation of 2% of the experimental data. The final values with corresponding standard errors of the salting-out binding constant, k_1, the salting-in binding constant, k_2, the salting-out

TABLE I

NATIVE SOY PROTEIN ISOLATE

Salt	k_1 (liter/mol)	k_2 (liter/mol)	S_1 (%)	S_2 (%)	n	m
NaCl, NH_4Cl	41 ± 9	4.7 ± 0.4	31 ± 2	59 ± 4	1	2
NH_4Br	53 ± 16	6 ± 2	28 ± 10	62 ± 09	1	2
NH_4NO_3	51 ± 17	6 ± 2	29 ± 12	63 ± 13	1	2
NaI	50 ± 6	2.9 ± 0.3	43 ± 2	74 ± 4	1	2
Na_2SO_4, $(NH_4)SO_4$	100 ± 1	1.6 ± 0.1	55.1 ± 0.3	44 ± 1	4	4

solubility, S_1, the salting-in solubility, S_2, and the values of n and m, i.e., the number of moles of salt bound to S_1 species for n and to S_2 species for m, are presented in Table I for the native soy isolate and Table II for the denatured soy isolate.

Once again, it must be stressed that the k values are not the actual stoichiometric equilibrium binding constants. They are merely average values representative of only 1 mol of salt bound to one protein site. The actual equilibrium constants are calculated by raising the k value to the corresponding n or m exponents. The salting-out constant, k_1, is essentially invariant within experimental error for NaCl, NH_4Cl, NH_4Br, NH_4NO_3, and NaI (Table I). Also, little change in values for k_2, the salting-in equilibrium constant, is observable for the same lyotropic series of salts. The n and m values are also the same, i.e., $n = 1$ and $m = 2$ for all of the above salts. However, the relatively low values of 1 and 2 for n and m, respectively, should not be interpreted literally as only a simple binding site, since it is well known that multiple binding sites with exactly the same equilibrium constant yield only a single binding isotherm (Tanford, 1961). Hence, a value of n or m represents a class of protein-binding sites rather than a single binding site linked to the solubility change of the protein.

TABLE II

DENATURED SOY PROTEIN ISOLATE

Salt	k_1 (liter/mol)	k_2 (liter/mol)	S_1 (%)	S_2 (%)	n	m
NaCl, NH_4Cl	383 ± 43	8 ± 4	21 ± 4	13 ± 8	1	4
NH_4Br	240 ± 22	1.9 ± 0.4	16 ± 1	28 ± 4	1	4
NH_4NO_3	265 ± 5	2.0 ± 0.1	20.2 ± 0.1	34.7 ± 0.1	1	4
NaI	238 ± 1	2.0 ± 0.1	23.4 ± 0.1	46.1 ± 0.2	1	4
Na_2SO_4, $(NH_4)SO_4$	273 ± 18	2.2 ± 0.6	10 ± 1	1.0 ± 0.5	1	4

The salting-out solubility, S_1, shows no trend with respect to the type of anion used, whereas a slight trend may exist for the salting-in solubility, S_2, which will be discussed later in this article. Since soy isolates at neutral pH have a net negative charge (Shen, 1981), the above results can easily be interpreted in terms of an isoelectric binding model, i.e., salt cations bind to negative sites on a protein surface, with an average constant of k_1, and produce a species of zero net charge with a corresponding solubility of S_1. The further salting-in of the protein may reflect either only cations binding, k_2, to the unbound negative protein sites yielding a species, S_2, with a net positive charge, or both salt cation and anion binding, k_2, to corresponding protein negative- and positive-charged sites, yielding a species with a zero or negative charge. The values of S_1 and S_2 are higher for NaI, 43 ± 2 and 74 ± 4, respectively, than for chloride, bromide, and nitrate, approximately 30 and 60, respectively.

The solubilities of native soy isolate, S_1, are high in $(NH_4)_2SO_4$ and Na_2SO_4 in comparison with the other salts mentioned in Table I. In addition, the k_1 value is significantly higher but the k_2 value is much smaller than the rest. However, the n and m values, namely, 4 and 4, respectively, were different from the corresponding 1 and 2 values for the other salts. Hence, only the sulfate salt-induced solubility profile for native soy isolate is presented and it is not compared with the others in this series. Nevertheless, it should be noted that even though the shape of the sulfate profile (Fig. 1B) is different from those of rest of the salts (Fig. 1A and B), inasmuch as the sulfate solubility decreases to a platcau at approximately 0.1 M and then further decreases to a limiting value (rather than decreasing to a minimum followed by an increase to a limiting value), this mechanism, quantitated by Eq. (4), can easily describe both solubility profiles. The only difference between these two profiles is that $S_2 < S_1$ for sulfate and $S_2 > S_1$ for the other salts.

The binding and solubility parameters for the heat-denatured soy isolate derived from the data in Fig. 2A and B are shown in Table II. With the exception of chloride, all k_1 values are invariant with the type of salt used in this study. All k_2 values, with the exception of chloride, show a similar invariant behavior. The latter difference is most likely due to experimental error, and the conclusion that the salt binding is invariant to the lyotropic series is warranted, especially since all n and m values were found to be equal to 1 and 4, respectively. Inspection of the k_1 values from Tables I and II for native and denatured soy isolates shows significant higher values for the latter form of the isolate. This effect is consistent with the notion that a protein in its native state has a more compact tertiary structure than the corresponding denatured form (Tanford, 1961). Hence, it is reasonable to conclude that k_1 and S_1 reflect an isoelectric salt binding mechanism.

TABLE III

SOY ISOLATE SOLUBILITY (S_1 AND S_2) AND MOLAR SURFACE TENSION INCREMENT (σ)

Salt	$\sigma \times 10^3$[a] (dyn g/cm mol)	S_{1N}[b] (%)	S_{2N}[c] (%)	S_{1D}[d] (%)	S_{2D}[e] (%)
NH_4NO_3	0.85	29 ± 12	63 ± 13	20.2 ± 0.1	34.7 ± 0.1
NaI	1.02	43 ± 2	74 ± 4	23.4 ± 0.1	46.1 ± 0.2
NH_4Br	1.14	28 ± 10	62 ± 9	16 ± 1	28 ± 4
NH_4Cl	1.39	31 ± 2	59 ± 4	21 ± 4	13 ± 8
NaCl	1.64	31 ± 2	59 ± 9	21 ± 4	13 ± 8
$(NH_4)_2SO_4$	2.16	55.1 ± 0.3	44 ± 1	10 ± 1	1.0 ± 0.5
Na_2SO_4	2.73	55.1 ± 0.3	44 ± 1	10 ± 1	1.0 ± 0.5

[a] Values from Melander and Horvath (1977a).
[b] S_{1N}, Salting-out for native protein.
[c] S_{2N}, Salting-in for native protein.
[d] S_{1D}, Salting-out for denatured protein.
[e] S_{2D}, Salting-in for denatured protein.

This mechanism is also corroborated by the fact that S_1s from the native protein (Table I) are somewhat larger in magnitude than the S_1s from the denatured form (Table II), while remaining relatively invariant to the type of salt used in this study. No trend for S_1 in either Table I or Table II exists with the lyotropic series.

S_2 for the denatured soy isolate (Table II), however, strongly follows the Höffmeister series for proteins. The solubility increases dramatically in the order of $SO_4 < Cl < Br < NO_3 < I$. An attempt was made to quantify this lyotropic trend of S_2 with either hydrophobic forces or anion binding. Although Melander and Horvath (1977a) postulated that the surface tension increment of the salt and the hydrophobic surface area are responsible for the salting-out phenomenon, we have compared all S_1 and S_2 values for both native and denatured soy isolate in Table III along with the molar surface tension increment σ (second column, Table III) (Melander and Horvath, 1977a) in increasing order of magnitude. No trend can be observed for any S_1 and S_2 value with increasing σ. Hence, it appears that the surface tension and, possibly, the hydrophobic interactions have little or no effect on the salt-induced solubility change of soy isolates. This is surprising, since there exists a strong trend in S_2 for denatured soy isolate with varying types of added salts, and it has been well documented that hydrophobic groups are more exposed to the solvent when protein denaturation has occurred (Tanford, 1961).

To test the concept of anion binding being the predominant contribution

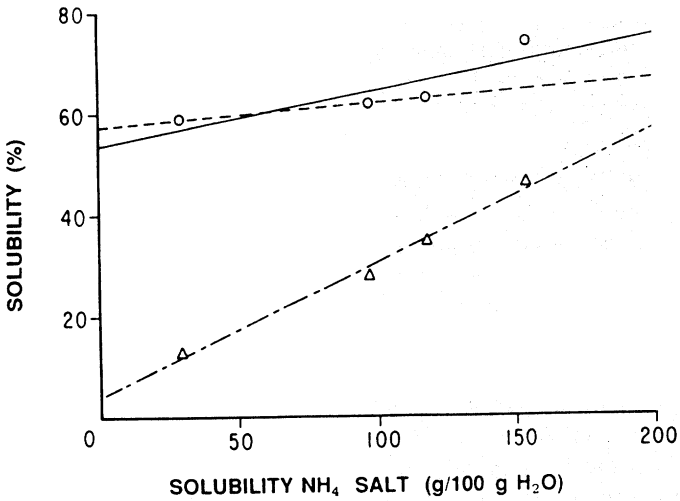

FIG. 3. Salting-in solubilities (S_2 from Table I and II) versus literature solubilities of ammonium salts with corresponding anions (Wagman, 1968) of Cl^-, Br^-, NO_3^-, and I^- (points marked from left to right with circles and triangles). O, Native soy isolate; ——, least-square straight line for only first three points; ---, least-square straight line for all four points; △, denatured soy isolate; —·—, least-square straight line for denatured soy isolate data.

to S_2 for the denatured protein, S_2values were plotted against literature values for the solubility of ammonium salts of Cl, Br, NO_3, and I (Wagman, 1968), presented in Fig. 3 as the open triangles. The dot-dashed line in Fig. 3 is the least-square straight line, which is in excellent agreement with the experimental values with a root-mean-square deviation (rms) of 1.2, yielding a slope of 0.26 ± 0.02 and an intercept close to zero, namely, 4 ± 2. This strong linear dependency of S_2 with the solubilities of corresponding ammonium salts is a strong indication that, for the heat-denatured soy isolate, the dominant contribution to the salting-in phenomenon is the salt anion binding to the positively charged amine groups on the protein surface.

A smaller but somewhat significant trend for S_2 versus the ammonium salts solubilities was also observed for native soy isolate (open circles in Fig. 3). Linear regression analysis on all four S_2 values yields an rms value of 3.5 with a slope of 0.11 ± 0.05 and a large intercept of 54 ± 5. Better statistics are obtainable if the iodide point is eliminated, yielding a rms of 0.3 with a slope of 0.045 ± 0.003 and an intercept of 57.6 ± 0.1. However, at this time, there is no valid reason for the incorporation or deletion of the iodide value. Furthermore, since both intercept values for the native

soy are much larger than that of denatured soy, i.e.,approximately 50% verses 4%, respectively, it can be concluded that anion binding has a small but real effect on the salting-in of native soy isolate. A possible explanation is that only a limited amount of anion binding can occur in native soy because of its closed tertiary structure. This hypothesis is consistent with the value of m for native protein, 2, being lower than that for the denatured protein, which was 4. If anion binding does not occur during the salting-in process and only salt cations are bound to native soy, then S_2 species would have a net positive charge, assuming that the S_1 state has a net charge of zero. Hence, a positive net charge of the S_2 species would indeed have a relatively large solubility, resulting in an S_2 value which is invariant with the Höffmeister series and large in magnitude. Therefore, for native soy isolate, the predominant driving force for the salting-in process appears to be caused only by the cation binding, leading to a protein complex with an apparent positive charge. For the heat-denatured soy isolate, the salting-in process is most likely caused by both salt anion and cation binding to the corresponding protein positive and negative sites, respectively, yielding a complex with a net zero charge. The salting-out process of both forms of the soy isolate is caused by salt cation binding to a protein with a net negative charge, leading to isoelectric precipitation.

In conclusion, the above results are a strong indication that the binding of salt cations and/or anions to proteins has a major influence on protein solubility, even though the magnitude of the binding constants is small. Furthermore, the binding parameters can be influenced by the secondary and tertiary structure of the protein, as in the present case for native and heat-denatured soy isolates.

B. BOVINE CASEIN

Following the above approach, a simple functionality test for the solubility of caseins as a function of calcium ion concentration was modeled. This system was selected because caseinate is an important commodity, and milk and dairy products are widely consumed for their calcium content. Second, the interactions occurring in this important colloidal-transport system are still not well defined, and a wealth of information of a qualitative nature is available in the literature on calcium-induced casein solubility curves (Bingham *et al.*, 1972; Thompson *et al.*, 1969; Waugh and Noble, 1965). In order to understand these calcium–protein interactions better, the precipitation and resolubilization reactions of selected caseins were reinvestigated. The data were analyzed with respect to computer-

generated models; preliminary analysis of the data indicates that a thermodynamic linkage occurs between calcium binding and salting-out and salting-in reactions.

1. *Procedures*

a. Materials. Purified caseins were prepared as described by Thompson *et al.* (1969) using DEAE-cellulose chromatography. Enzymatic dephosphorylations were conducted as previously described (Bingham *et al.*, 1976). Stock $CaCl_2$ solutions were prepared and their concentrations checked by atomic absorption analysis. Nomenclature of the genetic variants and abbreviations for casein are as recommended by the Milk Protein Nomenclature Committee (Eigel *et al.*,1984).

b. Solubility of Caseins. Solubility of caseins at each of two temperatures, 1 and 37°C, was carried out as follows:

Dissolve caseins (about 20 mg/ml) in water and adjust pH to 7.0 with 0.1 *N* KOH or NaOH. Equilibrate in a water bath at desired temperature for 15 to 20 min.

To 2 ml of protein solution (in thick-walled centrifuge tubes), add 2 ml of $CaCl_2$ solutions, with or without buffer + KCl. Invert the tube and let stand at desired temperature for 30 min.

Centrifuge for 15 min at 43,800 *g* max at desired temperature in a Model L-8 Beckman ultracentrifuge.

Transfer 500 μl of supernatant to a 5-ml volumetric flask containing 1 ml of 1 *N* sodium citrate plus a few milliliters of water; make up to volume with water. When solubility is determined at 1°C, pipettes must be prechilled to avoid precipitation of protein in the pipette. Read in 1-cm cuvettes at 280 nm. Extinction coefficients, ε, at 1 cm 1% 280 nm for α_{s1}-caseins A and B are 10.0, and for β-casein C, 4.7 (Eigel *et al.*, 1984).

c. Theory. Here, we assume that there are essentially two classes of binding sites for ligands responsible for the sequential salting-out and salting-in processes. Therefore, the concept of Wyman's (1964) linked functions can be used to treat these processes according to the theory developed in Section II,A,2 [Eqs. (1–5)].

2. *Analysis of Data*

From studies on casein, Linderstrom-Lang (1929) postulated that the colloidal milk complex (the casein micelle) is composed of a mixture

of calcium-insoluble proteins which are stabilized by a calcium-soluble protein. The latter protein would be readily split by the milk-clotting enzyme chymosin, destabilizing the colloid and allowing coagulation to occur. In the intervening years, individual caseins have been isolated and purified and the α_{s1}, α_{s2}, and β-caseins have been shown to be calcium insoluble, while κ-casein is not only soluble in the presence of calcium ions, but is readily split by chymosin (Farrell and Thompson, 1988).

a. Solubility at 37°C. The solubility of α_{s1}-caseins A and B (α_{s1}-A, α_{s1}-B) and β-casein C (β-C) at 37°C in 10 m*M* imidazole-HCl, pH 7.0, 0.07 *M* KCl at initial protein concentrations of 10 mg/ml had previously been reported (Thompson *et al.*,1969). KCl was chosen as the electrolyte because it predominates in the milk salt system (Farrell and Thompson, 1988). The proteins become increasingly less soluble at about 5 m*M* $CaCl_2$ (Fig. 4a,b) (Noble and Waugh, 1965). Comparison of the solubility profiles of α_{s1}-A and α_{s1}-B indicates that at 37°C α_{s1}-A is more soluble than α_{s1}-B, while β-C is the most soluble. In order to quantify the data, nonlinear regression analyses were performed. The data in Fig. 4a were fitted by Eq. (4) using iterative analysis. Values of k_1 were obtained at fixed integer values of n (range of n = 1 to 32); the correct value of n was taken to be the fit with the lowest root-mean-square deviation (RMS). Figure 4a shows the fit to n = 2, 4, and 8 for α_{s1}-A; values for n = 8 gave the minimum RMS. In each case, the parameters S_1, S_2, and S_i were also determined by the analyses. Analysis of the solubility profiles of α_{s1}-A, α_{s1}-B, and β-C at 37°C, where protein aggregations due to hydrophobic interactions are maximized with respect to temperature, showed no salting-in behavior, so that k_2 and m were essentially zero. Values obtained for k_1 (salting-out) and n are given in Table IV. Since the n values appear to correspond to the number of phosphate groups per mole of protein (8 and 4, respectively), for α_{s1}- and β-caseins (Eigel *et al.*, 1984) it may be hypothesized that calcium binds to the serine phosphates of casein, and that this binding in turn is linked to changes in the solubilities of the various protein species.

b. Solubility at 1°C. β-Casein C does not precipitate at 1°C at concentrations of Ca^{2+} of up to 400 m*M*. It is known that hydrophobic forces are dominant in the association reactions of β-caseins (Schmidt, 1984), and that β-casein binds Ca^{2+} at 1°C. In this case, binding is not linked to decreased solubility. Addition of calcium chloride to α_{s1}-casein solutions results in a rapid decrease in solubility; at 50 m*M* $CaCl_2$ the protein is mostly precipitated (Fig. 5). When the calcium chloride concentration exceeds 100 m*M*, a gradual salting-in of the protein occurs at 1°C. The data for α_{s1}-B were fitted to Eq. (4) and the salting-out parameters k_1 and

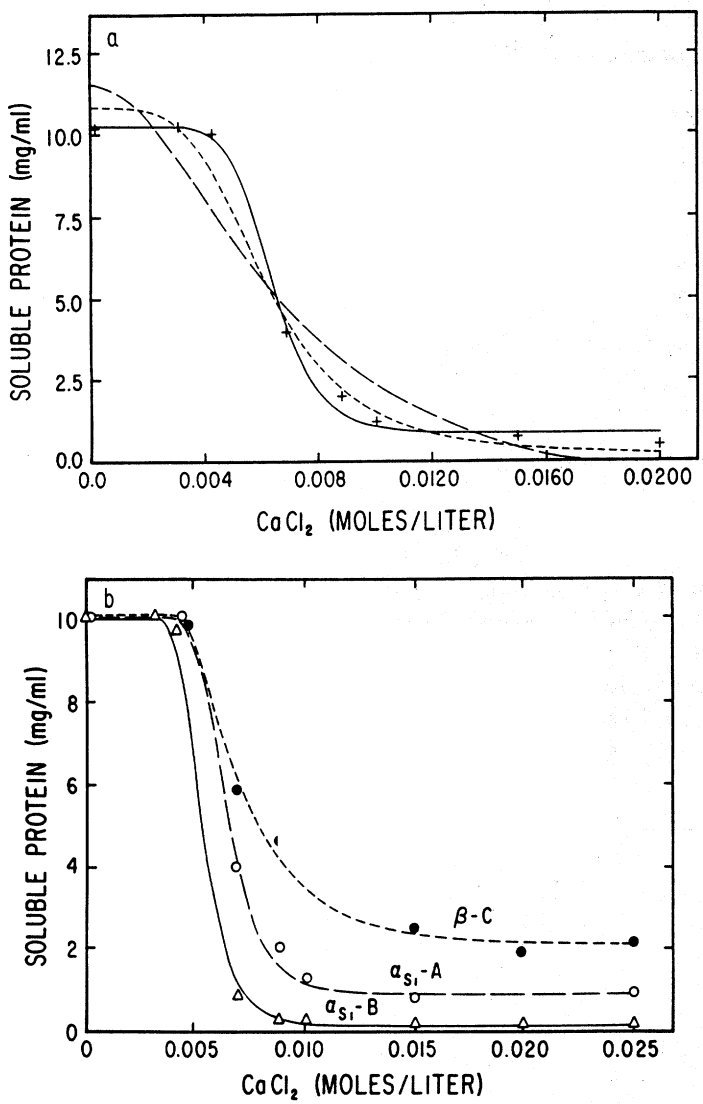

FIG. 4. Solubility at 37°C of the calcium salts of α_{s1}-caseins A and B (α_{s1}-A, α_{s1}-B), and β-casein C (β-C) as a function of increasing $CaCl_2$ concentration. Solutions buffered at pH 7.0, 10 m*M* imidazole-HCl with 0.07 *M* KCl. (a) The experimental data for α_{s1}-A (+) were fitted by Eq. (4) by nonlinear regression analysis with values of 2, 4, and 8 assigned to n. The best fit was obtained for $n = 8$. (b) Similar fits for α_{s1}-B and β-C, with α_{s1}-A repeated. Results of analyses are given in Table IV.

TABLE IV

CALCIUM-INDUCED INSOLUBILITY OF CASEIN AT 37°C[a]

Casein	k_1 (liter/mol)	n	S_1[b] (mg/ml)
α_{s1}-A	157 ± 3	8	0.9 ± 0.2
α_{s1}-B	187 ± 3	8	0.1 ± 0.1
β-C	156 ± 12	4	2.0 ± 0.3

[a] Solutions buffered at pH 7.0, 10 mM imidazole-HCl with 0.07 M KCl (Thompson *et al.*, 1969).

[b] S_1 denotes the soluble protein at elevated Ca^{2+} concentrations as defined in Eq. (1).

n, as well as the salting-in parameters k_2 and m, were determined (Table V).

The α_{s1}-A genetic variant, in contrast to the α_{s1}-B, exhibits solubility behavior over a range of calcium chloride concentrations. At 1°C (Fig. 5) α_{s1}-A, like α_{s1}-B, is precipitated with calcium at about 8 mM; in the presence of 0.07 M KCl after aliquot addition of $CaCl_2$, the protein is driven back into solution at 90 mM with $n = m = 8$. The protein is now positively charged, acting as a cation. This conclusion was previously verified by free-boundary electrophoresis at pH 7.0, 10 mM imidazole, 150

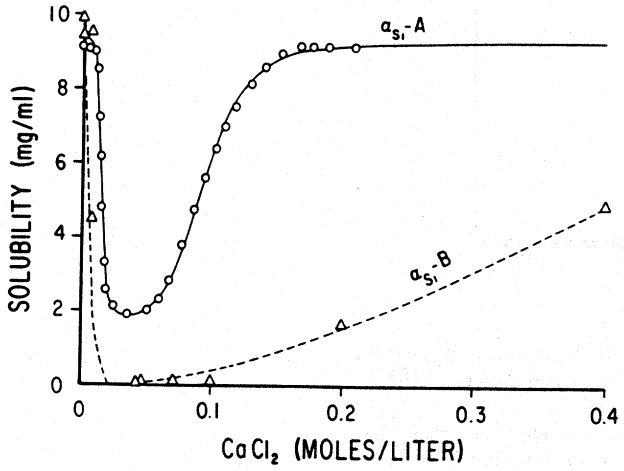

FIG. 5. Solubility at 1°C of calcium α_{s1}-B caseinate and calcium α_{s1}-A caseinate as a function of increasing $CaCl_2$ concentration at 1°C. Data were fitted by Eq. (4). Results of analyses are given in Table V.

TABLE V

CALCIUM-INDUCED INSOLUBILITY AND SOLUBILITY OF CASEINS AT 1°C[a]

Casein	k_1	n	k_2	m
α_{s1}-B	123 ± 5	8	2.5 ± 0.2	4
α_{s1}-A	68 ± 1	8	10.6 ± 0.3	8
β-C	Totally soluble			

[a] Conditions as in Table IV.

m*M* $CaCl_2$, where the protein is soluble at 1°C; it migrates ($+1.36$ cm^2 V^{-1} sec^{-1} $\times$ 10^{-5}) toward the cathode (Thompson *et al.*, 1969).

c. Influence of Electrolyte on Salting-Out at 37°C. When the 0.07 *M* KCl is omitted from these experiments and solubility is tested in $CaCl_2$ alone, somewhat different results are obtained (Fig. 6). The two genetic variants of α_{s1}-casein (A and B) show decreased solubility at 5 m*M* $CaCl_2$ and gave salting-out constants, k_1, of 180 and 204 liter/mol at 4 mg/ml; these values are significantly different, but, more surprisingly, the numbers

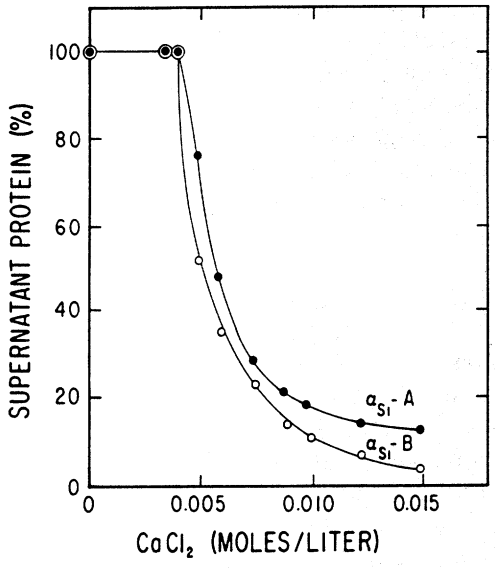

FIG. 6. Solubility at 37°C of calcium α_{s1}-A and B caseinates as a function of increasing $CaCl_2$ without KCl at 5 mg/ml. Data were fitted by Eq. (4).

TABLE VI

CALCIUM-INDUCED INSOLUBILITY OF α_{s1}-CASEIN B AT 37°C

Protein concentration[a]	k_1 (liter/mol)	S_0 (g/liter)	S_1 (g/liter)	n
5 + KCl	225 ± 2	5.31 ± 0.07	0.12 ± 0.04	8
10 + KCl	182 ± 4	11.11 ± 0.41	0.30 ± 0.20	8
4 − KCl	204 ± 4	4.31 ± 0.04	0.49 ± 0.04	16
10 − KCl	151 ± 1	9.42 ± 0.04	0.49 ± 0.04	16

[a] Initial concentration of protein in g/liter ± 0.07 *M* KCl.

of calcium binding sites (n) were 8 and 16, respectively. This difference was of interest since in the presence of KCl (Tables IV and V), the apparent number of calcium binding sites was equal to 8 for both genetic variants of the casein. Effects of KCl on the solubility of α_{s1}-B were tested at two different protein concentrations; data are summarized in Table VI. With no KCl present, k_1 is smaller for α_{s1}-B but n, the number of limiting sites, is 16. In the presence of 0.07 *M* KCl, the number of sites is reduced to $n = 8$ for both concentrations, but k_1 is larger. Apparently K^+ will compete with Ca^{2+} for a group of binding sites present in the α_{s1}-B genetic variant, but not in the α_{s1}-A. The α_{s1}-A genetic variant is the result of the deletion of 13 amino acid residues from α_{s1}-B (Fig. 7). The losses of glutamate residues 14 and 17 as well as arginine 22, which are surrounded by hydrophobic side chains, may cause this protein to have different physical properties. One explanation could be the loss of a hydrophobically stabilized intramolecular ion pair (Tanford, 1961). Increased K^+ concentrations may break this ion pair, lead to increased Ca^{2+} binding and altered equilibria among species present for α_{s1}-B. Indeed, α_{s1}-A, as noted above, is readily salted-in at 1°C whereas the B variant is not.

d. Influence of Phosphate Groups on Salting-Out and Salting-In. α_{s1}-Caseins A and B and β-C readily precipitate at 37°C in 0.07 *M* KCl (Fig. 4). Under these conditions, n was correlated with the number of phosphate residues in the native casein; hence, the importance of these residues in the precipitation reaction could be tested. In previous research, the phosphate groups of α_{s1}-B were removed enzymatically (Bingham *et al.*, 1972) and the effects of KCl on the precipitation of native (N) and dephosphorylated (O-P) caseins had been compared (Fig. 8a–c) but never quantified. Analysis of these data by use of Eq. (4) is summarized in Table VII. With no KCl present, dephosphorylation increases k_1 and some salting-in occurs for the O-P form; surprisingly, for both proteins (N and O-P), n =

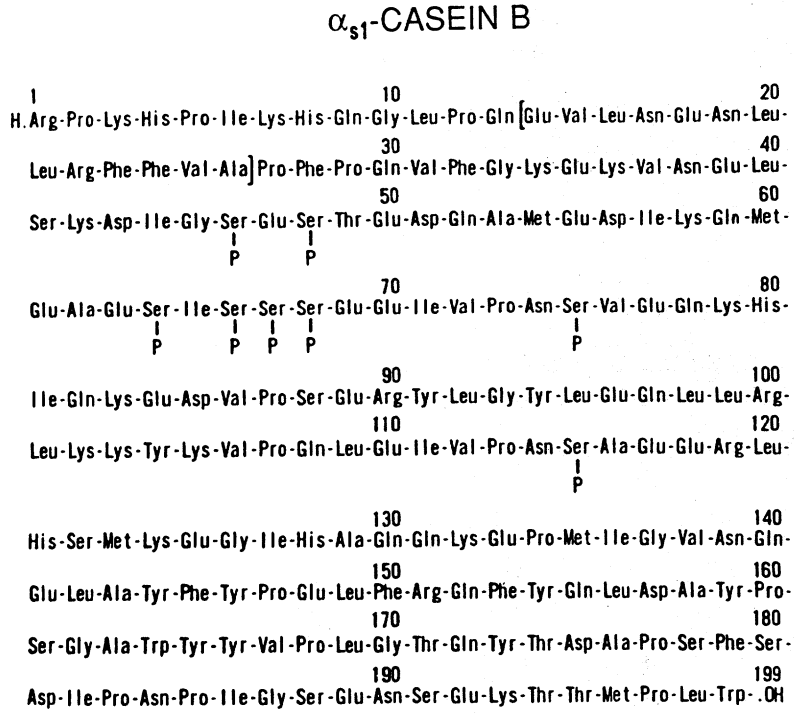

FIG. 7. Sequence of α_{s1}-casein B showing amino acids deleted to yield the α_{s1}-A variant. The deleted segment, residues 14–26, is enclosed in brackets.

16. In the presence of 0.07 *M* KCl, n is again reduced to 8 for both N and O-P forms of α_{s1}-B; the k_1s are similar to those found in the absence of KCl and salting-in occurs only for the O-P casein.

When α_{s1}-A is dephosphorylated it becomes almost completely soluble at 1°C and is salted-in even at 36°C (Fig. 9). In contrast, the N α_{s1}-A is not appreciably salted-in at 37°C (Fig. 4). Results are compared in Table VIII. For O-P α_{s1}-A without KCl $n = 8$, mirroring the numbers found for the N protein, but for the O-P form at 1°C $n = 2$ and $m = 4$. The k_2s observed for both N and O-P α_{s1}-A at both 1 and 36°C are similar to each other and to that of α_{s1}-B at 1°C. However, the small degree of salting-in which occurs for O-P α_{s1}-B does so with an elevated k_2 (Table VII), showing another significant difference between the A and B variants.

e. Effect of Various Cations at 1°C. The solubilities of α_{s1}-A in the presence of various cations are illustrated in Fig. 10. Cu^{2+} and Zn^{2+} are the most effective precipitants, as might be expected from their atomic

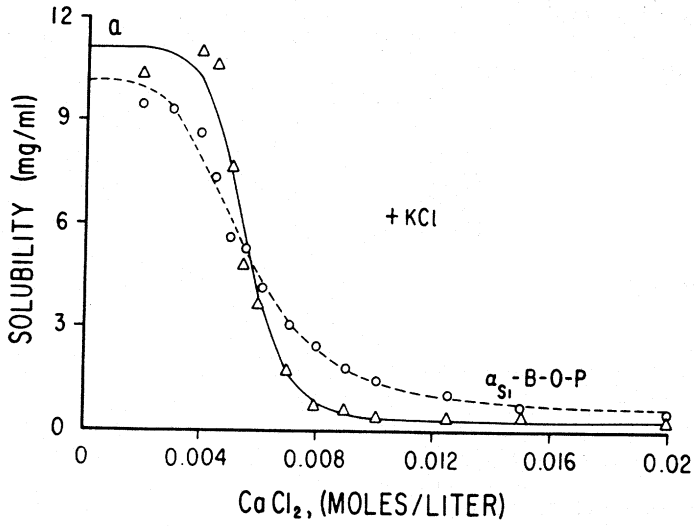
a
SOLUBILITY (mg/ml)
12
9
6
3
0
+KCl
α_{Si}-B-O-P
0
0.004
0.008
0.012
0.016
0.02
$CaCl_2$, (MOLES/LITER)

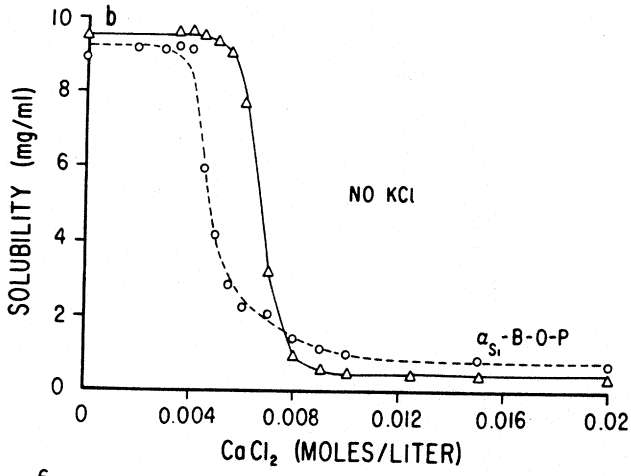
b
SOLUBILITY (mg/ml)
10
8
6
4
2
0
NO KCl
α_{Si}-B-O-P
0
0.004
0.008
0.012
0.016
0.02
$CaCl_2$ (MOLES/LITER)

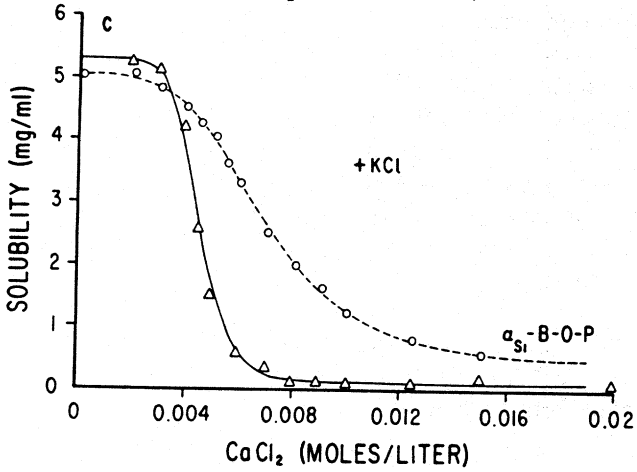
c
SOLUBILITY (mg/ml)
6
5
4
3
2
1
0
+KCl
α_{Si}-B-O-P
0
0.004
0.008
0.012
0.016
0.02
$CaCl_2$ (MOLES/LITER)

TABLE VII

CALCIUM-INDUCED INSOLUBILITY OF NATIVE (N) AND DEPHOSPHORYLATED (O-P) α_{s1}-CASEIN B AT 37°C

Protein	k_1 (liter/mol)	k_2 (liter/mol)	S_0[a]	S_1[a]	S_2[a]	n	m
N_{10} − KCl[b]	151 ± 1	—	9.42 ± 0.04	0.49 ± 0.04	—	16	0
O-P_{10} − KCl[c]	219 ± 2	135 ± 12	9.2 ± 0.1	2.6 ± 0.3	0.8 ± 0.6	16	8
N_{10} + KCl	182 ± 4	—	11.1 ± 0.4	0.3 ± 0.2	—	8	0
O-P_{10} + KCl	218 ± 10	154 ± 22	9.9 ± 0.2	6.4 ± 1.8	0.6 ± 0.6	8	4

[a] S_i denotes the soluble protein species defined in Eq. (1).

[b] N_{10}, Native protein at an initial concentration of 10 g/liter ± 0.07 *M* KCl.

[c] O-P_{10}, Dephosphorylated protein at an initial concentration of 10 g/liter ± 0.07 *M* KCl (Bingham *et al.*, 1972).

numbers. Coordinate complexes may be formed between α_{s1}-A molecules with Co^{2+}, Zn^{2+}, and Cu^{2+}. Ca^{2+} is effective as a precipitant to a lesser extent than Cu^{2+} or Zn^{2+}, whereas Mg^{2+} is the least effective of the five cations studied. The salting-out and salting-in constants were estimated from Eq. (4) for each cation and are given in Table IX. Cation variation (i.e., use of magnesium, calcium, cobalt, copper, and zinc) of these profiles showed k_1 and k_2 behavior consistent with concepts of phosphate- and carboxylate-ligand coordination, respectively. Clearly, an inverse relationship exists between casein solubility (as quantified by changes in k_1) and the atomic number of the divalent cations studied. The salting-in constant k_2 appears to decrease and then increase with atomic number; no apparent correlation with ionic radius is evident.

3. *Interpretation*

The caseins of milk can be subdivided on the basis of their solubility in Ca^{2+} solutions (Farrell and Thompson, 1988). Analyses of the solubility profiles of two genetic variants of the major bovine casein (α_{s1}) have been accomplished using Wyman's Theory of Thermodynamic Linkage. These analyses have yielded parameters which quantify the precipitation reactions. A notable feature of this analysis is that values of k_1 and k_2 obtained from the data of a variety of investigators are in excellent

FIG. 8. Solubility at 37°C of (△) native and (○) dephosphorylated α_{s1}-B as a function of $CaCl_2$ concentration (a) with 0.07 *M* KCl at 10 mg/ml, (b) without KCl at 10 mg/ml, and (c) with 0.07 *M* KCl at 5 mg/ml. Results of analyses are given in Tables VI and VII.

TABLE VIII

CALCIUM-INDUCED INSOLUBILITY OF NATIVE (N) AND DEPHOSPHORYLATED (O-P) α_{s1}-CASEIN A AT 36°C AND AT 1°C

Protein	k_1 (liters/mol)	k_2 (liters/mol)	S_1[a]	S_2[a]	n	m
N_{10} + 36°[b]	140 ± 3	—	0.90 ± 0.20	—	8	0
$O\text{-}P_{10}$ + 36°[c]	326 ± 7	36 ± 1	0.6 ± 0.3	10.0 ± 0.6	8	8
N_{10} + 1°	130 ± 4	13 ± 1	0.4 ± 0.2	—	8	8
$O\text{-}P_{10}$ + 1°	223 ± 59	46 ± 4	8.8 ± 1.8	10.0 ± 0.6	2	4

[a] S_i denotes the soluble protein species defined in Eq. (1).

[b] N_{10}, Native protein at an initial concentration of g/liter with no KCl and at the indicated temperature.

[c] $O\text{-}P_{10}$, Dephosphorylated protein at an initial concentration of 10 g/liter with no KCl and at the indicated temperature.

agreement [e.g., compare k_1 of Tables IV and VII for α_{s1}-β + KCl at 10 mg/ml with a value of 190 liter/mol calculated from Noble and Waugh (1965)]. The parameters k_1 and k_2 are taken to be related to the average association constants for the binding of calcium to casein. The logic behind this assumption is that, as the casein binds Ca^{2+} ions, a charge neutralization occurs, the complex approaches its isoelectric

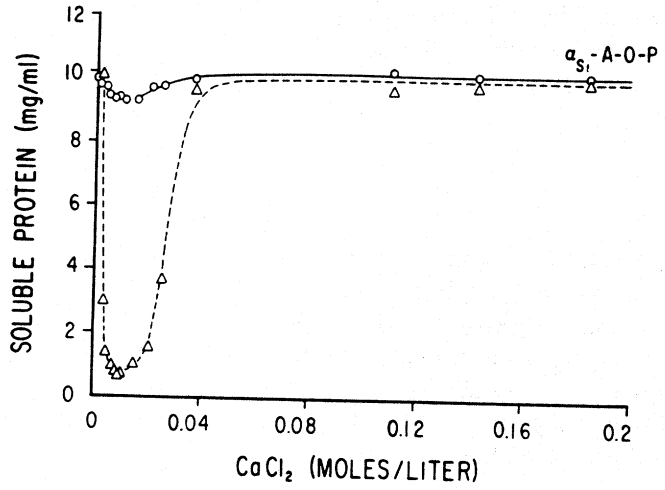

FIG. 9. Solubility of α_{s1}-casein A O-P as a function of calcium ion concentrations at 1°C (---) and at 36°C (——). Data were fitted by Eq. (1). Results of analyses are given in Table VIII.

TABLE IX

CATION-INDUCED SOLUBILITY OF α_{s1}-CASEIN A AT 1°C[a]

Cation	k_1 (liter/mol)	k_2 (liter/mol)	Atomic $S_2 - S_1$[b]	No.	R[c]
Mg^{2+}	76 ± 9	56 ± 7	8.4 ± 1.3	12	0.66
Ca^{2+}	150 ± 27	13 ± 2	8.2 ± 1.4	20	0.99
Co^{2+}	166 ± 4	8.1 ± 0.2	8.5 ± 0.2	27	0.72
Cu^{2+}	229 ± 2	18 ± 2	1.5 ± 0.1	29	0.72
Zn^{2+}	373 ± 27	202 ± 35	0.20 ± 0.03	30	0.74

[a] $n = m = 8$ for all calculations; no KCl present.

[b] $S_2 - S_1$ is the concentration of soluble α_{s1}-A in mg/ml [Eq. (1)].

[c] Cation atomic radius in angstroms.

point, and decreases in solubility. Previous research by Waugh and coworkers (Creamer and Waugh, 1966; Waugh *et al.*, 1971) has indicated that all of the various ionic species present are in true equilibrium, and as developed Section II,B,2, analysis of the soluble protein as a function of total calcium ion present should yield parameters (k) akin to association constants for calcium binding if the observed solubility changes are thermodynamically linked to the binding. The fit of the data corroborates this. A comparison of experimental binding constants

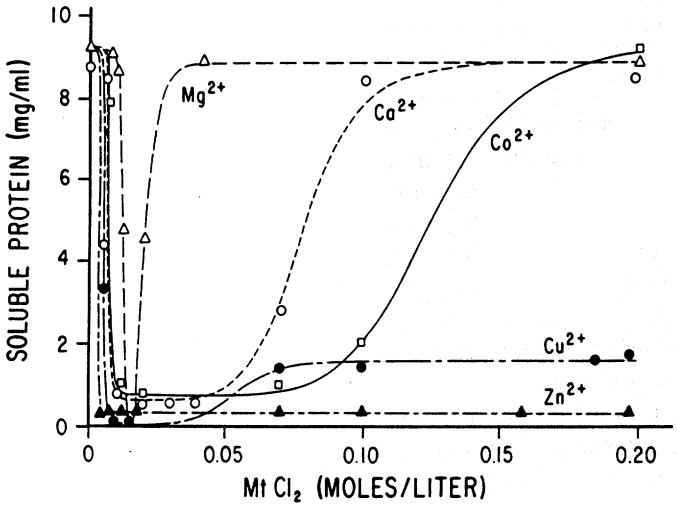

FIG. 10. Solubility at 1°C of various salts of α_{s1}-A as a function of increasing cation concentration. Data were fitted by Eq. (4). Results are given in Table IX.

TABLE X

COMPARISON OF ASSOCIATION CONSTANTS FOR VARIOUS CALCIUM COMPLEXES WITH VALUES OF k_1 AND k_2

Complex of Ca^{2+}	log k_a[a]	log k_1[b]	log k_2[b]
α_{s1}-Casein B	2.6	2.26	0.39
α_{s1}-Casein A	—	2.20	1.02
β-Casein	2.6	2.26	—
O-Phosphoserine	2.2		
Glutamate			0.8
Acetate			0.6

[a] Data from Dickson and Perkins (1971).
[b] Data from this study.

compiled by Dickson and Perkins (1971) with both values (log k_1, k_2) obtained in this study, both in the presence of added electrolyte, are shown in Table X. The k_1 values are in quite good agreement with literature values for calcium binding from dialysis experiments for the caseinates and for model phosphate compounds (Table X). Salting-in constants (k_2), however, appear to be more in agreement with association constants related to calcium binding by carboxylate groups. Thus, salting-in may be the result of further Ca^{2+} binding to carboxyl groups that increases the positive charge of the salt–protein complex, resulting in increased solubility.

The second parameter obtained by this method of analysis is n (or m). In the case of n, the values obtained in KCl (8 and 4 for α_{s1}- and β-caseins) appear to correspond to the number of moles of calcium bound as calculated from the data of Dickson and Perkins (1971) using in 0.1 *M* NaCl. These values also correspond to the number of phosphate residues found by sequence analyses for the respective caseinates. [Note β-C has only four groups as opposed to five found on A and B forms (Eigel *et al.*, 1984.)] α_{s1}-Casein A contains a total of 29 carboxylate groups and the net charge at neutral pH can be calculated to be -24; binding of 8 divalent calcium ions would decrease this number to -8, thus considerably reducing the molecule's net charge but not yielding an isoelectric precipitate. In a similar fashion, the net charge on β-C is -12 and binding of 4 divalent cations reduces this number to -4. These numbers (-8 and -4) may thus reflect that such binding leads to decreased solubility. Other binding, not linked to solubility, could first occur at higher affinity sites, and thus would not detected in this analysis; only that binding directly linked to solubility is revealed. It is interesting to note that in the case of α_{s1}-A, which is totally resolubilized

at 1°C, $n + m = 16$, reflecting a charge reversal to a cationic species with a net charge of +8. In fact, free boundary electrophoresis in calcium showed the molecule to have a cathodic mobility, and equilibrium dialysis experiments gave a value of 17 mol of Ca^{2+} bound at 1°C in 0.07 *M* KCl (Thompson *et al.*, 1969). It thus appears as though the parameters n and m correspond to the number of moles of Ca^{2+} bound per monomer, leading to solubility changes, while the values of k_1 and k_2 may relate to the association constants for phosphate and/or carboxylate binding of Ca^{2+}. Initially, the values of k_1 and n calculated for α_{s1}-B in 0.07 *M* KCl seemed to agree with literature values for binding of calcium to casein phosphate groups. If this is valid, a decrease in k_1 and n with dephosphorylation, with these values becoming more like those of k_2, is expected. In fact, k_1 increased upon dephosphorylation (Tables VII and VIII) and n remained the same; instead of abating calcium binding, dephosphorylation apparently enhanced it. Experiments conducted in the absence of KCl also showed similar trends: a class of tighter binding sites for the dephosphorylated form of α_{s1}-B, with $n = 16$ for both. For α_{s1}-A, $n = 8$ for both native and dephosphorylated caseins, and the dephosphorylated form had the highest value of k_1 observed (326 liter/mol). These observations are not contradictory; if altering the protein or its environment leads to decreased solubility, then the equations disclose those binding sites linked to this phenomenon under the specific conditions used.

One can visualize three classes of calcium binding sites on α_{s1}-casein, all with k_1 in the order of magnitude for calcium phosphocaseinate, and all thermodynamically linked to solubility changes under the selected test conditions. With the assumption that the protein is monomeric, these classes include (1) a class of sites with the highest calcium affinity observed (k_1) which are unmasked by dephosphorylation; $n = 8$ for this class. (2) A class of sites with k_1 between 160 and 180 for which $n = 8$ and which may correspond to phosphate groups (for β-casein $n = 4$ for this class). (3) A weaker set of sites which lower the average k_1 in the absence of KCl and which are expressed in α_{s1}-B with $n = 8$ but are not expressed in α_{s1}-A. (n without KCl $-$ n with KCl $= 16 - 8$.)

It is tempting to speculate that the calcium binding sites unmasked by dephosphorylation arise from changes in structure due to conversion of phosphoserine (P-serine) to serine. It is controversial as to whether or not P-serine disrupts secondary structures or promotes their formation. In theoretical calculations based on primary structures, Bloomfield and Mead considered P-serine to be a structure breaker, while Creamer *et al.* (1981) considered it to be neutral. In either event, most of the phosphate falls in areas of no regular structure or α-helix depending on the stance taken.

Here a change from 8 to 0 phosphate could induce a conformational change leading to tighter binding of calcium. For α_{s1}-A this change is most dramatic; the deleted residues (which occur in another area of uncertain structure) plus the deleted phosphate lead to even tighter binding of Ca^{2+} (Table VII). Thus the deleted segment may allow more carboxyl groups to act in concert and display the greatest affinity for calcium (k_1 = 326). In the α_{s1}-A variant, there are a total of 16 glutamic and aspartic residues in the sequence bounded by residues 35 to 85. In the native molecule, P-serines are interspersed with carboxylates, and dephosphorylation could allow structural changes which would signifcantly increase k_1. This is in contrast to dentin and salivary phosphoproteins, where higher than expected association constants for calcium are dramatically reduced by dephosphorylation (Linde, 1982). Dephosphorylation increased k_1 at 10 mg/ml and the amount of soluble casein also increased. Native α_{s1}-A can be salted-in at 1°C, but dephosphorylation of α_{s1}-A caused the molecule to be salted-in at 36°C as well as presumably through stronger Ca^{2+} protein interactions with carboxylate groups. Comparison of the k_2 values for the dephosphorylated forms of α_{s1}-A and B shows an important difference between the two genetic variants. Salting in of the dephosphorylated A variant is readily accomplished at 37 and 1°C and k_2 is of the order of magnitude expected for carboxylate interaction (see Table VIII). The limited salting-in observed for dephosphorylated α_{s1}-B, however, showed a K_2 nearly equivalent to k_1 (Table VII).

The curves for the α_{s1}-A calcium complexes, both native and dephosphorylated forms, show a strong tendency toward resolubilization at 1°C, whereas α_{s1}-B does not. α_{s1}-A represents a sequential deletion of 13 amino acid residues from α_{s1}-B (Fig. 7). Note that residues 14 and 17 are glutamic acids while residue 22 is an arginine, the remainder of the amino acid residues deleted are hydrophobic or noncharged. It is possible that a strong hydrophobically stabilized intramolecular ion pair (Tanford, 1961) occurs in α_{s1}-B. Upon addition of Ca^{2+} this bond is broken, and when precipitation occurs further binding of calcium leads to greater insolubility for the B variant. In the absence of this bond, α_{s1}-A can be readily salted-in at 1°C in whereas the B variant cannot. The genetic alteration of these electrostatic interaction sites produces a major change in the physical properties of the α_{s1}-A protein. Similar calcium-sensitive ion pairs may be of importance in other phosphoprotein systems such as dentin formation and plaque deposition (Linde, 1982). Examination of the sequences of salivary phosphopeptides, which have been implicated in the latter reaction, shows repeating sequences of Arg and Glu interspersed with hydrophobic residues (Oppenheim *et al.*, 1982). Future research on site-specific

III. CASEIN COLLOIDAL STABILITY PROFILES

A. CALCIUM-INDUCED MICELLE STABILITY

The complexes formed by the association of isolated α_{s1}- and κ-caseins can in turn aggregate to form model colloidal casein upon the addition of Ca^{2+} in 0.01 *M* imidazole buffer, pH 6.7. As viewed by electron microscopy, these model micelles are virtually identical with fresh milk micelles except for their somewhat increased size (Bingham *et al.*, 1972). The precise mechanism of formation of these stable model casein micelles is as yet uncertain, although several theories have been advanced (Schmidt, 1984). To understand the forces involved in regenerating stable colloid complexes, the precipitation by calcium ions of selected caseins (salting-out) and their stabilization into colloidal complexes (salting-in) were reinvestigated. In order to quantitate these observations, data were analyzed with respect to computer models (Farrell *et al.*, 1988) which have been developed to take into account the theromodynamic linkage (Wyman, 1964) that occurs between calcium binding and salting-out and salting-in constants. In this study, k_1, the salting-out constant, was correlated with the calcium–caseinate association constant and its exponent, n, with the number of moles of salt bound to decrease solubility. Salting-in was similarly correlated with k_2 and m. This model has now been extended to quantify interactions between calcium and mixtures of α_{s1}- and κ-caseins and to analyze the stability of model colloidal complexes.

1. Experimental Procedures

a. Materials. Purified caseins were prepared as previously described (Thompson, 1966) by DEAE-cellulose chromatography. Stock $CaCl_2$ solutions were prepared and their concentration checked by atomic absorption analysis. Nomenclature of the genetic variants and abbreviations for casein are as previously described (Eigel *et al.*, 1984).

b. Model α_{s1}-Casein Micelles (Colloidal Stability Test). Stabilization of α_{s1}-caseins by κ-casein in the presence of Ca^{2+} was performed at 37°C. The procedure was as follows:

One milliliter of stock α_{s1}-casein solution (40 mg/ml) was added to a 20-ml conical graduated centrifuge tube. The appropriate amounts of κ-casein were added to a series of tubes to achieve ratios of α_{s1}/κ of 40 : 1, 20 : 1, and 10 : 1 and the mixtures diluted to 5 ml with water.

Solutions were warmed to 37°C and 5 ml of the desired calcium chloride–imidazole–HCl buffered solution blown into the solution. The tubes were inverted twice and allowed to stand in a 37°C water bath for 30 min.

Tubes were centrifuged at 1500 *g* for 10 min.

One milliliter of the supernatant was added to a 5-ml volumetric flask containing 1 ml of 1 *N* sodium citrate, plus 2 ml water and the mixture was diluted with water. Turbid solutions were cleared by the addition of 100 μl of 0.1 *M* Na_2EDTA and the supernatant protein concentration determined at 280 nm.

c. Theory. The caseins of all species display characteristic changes in their colloidal stability as a function of added calcium. Individual calcium-sensitive caseins have known association constants for calcium (Farrell and Thompson, 1988), and, in a previous study, Farrell *et al.* (1988) demonstrated thermodynamic linkage between the free energy of salt binding and solubility. That theory assumed that there are essentially three classes of binding sites for ligands that are responsible for the triphasic sequential changes in colloidal stability; therefore, the concept of linked functions as developed by Wyman (1964) can be used to treat the above processes if the following equilibria are assumed:

$$\begin{array}{ccccc} (S_0) & \overset{k_1}{\rightleftharpoons} & (S_1) & \overset{k_2}{\rightleftharpoons} & (S_2) \\ \mathrm{P} + n\mathrm{X} & & \mathrm{PX}_n + m\mathrm{X} & & \mathrm{PX}_m\mathrm{X}_n \\ & & + & & + \\ & & q\mathrm{X} & & q\mathrm{X} \\ & & \Big\Vert\, k_3 & & \Big\Vert\, k_3 \\ & & (\mathrm{PX}_n\mathrm{X}_q & \overset{k_2}{\rightleftharpoons} & \mathrm{PX}_m\mathrm{X}_n\mathrm{X}_q \\ & & (S_4) & & (S_3) \end{array} \qquad (6)$$

where P is the unbound protein; X is the free salt; n, m, and q are the number of moles bound to species PX_n, PX_nX_m, and $PX_nX_mX_q$; and S_0, S_1, S_2, and S_3 are the solubilities of the species indicated. For this study, S_1 and S_2 will be relative to S_0. The mathematical relationship representing the above stoichiometry can be represented as

$$S_{app} = S_0 f(P) + S_1 f(PX_n) + S_2 f(PX_nX_m) + S_3 f(PX_nX_mX_q) \quad (7)$$

where S_{app} is the apparent protein solubility at a given salt concentration (S_T), $f(i)$ are the protein fractional component of species i, and the Ss are as defined above. Incorporation of the salt binding equilibrium constants as defined by Eq. (6) into Eq. (7) leads to the following:

$$S_{app} = \frac{S_0 p}{p + k_1^n p x^n} + \frac{S_1 k_1^n p x^n}{p + k_1^n p x^n} + \frac{(S_2 - S_1) k_2^m p x^m}{p + k_2^m p x^m + k_3^q p x^q + k_2^m k_3^q p x^m x^q} + \frac{S_3 k_2^m k_3^q p x^m x^q}{(p + k_2^m p x^m)(p + k_3^q p x^q)} \tag{8}$$

where p is the concentration in percent of the unbound protein and x is the concentration of unbound salt. Cancellation of common terms yields

$$s_{app} = \frac{S_0}{1 + k_1^n x^n} + \frac{S_1 k_1^n x^n}{1 + k_1^n x^n} + \frac{(S_2 - S_1) k_2^m x^m}{1 + k_2^m x^m + k_3^q x^q + k_2^m k_3^q x^m x^q} + \frac{S_3 k_2^m x^m k_3^q x^q}{(1 + k_2^m x^m)(1 + k_3^q x^q)} \tag{9}$$

It should be stressed here that the latter expression is valid only for sequential binding, i.e., $k_1 > k_2 > k_3$ and where n sites saturate prior to the binding of m sites on the protein. Also, for n or m values greater than one, k_1, k_2, and k_3 represent an average value for each of the n, m, or q binding sites. In reality n, m, or q moles of salt will bind with only one equilibrium constant (K_1), i.e., $K_1 = k_1^n$, $K_2 = k_2^m$, and $K_3 = k_3^q$.

Now, since the total salt concentration, X_T, is the sum of the free salt concentration, x, and the concentration of the bound salt of all species PX_n, PX_nX_m, and $PX_nX_mX_q$, it can be shown that

$$X_T = x\left(1 + \frac{n k_1^n P_T x^{n-1}}{1 + k_1^n x^n} + \frac{m k_2^m P_T x^{m-1}}{1 + k_2^m x^m} + \frac{q k_3^q P_T x^{q-1}}{1 + k_3^q x^q}\right) \tag{10}$$

where P_T is the total concentration of protein. From Eq. (10) it can be seen that X_T approaches x when P_T is small relative to x. In our experiments, this assumption is reasonable because the concentration range of the total salt is large, while the molecular weight of the aggregated calcium caseinates significantly reduces their molar concentration. Therefore, since the total

salt concentration instead of the free concentration could be used in Eq. (9), the salt-induced solubility profiles can be directly analyzed using a Gauss–Newton nonlinear regression analysis program developed at this laboratory by Dr. William Damert. All solubility profiles were analyzed by fixing the values of n and m or q and calculating the best least-squares fit for the optimum evaluated k_1, k_2, and k_3 values. The n, m, and q values were then fixed to new integer values and the whole procedure repeated. The n, m, and q values which yielded the minimum root-mean-square value for the analysis with the minimum error in k_1, k_2, and k_3 were then reported.

Thus, colloidal stability can be defined as the fraction which does not sediment at 1500 g, while colloidal instability (coagulation) is defined as the fraction sedimented under these conditions. As an extension of the previously developed theories on solubility (Farrell *et al.*, 1988), k_1 may still be considered as calcium binding linked to precipitation (salting-out), while k_2 may be more appropriately defined as a colloidal stability constant (salting-in) whose linkage is affected by casein–casein interactions. Moreover, instability of the system as a whole can be measured through the linkage of k_3 with calcium binding (colloidal destabilization). In this light, the S_n terms represent concentrations of stable colloid.

2. *Analysis of Data*

Model Casein Colloids. Colloidal stability tests as defined above show the comparison of Ca^{2+} stability profiles of model micelles made from mixtures of the purified α_{s1}-caseins A and B and κ-casein (Fig. 11a,b). While the α_{s1}-A micelles (Fig. 11a) are soluble at 16 mM Ca^{2+}, α_{s1}-B micelles are less soluble at this concentration (Fig. 11b). In the case of α_{s1}-B, κ-casein initially enhances stability at lower Ca^{2+} concentrations, but increased Ca^{2+} leads to precipitation. For α_{s1}-A, increased Ca^{2+} does not lead to decreased stability. The data for α_{s1}-A were analyzed by use of the first and second terms of Eq. (9), with $q = 0$; results are summarized in Table XI. As κ-casein is added to α_{s1}-casein, increased stability occurs across the profiles. The salting-out constant (k_1) is not appreciably different for α_{s1}-A as κ-casein is varied, but salting-in (k_2) is lower than k_1 and, although it does not vary with κ-casein concentration, its value is 10× greater than salting-in (k_2) for α_{s1}-A in the absence of κ-casein (Farrell *et al.*, 1988). Thus κ-casein facilitates colloidal stability.

The α_{s1}-B variant, as noted above, shows significant destabilization of the colloidal complexes as the Ca^{2+} concentration exceeds 10 mM, even at elevated κ-casein concentrations. In order to analyze these data the

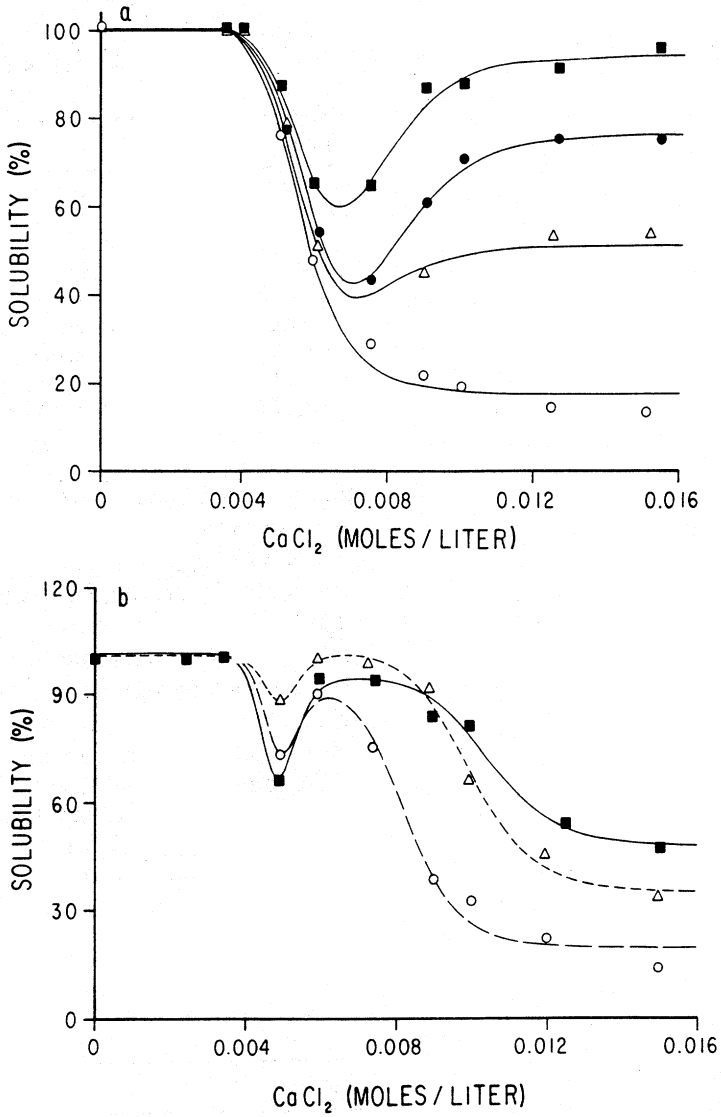

FIG. 11. (a) Supernatant protein at 37°C resulting from the incremental addition of $CaCl_2$ to α_{s1}-A with no κ-casein present (○); α_{s1}-A + κ-casein, 40 : 1 (△); α_{s1}-A + κ-casein, 20 : 1 (●); and α_{s1}-A + κ-casein, 10 : 1 (■). Solutions buffered at pH 7.0, 0.01 *M* imidazole-HCl. Initial protein concentration was 4 mg/ml. Data were fitted with Eq. (9). Results are given in Table XI. (b) Supernatant protein at 37°C resulting from the incremental addition of $CaCl_2$ to α_{s1}-B + κ-casein, 40 : 1 (○); α_{s1}-B + κ-casein, 20 : 1 (△); and α_{s1}-B + κ-casein, 10 : 1 (■). Solutions buffered at pH 7.0, 0.01 *M* imidazole-HCl. Initial protein concentration was 4 mg/ml. Data were fitted with Eq. (9). Results are given in Table XII.

TABLE XI

EFFECT OF κ-CASEIN ON CALCIUM-INDUCED INSOLUBILITY OF α_{s1}-CASEIN A AT 37°C

Ratio[a]	k_1[b]	k_2[b]	S_1[c](%)	S_2[d](%)
No κ-C	180 ± 3	—	17 ± 2	—
40:1	174 ± 4	138 ± 4	1.6 ± 0.9	51 ± 3
20:1	170 ± 2	127 ± 2	1.5 ± 0.9	77 ± 1
10:1	169 ± 3	137 ± 2	1.4 ± 0.9	95 ± 2

[a] Ratio of α_{s1}-A to κ-casein. Initial concentration: 4 g/liter α_{s1}-A.
[b] $n = m = 8$ for all calculations; k is expressed in liters/mole.
[c] S_1, Percentage of total protein soluble after initial precipitation.
[d] S_2, Percentage of resoluble casein at elevated calcium concentration.

parameters k^q and x^q were used. The results of the nonlinear regression analysis are given in Table XII. Again, k_1 does not vary with κ-casein and is not different from the salting-out constant obtained in the absence of stabilizing protein (κ-casein). Like α_{s1}-A, the k_2 for the B variant is significantly increased over values found in the absence of κ-casein at 1°C; in fact, this variant is usually nearly completely insoluble without κ-casein. The amount of soluble protein (S_3) here represents that which remains after colloid formation and subsequent destabilization. This parameter varies with κ-casein content, and q has an unusually large value of 12.

The data of Nobel and Waugh (1965) for native α_{s1}-B at higher Ca^{2+} concentrations in 0.07 *M* KCl (Fig. 8a) were used to find the values of k_3 and S_3 by analysis with Eq. (9) (Table XIII); the values are smaller, but $n = 16$ and $m = q = 8$. When compared to α_{s1}-B alone and to α_{s1}-B micelles

TABLE XII

EFFECT OF κ-CASEIN ON CALCIUM-INDUCED INSOLUBILITY OF α_{s1}-CASEIN B AT 37°C

Ratio[a]	k_1[b]	k_2	k_3	S_3[c](%)
No κ-C	204 ± 10	—	—	—
40:1	211 ± 21	197 ± 22	121 ± 4	20 ± 3
20:1	206 ± 21	198 ± 20	100 ± 2	35 ± 3
17:1	214 ± 11	189 ± 10	95 ± 3	36 ± 3

[a] Ratio of α_{s1}-B to κ-casein. Initial concentration: 4 mg/ml α_{s1}-B (S_0).
[b] $n = m = 16$ for all calculations and $q = 12$. k is expressed in liters/mole.
[c] All S_2 values at 100%; S_1 at 0; S_3 represents percentage of soluble α_{s1}-B at elevated calcium concentrations.

TABLE XIII

COMPARISON OF THE EFFECTS OF κ-CASEIN ON THE SALTING-OUT AND SALTING-IN PARAMETERS OF α_{s1}-CASEIN B AT 37°C

Sample[a]	k_1[b]	k_2	k_3	S_1[c]	S_2	S_3	n	m	q
Buffer, no KCl									
10:1	165 ± 8	164 ± 8	67 ± 1	0	10.2 ± 0.9	4.1 ± 0.5	16	16	12
Nobel and Waugh, with 0.07 *M* KCl									
10:1	195 ± 2	155 ± 2	21 ± 1	0	10.1 ± 0.2	2.5 ± 0.1	16	8	8
5:2	261 ± 3	254 ± 3	—	0	7.0 ± 0.1	—	16	16	—

[a] Ratio of α_{s1}- to κ-casein is given.
[b] k values expressed in liters/mole.
[c] S values given in mg/ml.

in the absence of KCl, differences in n and q are apparent. For α_{s1}-alone in KCl $n = 8$, but with κ-casein present it increases to 16, which is similar to its value alone without KCl. The interaction with κ-casein induces some change which affects calcium interaction sites, in a sense, "screening out" the KCl effect. Since this does not happen for α_{s1}-A, it indicates electrostatic involvement due to the deleted, but predominantly hydrophobic, segment. KCl does have an effect on m and q in α_{s1}–κ complexes (Table XIII); here, the KCl may make the micelles less sensitive to calcium precipitation (lower k_3 at 10 mg/ml by about 3-fold).

In contrast to the situation shown in Fig. 12a, precipitation of micelles (k_3) does not occur at 5 mg/ml (Fig. 12b) because the α_{s1}- to κ-casein ratio is decreased. The κ-casein protects α_{s1}-B, Ca^{2+} binding does not occur at sufficient levels, and the colloidal micelles remain stable. Nonlinear regression analyses of these data are summarized in Table XIII.

3. *Interpretation*

Calcium-Induced Colloidal Stability. Model colloidal complexes were previously defined by their stability at 1500 *g* (Noble and Waugh, 1965). The effects of the genetic variants A and B were tested in this system. Figure 11a,b shows the stabilization of α_{s1}-A and B by κ-casein (pH 7.0, imidazole-HCl buffer, 37°C) as a function of increasing calcium ion concentration. While these experiments were performed in the absence of KCl, the dip at 5 m*M* $CaCl_2$ reported by Noble and Waugh (1965) was apparent. In their early experiments on the colloidal system, Waugh and Nobel (1965) established that, under these conditions, the various soluble species of protein present are in thermodynamic equilibrium, and, as noted above,

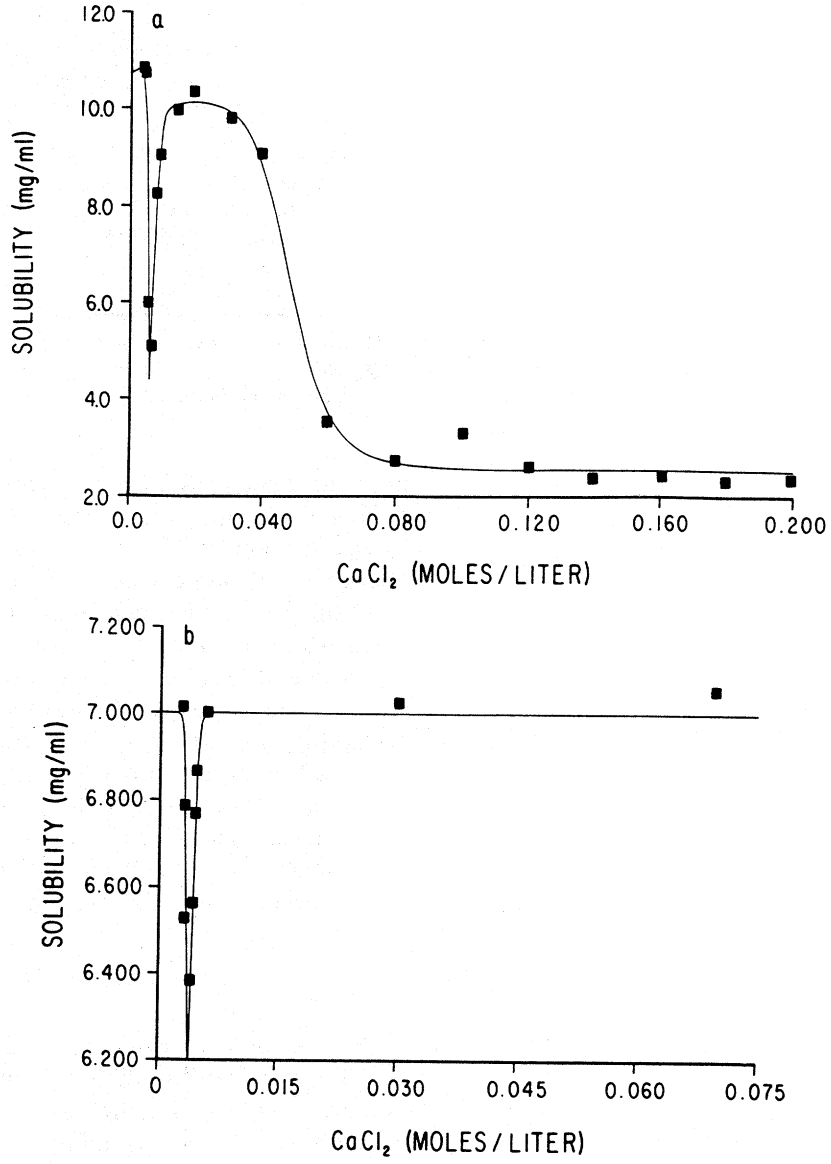

FIG. 12. Precipitation of α_{s1}-B/κ-casein micelles at elevated salt concentrations: (a) a ratio of α_{s1}-B to κ-casein of 10:1, (b) a ratio of 5:2.

calcium binding occurs. Thus Eq. (6) in the form of a binding isotherm relates the proposed stoichiometric terms (p, PX_m, etc.) to the soluble species (S_0, S, etc). Analysis of these data for α_{s1}-B complexes with Eq. 9 showed no substantial changes in k_1 from those found at 37°C with no κ-casein present (Table XII). On the other hand, κ-casein caused a 40-fold increase in k_2 over the salting-in constants found for salt alone at 1°C for the α_{s1}-caseins (Farrell *et al.*, 1988). In the absence of κ-casein at 37°C, α_{s1}-A and B are nearly completely insoluble (Fig. 11a,b).

κ-Casein could act in three ways to induce formation of stable colloidal complexes. In the first case, κ-casein could simply bind calcium and thus prevent calcium precipitation; however, equilibrium dialysis experiments (Dickson and Perkins, 1971) show that κ-casein has a lower K_a for calcium than α_{s1}-casein and has only 1–2 binding sites under these conditions. A second alternative is that κ-casein interacts with the α_{s1}-casein in such a way as to prevent calcium binding totally; this can be argued against since k_1 and n are essentially independent of κ-casein concentration for both genetic variants (Tables XI and XII) and since mixtures of caseins do bind calcium (Dickson and Perkins, 1971). The third alternative is that the α_{s1}- and κ-caseins form complexes with altered affinity for calcium which have the ability to go on to produce collodial particles. This latter alternative appears most likely. Formation of protein complexes in the absence of Ca^{2+} has been demonstrated by free boundary electrophoresis, analytical ultracentrifugation (Schmidt, 1984), and gel permeation chromatography (Pepper and Farrell, 1982), and, as clearly shown in these articles, calcium does generate complexes of colloidal dimensions. Considering α_{s1}-B in 0.07 M KCl as the starting point, either addition of κ-casein or omission of salt decreases k_1 but increases n to 16. This indicates that more weaker sites for calcium binding are exposed by either treatment. Thus, a structural change accompanying protein–protein interactions could occur in α_{s1}-B but not in α_{s1}-A. Evidence for an increase in the number of β-turns in mixtures of caseins (B variant) over the sum of the individual proteins has recently been given by Raman spectroscopy (Byler *et al.*, 1988). These data support the hypothesis that protein–protein interactions induce structural changes in the caseins. κ-Casein thus facilitates colloidal stability.

In these studies k_2 is increased nearly 10-fold by κ-casein over the value for salting-in of the α_{s1}-caseins alone. This too argues that the sites responsible for salting-in have had their affinity for calcium altered as a result of complex formation with κ-casein; k_2 may thus be a measure of colloidal stability rather than salting-in. A monotonic increase in total amount of soluble protein was observed for α_{s1}-A (Fig. 11a) with increasing κ-casein; these data are quantitated in Table XIII.

Comparison of Fig. 11a and b shows another important difference between α_{s1}-caseins A and B. As the Ca^{+2} concentration is increased the colloidal complexes containing α_{s1}-B begin to destabilize and start coagulating; those containing α_{s1}-A do not. These data were treated by an extension of the general salting-out theory (Farrell *et al.*, 1988); addition of a third term for the colloidal destabilization [Eq. (7)] yields a third set of terms, k_3 and q, which have the same meanings as k_1 and n, but are applied to the larger complexes of the α_{s1}–κ–calcium caseinates. Here the κ-casein is able to protect α_{s1}-B from precipitation at lower Ca^{2+} concentrations, but as Ca^{2+} increases more binding occurs. In contrast, α_{s1}-A–κ–casein complexes remain stable. The basis for this may be as follows: α_{s1}-A represents a sequential deletion of 13 amino acid residues. Note that residues 14 and 17 are glutamic acids while residue 22 is an arginine; the remainder of the amino acid residues deleted are hydrophobic

THOMAS F. KUMOSINSKI

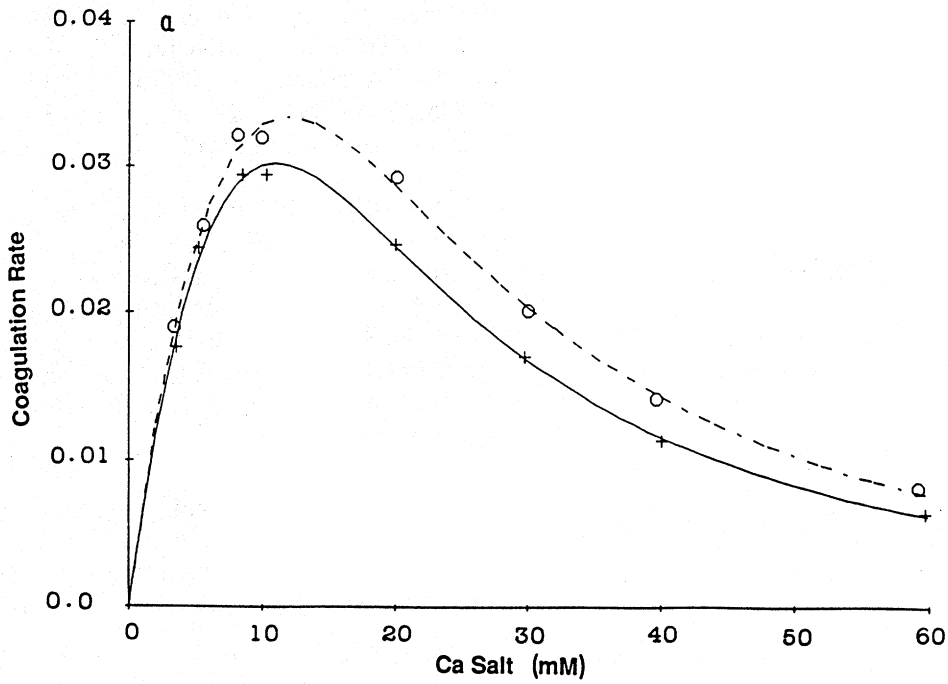

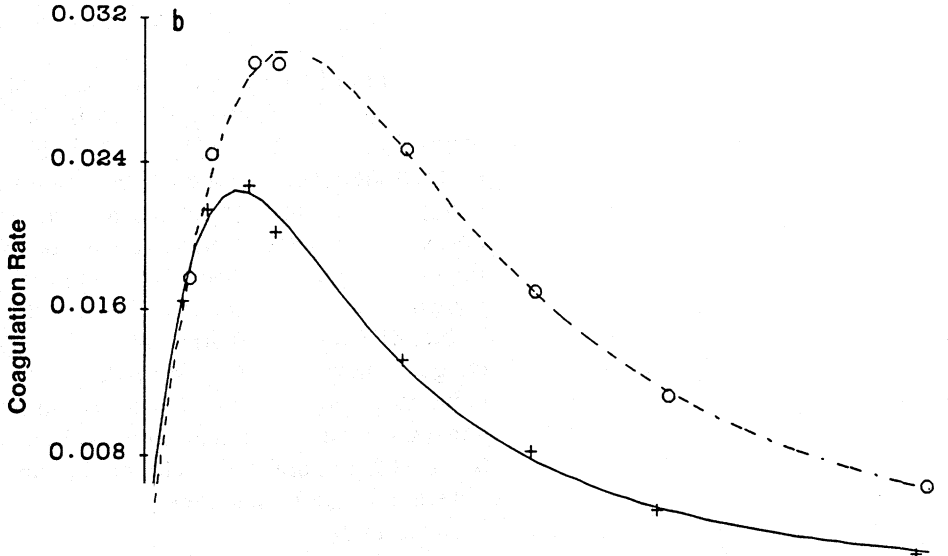

TABLE XIV

VARIATION OF THERMODYNAMIC LINKAGE PARAMETERS WITH ANION TYPE FOR THE CALCIUM-INDUCED COAGULATION OF CASEIN MICELLES

Anion	k_1 (liter/mol)	k_2 (liter/mol)	n	m
Cl	70 ± 23	47 ± 1	1	2
Br	80 ± 22	49 ± 1	1	2
NO_3	66 ± 23	58 ± 1	1	2
SCN	149 ± 40	77 ± 1	1	2

destabilization, i.e., k_2 and k_3, respectively, with the k_1 and k_2 values from Table XIV indicates a possible relationship between colloid stability and the rennin-induced coagulation rate. This can be seen qualitatively by comparison of Figs. 12a and 13a. Even though absolute magnitudes of these k values differ by up to a factor of two, there appears to be an optimum concentration of calcium chloride for a stable colloid which in turn exhibits a maximum coagulation rate. The differences in the parameters are probably due to the fact that the starting protein sample for the coagulation experiments contained calcium, whereas the colloidal stability measurements were performed on starting protein samples where calcium was totally eliminated. Nevertheless, the correlation between a stable colloidal micelle and optimum rennin-induced coagulation rate is apparent.

IV. GEL STRENGTH OF WHEY PROTEIN ISOLATE

A. VARIATION WITH ADDED COSOLUTE

1. Introduction

The importance to the food industry of variation of the functional properties of protein gels with added cosolutes is well documented. Many clear gels become opaque with even a slight addition of salt to the solution prior

FIG. 13. (a) Effect of calcium salts of Cl^- (O) and Br^- (+) on the average rate of chymosin-initiated coagulation of casein micelles (Bringe and Kinsella, 1986). The dotted and solid lines are the best fit using nonlinear regression analysis and thermodynamic linkage for the Cl^- and Br^- data, respectively. (b) Same as in a but O and + are NO_3^- and SCN, respectively.

to heating. Other rheological properties such as gel strength also vary drastically with the added cosolutes. Since no molecular model has successfully quantitated this behavior, the possibility of predicting gel strength behavior is at most limited. Hence, it would be prudent to employ the concept of thermodynamic linkage to the behavior of a rheological property of a protein gel. In this section, we attempt to link thermodynamically the gel strengths of whey protein isolates (WPI) with interaction of cosolutes with the protein prior to the gelation process. In this section, the data and methodologies are adapted from Schmidt.

2. *Experimental Procedures*

The gelation of WPI with added NaCl, $CaCl_2$, and cystine was described by Schmidt *et al.* (1978). What is noteworthy here is that each solution contained a constant amount of WPI, while the cosolute concentration was varied prior to the heating and cooling process. It should also be noted that the concentration of protein used at zero concentration of cosolute must be of a large enough magnitude so that gelation will take place.

Theory. The mechanism employed follows Eqs. (2)–(5) for the solubility of soy protein isolate. Here, the S values will denote gel strength instead of the usual solubility of the free and bound species. All other parameters, i.e., species and k values, and methods of analysis remain the same.

3. *Analysis of Data*

The variation of gel strength of WPI with added NaCl and $CaCl_2$ is shown in Fig. 14. Only monophasic behavior is observed at these concentrations. Here both the NaCl and $CaCl_2$ results were analyzed via nonlinear regression analysis using Eq. (5). The lowest root-mean-square results were obtained with n values of 2 and 4 for NaCl and $CaCl_2$, respectively, yielding corresponding binding constants, k_1, of 6.2 ± 1.8 liter/mol and 93.3 ± 0.8 liter/mol. It is apparent from these results that the cations of sodium and calcium bind the WPI in a cooperative manner whereby an increase of gel strength occurs. Obviously, an electrostatic mechanism is involved, i.e., the average charge of the WPI has decreased upon the cooperative binding of these cations to the negatively charged carboxyl groups on the WPI. This binding would then decrease the protein–protein repulsive interactions, allowing the new hydrophobic or other attractive forces (introduced by heat denaturation during preparation) to cause efficient formation of a

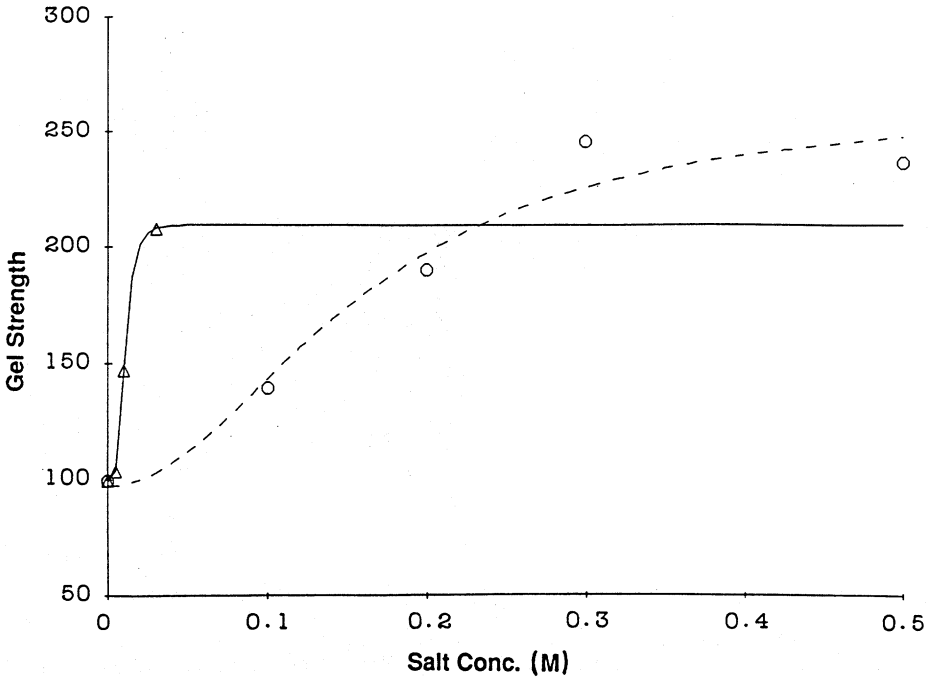

FIG. 14. Variation of gel strength of whey protein isolate in the presence of added NaCl, (○) and $CaCl_2$ (△). Dashed and solid lines are the best fit of the NaCl and $CaCl_2$ data, respectively, using thermodynamic linkage and nonlinear regression analysis (see text). [Data from Schmidt *et al.* (1978).]

more stable gel. The difference between the n and k values of calcium and sodium may reflect calcium–carboxylate interactions rather than intramolecular cross-linking.

The gel strength variation of WPI with added cysteine is shown in Fig. 15. Here, unlike the previous sodium and calcium results, the gel strength plot exhibits biphasic behavior. Qualitative observation of the results shows an optimum concentration of 0.05 M cysteine for the gel strength of WPI. All other values result in a less stable gel. Analysis via thermodynamic linkage and nonlinear regression analysis yielded n and k values of 1 and 43 ± 5 liter/mol for stabilization of the gel, and m and k_2 values of 8 and 15 ± 1 liter/mol for destabilization, respectively. It is apparent from these results that since cysteine is capable of interacting with protein sulfhydryl and disulfide groups that one such group of WPI is necessary for increasing gel strengths of WPI, whereas eight others are responsible for inhibiting the gelation process. However, no speculation concerning

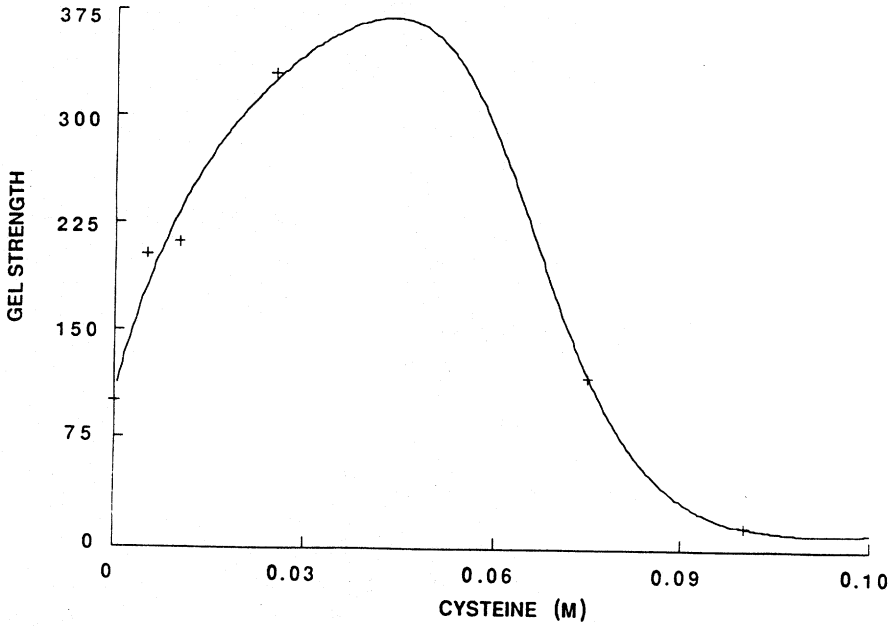

FIG. 15. Effect of cysteine on the gel strength of whey protein isolate. Solid line is best fit for data using thermodynamic linkage and nonlinear regression analysis (see text). [Data from Schmidt *et al.* (1978).]

which groups responsible for this phenomenon is possible until detailed structural analysis of these proteins is performed under gelation conditions. Since the X-ray crystallographic three-dimensional structures of both α-lactalbumin and β-lactoglobulin are now available, it may be possible in the future to use this structural information in conjunction with other methodologies to answer this question.

B. VARIATION WITH PROTEIN CONCENTRATION

1. Introduction

The gelation of a protein involves protein–protein interactions. The process of heating the protein above 80°C at a minimum concentration, which depends on the nature of the protein, clearly necessitates protein conformational changes. The cooling process whereby a gel is formed from this new (nonnative) protein structure establishes a need for a measure of the free energy, i.e., the equilibrium constant for the aggregation of the

new conformationally changed protein monomer units. Whether these units are cooperative in nature or nonspecific, however, needs to be clarified. Most investigators have speculated that heat denaturation produces a conformational change in the protein mimicking a random coil with exposed hydrophobic groups which in turn can self-associate during cooling. However, such a mechanism would not involve a cooperative protein–protein interaction. Thus, the protein concentration dependence of the gelation process may not involve a unique number of protein monomer units. To test the cooperative mechanism of protein–protein self-association, a thermodynamic linkage of the gel strength of a WPI with protein concentration was attempted. This allows us to obtain the number of cooperative monomer units which leads to gel formation, and to calculation of free energy, i.e., the equilibrium constant for the aggregation process. This equilibrium constant can then be compared with other homogeneous or heterogeneous protein constituents to obtain a quantitative free energy scale for gel formation.

2. *Experimental Procedures*

The data were obtained from the results of Schmidt *et al.* (1978). The system used in this study was WPI dissolved at various protein concentrations.

Theoretical Treament. The stoichiometry necessary for quantitating the variation of gel strength with protein concentration is

$$nP \overset{k_1^n}{\rightleftharpoons} P_n \xrightarrow{\text{cold}} \text{Gel} \tag{11}$$

where

$$k_1^n = [P_n]/[P]^n \tag{12}$$

P is the monomer protein, k_1^n is the equilibrium constant for self-association, and n is the degree of self-association. The degree of self-association is the number of protein monomer units within one cell which contain protein and trapped water. The cell units then aggregate irreversibly in the cold to form a gel. Now the Ss are the functional rheological parameters, e.g., gel strength, while C is the total protein concentration.

S_{app} is measured, S_0 is a nongel parameter, and S_1 is the gel rheological property.

$$S_{app} = f_{P_n} S_1 + f_P S_0 \tag{13}$$

where the f are the fractional amounts of protein in the P_n and P states, respectively.
Now,

$$f_{P_n} = \frac{k_1^n p^n}{p + k_1^n p^n} = \frac{k_1^n p^{n-1}}{1 + k_1^n p^{n-1}} \tag{14}$$

and total protein concentration (C) is

$$C = p(1 + k_1^n p^{n-1}) \tag{15}$$

Substituting Eq. (15) in Eq. (14) yields

$$f_{P_n} = \frac{k_1^n C^{n-1}}{1 + k_1^n p^{n-1} + k_1^n C^{n-1}} \tag{16}$$

Now, since k is large and the concentration of the monomer protein is small within a gel, then

$$k_1^n p^{n-1} \ll 0 \tag{17}$$

Therefore,

$$f_{P_n} = \frac{k_1^n C^{n-1}}{1 + k_1^n C^{n-1}} \tag{18}$$

and, since,

$$f_P = 1 - f_{P_n} \tag{19}$$

then

$$S_{app} = \frac{S_1 k_1^n C^{n-1}}{1 + k_1^n C^{n-1}} + \frac{S_0}{1 + k_1^n C^{n-1}} \tag{20}$$

If $S_0 = 0$ as is the case when using rheological functional parameters,

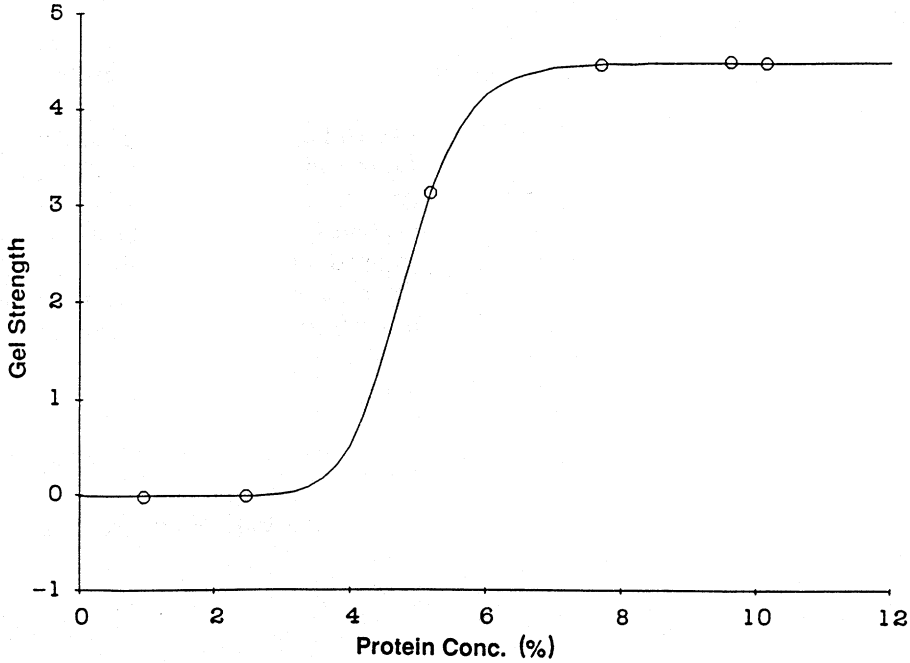

FIG. 16. Variation of gel strength with protein concentration of whey protein isolate. Solid line is best fit of data using Eq. (21) and nonlinear regression analysis (see text). [Data from Schmidt *et al.* (1978).]

$$S_{app} = \frac{S_1 k_1^n C^{n-1}}{1 + k_1^n C^{n-1}} \tag{21}$$

Finally, it should be noted that the free energy of self-association, $\Delta F = -nRT \ln k_1$. Therefore, using data of S_{app} versus C for any rheological property will yield k_1 and n by nonlinear regression analysis. ΔF, n, and k_1 can now be related to the chemical composition of the protein and may be used as a standard functional test for gelation.

3. *Analysis of Data*

The protein concentration dependence of the gelation of WPI according to Schmidt *et al.* (1978) is given in Fig. 16. Fitting these results by nonlinear regression analysis using the previously derived expressions [i.e., Eq. (21)] yields an n value of 12 for the cooperative protein self-association stoichiometry, and a corresponding equilibrium constant of 0.0237 ± 0.0001 liter/g for this interaction. It should be noted that the latter value

is not the total equilibrium constant, as defined by the previous equations, but a measure of a single protein–protein interaction within a cooperative structure. Thus, these values can be directly compared with other proteins even though their n values or degree of cooperative self-association differ. Moreover, the high value of 12 for the degree of cooperative protein self-association argues for a mechanism whereby a heat-induced nonnative protein can self-associate to a repeating unit in which water would be trapped. However, more structural work on the systems that have been thermodynamically linked using this methodology must be performed in order to prove this mechanism of protein gelation.

V. KINETIC PROCESSES

A. VARIATION OF ACID PHOSPHATASE WITH METAL IONS

1. Overview

Most plant cell walls form an extracellular network which is composed of cellulose fibers interconnected by the pectic-type polysaccharides (McNejl *et al.*, 1979). In addition to the carbohydrate components, the primary cell walls also contain several different types of proteins. One type of structural protein is the hydroxy proline-rich glycoproteins (HPGP) which may be important for cell recognition and disease resistance (Lamport and Catt, 1981). Functionally identifiable enzymes are also found in the primary cell wall (Lamport, 1970), including peroxidases (Fry, 1979), glycosidases (Lamport, 1970), and phosphatases (Crasiner *et al.*, 1980). Presumably, these enzymes are important in cell wall metabolism, nutrient transport, recognition, and disease resistance.

Plant cell walls contain many ionizable groups. Thus, they may be regarded as immobilized polyelectrolytes. The ionic behavior of cell walls has been described by the well-known theoretical models of Donnan (Pitman *et al.*, 1974) or Gouy–Chapman (Shone, 1966). More recently, the classical Donnan theory and activity coefficient concept were used to describe ion–ion and ion–water interactions in cell walls (DeMarty *et al.*, 1978). On the other hand, the relative adsorption of cations on isolated cell walls was shown to be accountable by mass-action expressions of ion exchange (Bush and McColl, 1987). A model simultaneously taking electrostatic interactions and specific binding into consideration was also developed for predicting ionic equilibrium concentrations in cell walls

is modulatory; sites with K_D equal to 1.54 mM produce an apparent reactivation or alleviation of inhibition (V_3 = 39.1). The curve of Fig. 20 is the composite of all these interactions. The linked-function analysis [Eq. (30)] thus appears to provide a more quantitative basis for discussion of these phenomena than the Dixon plot. Since the best data (lowest [I]) are used, the statistical fits are better, although qualitatively the Dixon plot (inset of Fig. 20) suggests the same result. As determined by Faulkner and Peaker (1982), the average total citrate content of lactating bovine mammary gland is >3 mM, so these effects could occur in the physiological range. Equation (30) implies no interaction between sites n, m, and q; a more complex model with interaction was tested, but statistical analysis did not allow discrimination between it and the simpler model (no valid improvement in the fit by the F test), thus the simpler equation was applied here. Interpretation of n, m, and q is somewhat more speculative than that of k_1, k_2, and k_3. In protein–ligand studies, n, m, and q may be correlated with the number of bound ligands giving rise to a selected change in properties (Farrell *et al.*, 1988). Here it may mean that 2 mol of metal–citrate bind per dimer for activation to occur, then additional binding of 2 mol of metal–citrate complex leads to strong inhibition (k_2) but an additional 4 mol (k_3) leads to reactivation and thus modulation. Further clarification of these numbers is necessary, but with the qualification that only binding which leads to change in V_{max} is disclosed by linkage; other binding not associated with activity can occur (Farrell *et al.*, 1988).

The importance of enzyme–substrate interactions in the regulation of enzymes has long been recognized (Frieden, 1979; Cleland, 1967), as have the principles of allosteric regulation (Gabriel and Plaut, 1984; Plaut *et al.*, 1983). The more recent focus on regulation through metal ion-activated cascades has emphasized the importance of regulatory binding sites with $K_A \approx 10^9$ (Cheung, 1984). The data reported above point to the potential significance of weaker binding sites as regulators of enzyme activity. This is especially true when metabolite concentrations in a tissue occur in the same range as the K_D for such sites. The effects of metal–citrate on the enzyme are noteworthy, particularly if the pools of Krebs cycle metabolites in mammary tissue fluctuate in the same fashion as the glycolytic pools do in other tissues (Neet and Ainslie, 1980). At very low isocitrate and citrate concentrations (<μM), the $NADP^+$: IDH would be mostly in the inactive form; a sudden upswing in Krebs cycle activity would presumably produce citrate first, and the citrate which is shunted to the cytosol could, as metal–citrate, activate NADP : IDH in advance of the production of isocitrate, so that the enzyme is primed for activity. Higher metal–citrate concentrations produce a strong inhibition (k_3^{-1}, 1.54 mM), and inhibition is modulated by the binding sites above 3 mM (k_2^{-1}, 3.83

m*M*). Thus, soluble $NADP^+$: IDH can be both positively and negatively controlled by the metabolite of the first step in the Krebs cycle, citrate synthesis, which occurs within the mitochondria (Greville, 1969; Farrell *et al.*, 1987). The activation reaction observed for bovine mammary gland apparently could also occur in bovine liver and heart since both display hysteretic behavior; it may be a common regulatory mechanism for all animal $NADP^+$: IDH. Since it was recently shown by Gabriel and Plaut (1984) that metal–citrate may control NAD^+ : IDH as well, it could thus be speculated that metal–citrate plays a more important role than previously expected in Kreb's cycle metabolism.

VI. DIFFUSION PROCESSES

A. RIPENING OF CHEDDAR CHEESE WITH TIME

1. Overview

This section addresses the ripening of Cheddar cheese by initially examining electrophoretic and densitometric data of Cheddar cheese at selected ages while stored under commercial conditions. Information on the degradation of caseins in the Cheddar during the storage time was gathered. Subjective analyses of the changes in protein concentrations with time suggested that a link with the thermodynamic property of diffusion might be the controlling factor. To achieve proteolytic cleaveage, the enzymes chymosin and plasmin must, with time, make their way (diffuse) through the cheese matrix and cause the observed changes.

2. Materials and Methods

a. Acquisition, Identification, and Preparation of Cheese Samples. Two and five 40-lb blocks of Cheddar cheese and stirred curd cheese, respectively, were received from a local commercial dairy. These cheeses were manufactured according to government specifications. The dimensions of the bottom layer were the same as those of the top layer. Each block was cut into smaller subblocks, 115 mm long, 115 mm wide, and either 51 mm or 13 mm thick. Several subblocks were used for immediate sampling while the others were stored for the ripening process. The number of weeks in cooler storage ranged between 3 and 52 weeks.

After a determined time of cheese ripening, a sample subblock was

removed from cooler storage. A cylinder, 100 mm in diameter and 50 mm thick, was cut out with a cork borer from the center of a subblock and used for analysis.

b. Extraction of Proteins from Cheeses. Approximately 2 g of cheese was solubilized in 5 ml of protein solvent (0.166 *M* Tris/1 m*M* EDTA, pH 8.0) by homogenization with a Polytron ST-20. Five milliliters of 7% SDS (w/v) was added and the sample was gently homogenized by hand to minimize foaming. For protein reduction, 2 ml of 10 m*M* dithiothreitol was added to the homogenized sample, which was then stirred for 15 min, and centrifuged for 1 hr at 40,000 *g* and 5°C. Three fractions were obtained: a lipid layer, supernatant, and a pellet. The chilled lipid plugs were carefully removed with a spatula and the clear orange–yellow supernatant was decanted through wiping tissue paper to entrap pieces of lipid plug. The lipid plugs and the pellets were washed with the same solvents (for the pellet only, the volume was reduced 1/10), homogenized, and centrifuged in order to obtain additional supernatants from both fractions. All three supernatants from the lipid layer (fs), original supernatant (cs), and from the pellet (ps) were lyophilized. The washed pellet (pp) was resuspended by homogenization in a minimum amount of deionized water before lyophilization.

c. Polyacrylamide Gel Electrophoresis. Proteins derived from the fractions of cheese were examined by polyacrylamide gel electrophoresis (PAGE) by the discontinuous system described by Laemmli (1970), as modified for an E-C Vertical Slab Gel Apparatus by Basch *et al.* (1985). The stacking and separating gels were 4 and 15% acrylamide (% T), respectively, cross-linked with bisacrylamide (2.67% C). The gels were run for 13 hr and stained for protein with Coomassie blue R250. Quantitative analyses of electrophoretic separations were accomplished by scanning the gels at 550 nm in a Gelman Model 18 automatic computing densitometer. Total milk protein concentrates (TMP) was used as a standard for every gel.

Graphical analysis of the protein composition data was carried out on an IBM-XT computer using the Lotus 1-2-3 program.

d. Theory. Preliminary analysis of the disappearance of total casein with time showed good correspondence with first-order decay. However, inspection of the changes of individual components with time showed more complex patterns. In the conversion to the log form some of these inflections are suppressed. To analyze these time-dependent changes more accurately by nonlinear regression, the following theory was developed.

It was first assumed that decreases in individual components (α_{s1}-, α_{s2}-, β-, etc.) are due to proteolytic cleavages; this of course is substantiated by the data of Fox (1981) and others. Furthermore, these changes could be due to the time-dependent action of different enzymes, e.g., chymosin (rennin), plasmin, and acid proteases. Thus, for such consecutive events the change in content of a given component would be

$$\begin{array}{ccccc} \underset{(C_0)}{P_0} + nE_1 & \xrightarrow{k_1} & \underset{(C_1)}{P_1} + mE_2 & \xrightarrow{k_2} & \underset{(C_1 - C_2)}{P_2} \\ & & + & & + \\ & & qE_3 & & qE_3 \\ & & \Big\vert & & \Big\vert \\ & & \Big\vert\, k_3 & & \Big\vert\, k_3 \\ & & \downarrow & & \downarrow \\ & & \underset{\text{(Not observed)}}{P_4} & & \underset{(C_3)}{P_3} \end{array} \qquad (31)$$

Here P_1 represents various possible reactions undergone by a casein component P_0. The quantities in parenthesis represent the concentration of these components, E_i represent different proteolytic enzymes responsible for observable changes in molecular weight such that the SDS gel mobility of the component is changed, and k_i are the rate for the conversion carried out by enzyme i. In all of these experiments, the cheese blocks are considered to be homogeneous and representative due to the sampling as described above. Since the reaction is occurring in a solid-state matrix the actual change in C_0 will depend not only on the actual catalytic rate constant, k_{cat}, but also on the diffusion coefficient of the enzyme in the matrix. Although such relationships are complex, data relating changes in C_0 with time can be thought of as linked thermodynamically through diffusion, so that the equations developed by Wyman (1964) could be tested here. Thus, the apparent concentration of a casein component at any time can be given as

$$C_{app} = C_0 f(P_0) + C_1 f(P_1) + (C_1 - C_2) f(P_2) + C_3 f(P_1) \qquad (32)$$

where f represents a "collisional binding function" for the enzyme with the component fixed in the matrix and the following relationship for reaction of enzyme with protein can be empirically derived from Wyman's (1964) binding isotherms as previously shown (Farrell and Kumosinski, 1988):

$$C_{app} = \frac{C_0 P_0}{P_0 + P_0 E_1^n} + \frac{C_1 P_0 E_1^n}{P_0 + P_0 E_1^n} \qquad (33)$$

(Sentenac and Grignon, 1981). These ionic properties may significantly modify the activity of certain cell wall-bound enzymes.

It was reported that cell wall-bound acid phosphatase, but not the solubilized enzyme, is activated by increasing the ionic strength of the reaction mixture (Noat *et al.*, 1980). The apparent activation may be attributed to a decrease of the Donnan potential which can inhibit the movement of negatively charged substrate to the structure of cell walls. This explanation was later supported by the Ca^{2+} binding experiment at low ionic strength (Crasiner *et al.*, 1985). The cell wall acid phosphatase, like other phosphatases, may be important in hydrolyzing and solubilizing organic soil phosphate-containing macromolecules independently of soil microbial activity (Chang and Bandurski, 1964). Wall-bound acid phosphatases of different plant sources have been isolated (Crasiner *et al.*, 1980; Sugawara *et al.*, 1981). The minimum MW of cell wall acid phosphatase is ~100,000 (Crasiner *et al.*, 1985). However, detailed characterization of these isolated enzymes has still to be carried out.

Since little information is available on the effects of metal ion binding on the cell wall-bound acid phosphatase activity under the condition of a minimum Donnan potential, the influence of different multivalent cations on both bound and salt-solubilized acid phosphatase activity associated with the primary cell walls of potato tubers and corn roots was investigated. The results were analyzed in terms of function-linked binding equilibria and are discussed below.

2. *Experimental Procedures*

a. Isolation of Plant Cell Walls. Corn seeds (*Zea mays* FBR 73, Illinois Foundation Seeds) were germinated on filter paper saturated with 0.1 m*M* $CaCl_2$ in the dark at 28°C for 3 days as previously described (Tu and Brouillette, 1987). About 16 to 20 g fresh weight of cortex tissue stripped from stele of the primary roots was frozen with liquid nitrogen and pulverized with a mortar and pestle. The pulverized cortex was suspended in 500 ml of isolation medium containing 0.1 *M* [4-(2-hydroxyethyl)-1-piperazine ethanesulfonic acid)]–(4-morpholinoethanesulfonic acid) (HEPES-MES), pH 7.8, 0.3 *M* sucrose, 5 m*M* 2-mercaptoethanol, 2 m*M* $Na_2S_2O_5$, and 5 m*M* sodium ethylenediaminetetraacetate (EDTA). The suspension was placed in a Parr Bomb under nitrogen pressure (1500 psi) for 10 min at 4°C before extrusion to atmospheric pressure. The cell wall material was twice washed with cold deionized water and trapped on a cheesecloth sieve. The cell walls were then suspended in 200 ml of fresh homogenization solution and sonicated with a Heat System 225 sonicator

at 4°C with 50% pulsed cycle at power setting 7 for 7 min. After this treatment, the cell walls were washed extensively with a cold, aqueous solution of 1 m*M* 2-mercaptoethanol. For potato tuber cell wall preparation, tubers were peeled and parenchyma tissue was processed as described previously (Noat *et al.*, 1980). The homogenized tissue was then subjected to Parr bomb treatment and other further purification procedures identical to those described for corn roots. Based on electron microscopic observation and marker enzyme analysis, the cell walls obtained were free from cytoplasmic contamination (Noat *et al.*, 1980).

b. Salt Extraction of Cell Wall Acid Phosphatase Activity. The acid phosphatase activity of both corn cell walls (CCW) and potato cell walls (PCW) was also partially solubilized by salt extraction method as described by Sugawara *et al.* (1981) for potato tuber cell walls and by Crasiner and Giordani (1985) for sycamore cell walls. PCW and CCW obtained from 20 g of tissues were incubated in 100 ml of 1.5 *M* NaCl solution containing 1 m*M* 2-mercaptoethanol for 16 hr at 4°C. The volumes of the protein solutions were reduced to ~8 ml by the use of an Amicon ultrafiltration cell (cut-off MW ~10,000). The concentrated protein solutions were then dialyzed against ice-cold H_2O (36 hr) to remove residual 2-mercaptoethanol.

c. EDTA Treatment of Isolated Cell Walls. Cell walls isolated from corn roots and potato tubers were suspended in 100 ml of a solution containing 50 m*M* EDTA, pH 7.5, and were constantly stirred for 90 min at 4°C. After this treatment, the cell walls were repeatedly washed with cold deionized water (resistivity > 10 mΩ) by suspension and filtration. The treated cell walls were finally resuspended in 50 m*M* sodium acetate, pH 4.2. This procedure effectively removed most of the divalent cations bound to CCW. For example, the calcium contents of CCW used in this study were typically 0.134% (33.5 nmol Ca^{2+}/mg cell walls) and 0.019% (4.75 nmol Ca^{2+}/mg cell walls) by weight before and after the EDTA treatment, respectively. The PCW contained only small amounts of Ca^{2+} (0.020% by weight, 5.0 nmol/mg cell walls), and further EDTA treatment did not significantly alter this Ca^{2+} content. For calcium content determination, cell walls (~20 mg) were first dried in a crucible and then completely oxidized by flame. After dissolving the residue in the crucible with 5 ml of deionized water, the calcium concentration was determined with a radiometer Model F2002 calcium-ion electrode. We observed that the cell wall samples developed a deep yellow color in alkaline medium. To prevent possible permanent changes of the sample, pH 7.5 was chosen as a compromise for EDTA treatment.

d. Measurement of Acid Phosphatase Activity. The acid phosphatase activity of cell walls was measured by hydrolysis of *p*-nitrophenyl phosphate (PNP-P). An appropriate amount (~0.1 mg) of cell walls was suspended in 1 ml of a solution containing 50 m*M* sodium acetate, pH 4.2, and various concentrations of sulfates (Cu^{2+}, Hg^{2+}, Mg^{2+}, Al^{3+}) or chlorides (Zn^{2+}, Mn^{2+}, Ba^{2+}, Cd^{2+}, Ca^{2+}, Pb^{2+}) of different di- or trivalent cations. After an incubation for 10 min at 22°C, PNP-P (4 m*M*, unless indicated otherwise) was added to start the reaction. After 10 min, the reaction was stopped by the addition of 1 ml of 0.1 *M* Na_2CO_3. This addition changed the pH of the solution from 4.2 to higher than 10. The amount of *p*-nitrophenol produced was determined by its absorbance at 405 nm (extinction coefficient ε at 405 nm = 8.71 mM^{-1} cm^{-1}). The hydrolysis rate was linear within 10 min under the employed conditions. Furthermore, the nonenzymatic hydrolysis and the enzymatic hydrolysis in basic medium (adding Na_2CO_3 prior to PNP-P) over the period of 10 min was negligible. The solubilized acid phosphatase activity was determined in a similar manner.

e. Calculation of Function-Linked Binding. The theoretical details of employed function-linked binding analysis are discussed in Section V,A,3,d of this report. For example, in the computation of values of the parameters in the equation

$$A = \frac{A_1}{1 + K_a[\mathrm{M}]^n} + \frac{CA_1K_a[\mathrm{M}]^n}{1 + K_a[\mathrm{M}]^n} \tag{22}$$

n was first assigned an integral of 1. From input data of A, A_1, C, and [M], the value of K_a was estimated by a Gauss–Newton nonlinear regression program developed in our Research Center. In the regression process, the K_a value was varied until a minimum of an overall root-mean-square deviation between observed and calculated activity was reached. The value of *n* was then increased by 1 and the nonlinear regression repeated. The *n* value chosen to describe the function-linked binding was the one which gave the lowest root-mean-square deviation for the fit and minimum error in K_a.

3. *Analysis of Data*

The activity of plant cell wall acid phosphatase has been shown to be modulated by the binding of Ca^{2+} and the ionic strength of the bulk solution (Crasiner *et al.*, 1985; Noat *et al.*, 1980). Since cell walls are known to

TABLE XV

EFFECT OF MULTIVALENT CATIONS ON CELL WALL-BOUND ACID PHOSPHATASE ACTIVITY[a]

Cation[b] (5 m*M*)	Corn root cell wall		Potato tuber cell wall	
	Activity (μmol P_i/mg hr)	Relative activity	Activity (μmol P_i/mg hr)	Relative activity
None	0.217	100.0	0.054	100.0
Cu^{2+}	0.225	103.3	0.256	475.1
Mg^{2+}	0.206	94.7	0.222	411.0
Zn^{2+}	0.220	101.3	0.190	351.6
Mn^{2+}	0.209	96.0	0.148	274.4
Ba^{2+}	0.216	99.3	0.075	139.7
Cd^{2+}	0.215	98.7	0.065	119.9
Ca^{2+}	0.213	98.0	0.062	114.8
Pb^{2+}	0.222	102.0	0.055	102.0
Al^{3+}	0.099	45.4	0.025	46.9
Hg^{2+}	0.023	10.7	0.000	0.0

[a] The acid phosphatase activity of EDTA-treated CCW and PCW was determined as described in Section V.A.2 and expressed as micromoles P_i released per milligram of dry cell walls per hour. The values shown represent an average of determinations with an error as ±10%.

[b] In addition to 50 m*M* sodium acetate, salts of indicated cations were also added at a concentration of 5 m*M*.

contain a high percentage of negatively charged residues, the observed modulation is attributable to an electrostatic interaction between cell walls and the negatively charged enzyme substrate (PNP-P). Whether the effect of Ca^{2+} is unique or not has not been systematically investigated. In order to gain certain insights into this question, the effects of multivalent cations such as Ca^{2+} which may show comparable interaction with the immobilized negative charges of cell walls were determined on PCW-bound and CCW-bound acid phosphatases.

As shown in Table XV under the condition of nearly constant ionic strength, the addition of various cations produced different effects on bound acid phosphatase activity. In the case of CCW-bound acid phosphatase, with the exception of Al^{3+} or Hg^{2+}, all other tested cations including Ca^{2+} appear to have negligible effect. In contrast, the PCW-bound acid phosphatase was strongly stimulated (>100% increase in activity) by the presence of 5 m*M* of Cu^{2+}, Mg^{2+}, Zn^{2+}, and Mn^{2+}. The rest of the tested cations (Ba^{2+}, Cd^{2+}, Ca^{2+}, Pb^{2+}) showed weak or no stimulatory effects to PCW acid phosphatase. For both PCW and CCW, the bound enzyme was inhibited by Al^{3+} and Hg^{2+}.

a. Concentration-Dependent Multivalent Cation Effects. The results (Table XV) clearly demonstrate that, depending on the source of cell walls, the tested cations may be either stimulatory, inhibitory, or have no effect on acid phosphatase activity. The electrostatic interaction model which emphasizes the effect of increasing the concentration of PNP-P near the catalytic site of the enzyme by neutralization of cell wall negative charges with cation binding has been suggested as the origin of Ca^{2+} modulation of acid phosphatase in sycamore (Noat *et al.*, 1980) and cultured soybean cells (Crasiner *et al.*, 1985). It appears that this model may not be adequate to account for the observed effects mentioned in Table XV.

In order to gain further insight, a more detailed study of the cation concentration dependence of the enzyme activity was performed. Because of their physiological or toxicological importance, we have chosen Mg^{2+}, Hg^{2+}, and Al^{3+} for the study. By keeping the substrate concentration at a constant level (4 m*M*), the effect of increasing cation concentration on the bound acid phosphatases was determined. The results are summarized in Figs. 17 and 18. It should be mentioned that the results shown are not due to the variation of ionic strength of the solution. The addition of salts of multivalent cations changed at most the ionic strength of the solution from 0.03 (50 m*M* sodium acetate at pH 4.2) to 0.045 [50 m*M* sodium acetate + 2 m*M* $Al_2(SO_4)_3$]. The bound acid phosphatase activity of both PCW and CCW observed in 50 m*M* sodium acetate ($I = 0.03$) is essentially the same as that measured in 50 m*M* sodium acetate + 25 m*M* KCl ($I = 0.055$). It appears that the effects of Donnan potential generated by the polyanionic PCW and CCW may be sufficiently minimized by 50 m*M* sodium acetate at pH 4.2.

The data in Fig. 17 indicate that the bound acid phosphatase of PCW reaches a 50% maximum stimulation in the presence of 0.3 m*M* Mg^{2+}. The PCW-bound acid phosphatase activity is first stimulated and then inhibited by Hg^{2+} or Al^{3+}. However, the stimulation caused by Hg^{2+} or Al^{3+} at low concentration levels is not observed for CCW-bound acid phosphatase (Fig. 18). These results suggest that there are two, rather than one, types of function-linked binding processes for Hg^{2+} and Al^{3+} in PCW.

b. Combined Effects of Multivalent Cations. When the bound acid phosphatase activity was determined in the presence of two different multivalent cations, the combined effects could be determined. As shown in Table XVI, we observed that the inhibitory efficiency of Hg^{2+} or Al^{3+} to the bound acid phosphatases was not significantly affected by the presence of Mg^{2+}. On the other hand, the presence of Ca^{2+} substantially decreased the inhibitory power of Hg^{2+} and Al^{3+}. Figure 19 clearly shows that the inhibition efficiency of $Hg^{2+}$and Al^{3+} decreases as the concentra-

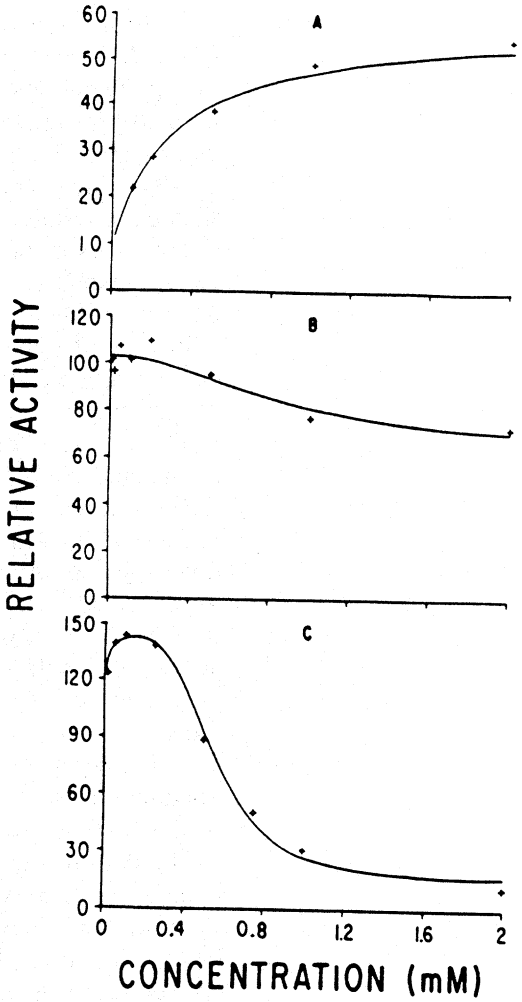

FIG. 17. Effects of multivalent cations on the acid phosphatase activity of PCW. The enzyme activity was measured as described in Section V,A,2,d with the addition of various concentrations of indicated cations: (A) Mg, (B) Al, (C) Hg. The acid phosphatase activity obtained, in the absence of added cations, was assigned as 10 in A and as 100 in B and C. The solid lines represent the best fit obtained by function-linked binding analysis.

tion of Ca^{2+} increases. In terms of enzyme kinetics, the presence of the two different cations (Mg^{2+} + Ca^{2+}, Mg^{2+} + Hg^{2+}, Hg^{2+} + Ca^{2+}) did not alter the linear response ($1/V$ versus $1/S$) of CCW-bound acid phosphatase. However, for PCW-bound acid phosphatase, the linear response obtained

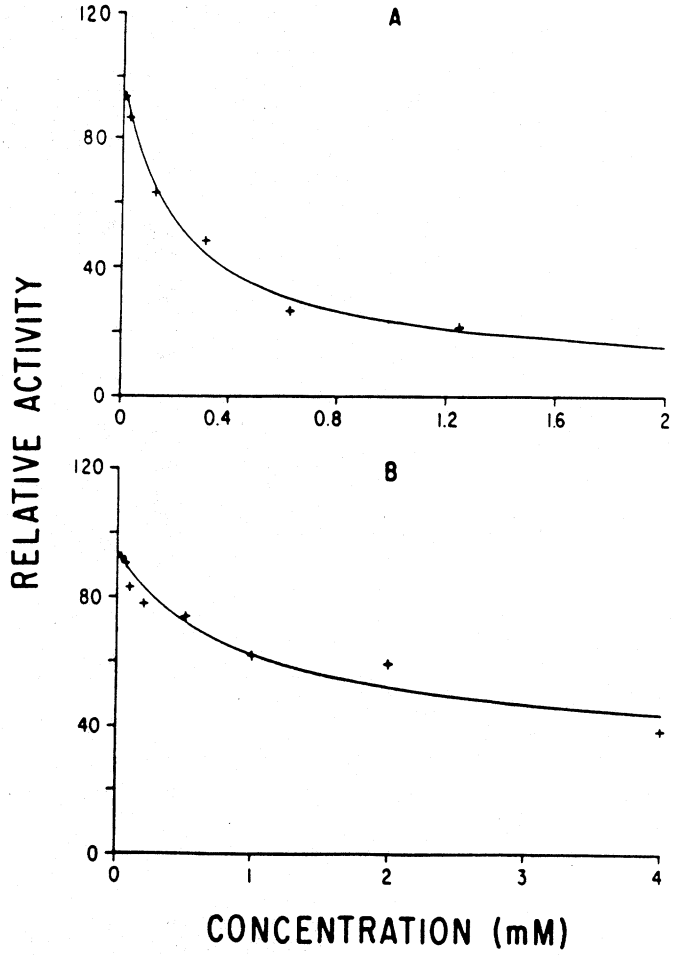

FIG. 18. Effect of multivalent cations on the acid phosphatase activity of CCW. The enzyme activity, in the presence of various concentrations of (A) Hg and (B) Al, was measured as described in Section V,A,2,d. The acid phosphatases activity (basal) obtained in the absence of added cations was assigned as 100. The addition of $MgSO_4$ up to 5 m*M* did not cause any significant change in the basal activity. The solid lines represent the best fits obtained by function-linked binding analysis.

in the presence of Mg^{2+} (Fig. 19B), was changed to a negative-cooperativity pattern by the addition of Hg^{2+} but not Ca^{2+}.

These results seem to suggest several possibilities (Bieleski, 1974): Mg^{2+} and Ca^{2+} probably do not share the same binding site(s) (Bush and McColl, 1987), Ca^{2+} is likely to compete with Hg^{2+} and/or Al^{3+} for some common

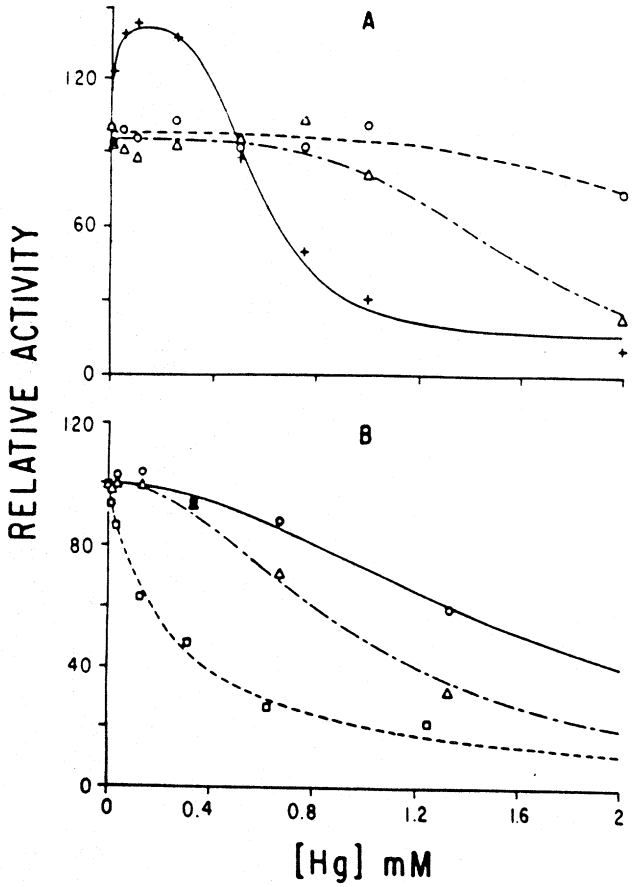

FIG. 19. Effects of Ca^{2+} on Hg^{2+} inhibition. The acid phosphatase activity of (A) PCW and (B) CCW was measured in the presence of various amounts of Hg^{2+} but keeping Ca^{2+} concentration at indicated levels: (A) ○, 1.25 m*M*; △, 0.0 m*M*; +, 0.00 m*M* Ca. (B) ○, 1.33 m*M*; △, 0.67 m*M*; □, 0.00 m*M* Ca. The activity obtained in the absence of Hg^{2+} was assigned as 100, and was not affected by the concentration of Ca^{2+}. The best fit lines, based on function-linked binding analysis, are also shown.

binding site(s) (Chang and Bandurski, 1964), and only some of the Hg^{2+} and/or Al^{3+} binding site(s) may be common for Mg^{2+} or, alternatively, Mg^{2+} does not share any site(s) with Hg^{2+} but the effect of Hg^{2+} binding overrides Mg^{2+} stimulation. The exact origin of observed combined effects remains to be established.

To express these metal ion-binding effects quantitatively, the simple Michaelis–Menten kinetic analysis would be of limited value. For exam-

TABLE XVI

COMBINED EFFECTS OF METAL IONS ON BOUND ACID PHOSPHATASE ACTIVITY

Experiment	Acid phosphatase activity[a] (%)
Corn root cell wall	
Control (no cations)[b]	100
5 mM Hg^{2+} + 5 m*M* Mg^{2+}	14
5 m*M* Hg^{2+} + 5 m*M* Ca^{2+}	35
5 m*M* Hg^{2+}	11
5 m*M* Al^{3+} + 5 m*M* Mg^{2+}	37
5 m*M* Al^{3+} + 5 m*M* Ca^{2+}	48
5 m*M* Al^{3+}	37
Potato tuber cell wall	
Control (no cations)[b]	100
2 m*M* Hg^{2+} + 2 m*M* Mg^{2+}	8
1.25 m*M* Hg^{2+} + 1.25 m*M* Ca^{2+}	95

[a] The values represent an average of three determinations with ±5% error.

[b] No di- or trivalent cations were added to the basic assaying solutions.

ple, in order to obtain the inhibition constant K_i of Hg^{2+} for CCW acid phosphatase, the linear transformation of the conventional enzyme kinetic method requires substantially more experimental information for a reasonable estimation. However, this information may be obtained by the use of the thermodynamic linkage concept (Sentenac and Grignon, 1981; Shone, 1966) in combination with nonlinear Gauss–Newton data analysis of the experimental results.

c. Effects of Multivalent Cations on Solubilized Acid Phosphatase Activity. The acid phosphatase activity associated with plant cell walls may be partially solubilized by salt treatment (Crasiner and Giordani, 1985; Nagahashi and Seibles, 1986; Sugawara *et al.*, 1981). When CCW was treated with 1.5 *M* NaCl, approximately 15% of the total acid phosphatase activity was released to the solution. On the other hand, similar treatment to PCW released ~50% of the acid phosphatase activity. The sensitivity of solubilized acid phosphatase activity to the presence of multivalent cations was tested and the results are summarized in Table XV. For convenience, we defined the solubilized activity obtained from CCW and PCW as C-APase and P-APase, respectively. For C-APase, the presence of cations yielded the similar effects observed for bound acid phosphatase of CCW (see Tables XV and XVI). However, unlike the bound acid phosphatase of CCW, Ca^{2+} failed to relieve the inhibitory effect of either

Hg^{2+} or Al^{3+} on the solubilized enzyme activity. The effects of the cations on P-APase activity, as shown in Table XVI, are quite different from these of bound acid phosphatase of PCW. A comparison with the data described in Tables XV and XVI indicated that none of the tested cations could stimulate the activity of P-APase. Furthermore, the presence of Ca^{2+} provided no protection against the inhibition caused by Hg^{2+} and Al^{3+}. These results strongly suggest that the structures of CCW and PCW can regulate the responses of bound acid phosphatases to the presence of multivalent cations. The specific activities of the bound acid phosphatases of PCW and CCW, when expressed in terms of protein content, as listed in Tables XV and XVI, would be in the same general ranges of solubilized enzymes since the protein accounts for about 10% of the dry weight of plant cell walls (O'Neill and Roberts, 1981).

d. Function-Linked Multivalent Cation Binding. To express the effects of metal ion binding to bound acid phosphatase quantitatively, the simple Michaelis–Menten kinetic analysis would be of limited value. For example, in order to obtain the inhibition constant K_i of Hg^{2+} for CCW-bound acid phosphatase, the linear transformation of the conventional enzyme kinetic method requires substantially more experimental information for a reasonable estimation. However, this information may be obtained by the use of the thermodynamic linkage concept (Wyman, 1964) in combination with nonlinear Gauss–Newton data analysis of the experimental results. We assume that the observed functional change in the acid phosphatase activity is due to a certain rather unique binding which may constitute only part of the total binding of tested cations to the components of cell walls. In order to simplify the analysis, we further assume that the molecules of acid phosphatase are uniformly distributed among many equivalent subdomains in the structure of cell walls. Certain binding of n, and only n, metal ions to the subdomain (either to the enzyme directly or to its immediate environment, or both) will cause a concentration-dependent change in the activity of the enzyme.

For the simplest case, consider the following binding equilibrium between the subdomain (D) containing the enzyme and metal ions (M):

$$D + nM \rightleftharpoons DM_n \qquad K_a = [DM_n]/[D][M]^n \tag{23}$$

in which DM_n and D represent the domains with and without functionally effective (stimulation or inhibition) metal ion binding, respectively, and K_a is the association equilibrium constant. By keeping the substrate concentration (4 m*M* PNP-P) in large excess over the K_M values, i.e., K_M =

$1/K_a$, the observed apparent enzyme activity, A, in the presence of tested cations, as determined by the hydrolysis of PNP-P, is then

$$A = (A_1[D] + A_2[DM_n])/([D] + [DM_n]) \tag{24}$$

in which A_1 and A_2 are the activities of D and DM_n, respectively. A_2 may be either greater or smaller than A_1. Or

$$A_2 = CA_1 \tag{25}$$

C is greater than 1 for stimulation, or smaller than 1 for inhibition of the activity. The values of A_1 and C can be easily estimated from the data shown in Figs. 17 and 18. Equation (24) may be reduced to

$$A = \frac{A_1}{1 + K_a[M]^n} + \frac{CA_1K_a[M]^n}{1 + K_a[M]^n} \tag{26}$$

Plant cell walls contain relatively small amount of protein. It has been shown that proteins constitute about 10% of the total dry weight of cell walls (O'Neill and Roberts, 1981). The majority of cell wall protein is in the form of hydroxyproline-rich glycoproteins which are characteristic structural components of cell walls of higher plants (Bush and McColl, 1987). The acid phosphatase isolated from various cell wall preparations (Crasiner *et al.*, 1985; Sugawara *et al.*, 1981) has a MW of ~100,000. Thus, even if we assume all the protein in PCW and CCW is in the form of acid phosphatase, the maximum enzyme content would be 1.0 nmol/mg cell wall (dry weight). Since the maximum function-linked binding of tested cations as shown by Eq. (23) would be in the same order of magnitude as the enzyme content, the concentration term [M] in Eq. (26) may be approximated by the total concentration of M added. With the quantities A, A_1, C, and [M] known, the application of a nonlinear Gauss–Newton regression of the data shown in Fig. 17 is possible. The results of this analysis are summarized in Table XVII. In most cases, the best fits were obtained by the use of Eq. (26). However, for the function-linked Hg^{2+}-binding to PCW, this equation is obviously insufficient. The activity versus Hg^{2+} concentration dependence shown in Fig. 17 indicates that the binding of Hg^{2+} at low concentration levels stimulates the activity, and at higher concentrations of Hg^{2+}, inhibition becomes predominant. A simple model to account for this observation is to assume that there are two independent function-linked binding sites of Hg^{2+} which may occur in the subdomains of PCW. The binding involved may be represented as

TABLE XVII

FUNCTION-LINKED METAL ION-BINDING PARAMETERS[a]

Experiment	K^b (association)	n^b	±RMS[c] (%)	Effect
PCW and Mg	3.78 mM^{-1} ±18%	1	15	Stimulation
PCW and Al	1.40 mM^{-1} ±41%	2	4	Inhibition
PCW and Hg[d]	108.4 mM^{-1} ±58%	1	8	Stimulation
	1.38×10^4 mM^{-4} ±10%	4	3	Inhibition
PCW and Hg (0.6 mM Ca)	6.55×10^{-4} mM^{-4} ±8%	4	6	Inhibition
PCW and Hg (1.2 mM Ca)	1.60×10^{-7} mM^{-4} ±7%	4	4	Inhibition
CCW and Hg	4.82 mM^{-1} ±18%	1	2	Inhibition
CCW and Hg (0.7 mM Ca)	1.06 mM^{-2} ±5%	2	2	Inhibition
CCW and Hg (1.3 mM Ca)	0.13 mM^{-2} ±8%	2	3	Inhibition
CCW and Al (5.0 mM Mg)	1.08 mM^{-1} ±51%	1	4	Inhibition

[a] Function-linked metal ion binding was analyzed as described in text using data shown in Figs. 16 and 18.

[b] In the case of only one set of K and n, best fitting was obtained with Eq. (21).

[c] RMS refers to the overall deviation between observed and calculated values of A (activity).

[d] For the effect of Hg on PCW acid phosphatase activity, Eq. (27) was used.

$$\begin{aligned} D + nM &\rightleftharpoons M_nD && K_n \text{ (stimulation)} \\ D + mM &\rightleftharpoons DM_m && K_m \text{ (inhibition)} \\ M_nD + mM &\rightleftharpoons M_nDM_m && K_m \text{ (inhibition)} \\ DMm + nM &\rightleftharpoons M_nDM_n && K_n \text{ (inhibition)} \end{aligned}$$

The observed activity, A, can then be expressed as

$$A = \frac{A_1}{Z} + \frac{CA_1K_n[M]^n}{Z} + \frac{C'A_1(K_n[M]^n + K_nK_m[M]^{m+n})}{Z} \qquad (27)$$

where

$$Z = 1 + K_n[M]^n + K_m[M] + K_nK_m[M]^{m+n}$$

in which C and C' are greater and smaller than 1.0, respectively. While Eq. (27) appears to be complex, the actual data fitting turns out to be rather simple because the term of $[M]^{m+n}$ has a relatively negligible contribution. Using this model, the data were best fitted with $n = 1$ and $m = 4$. On the other hand, a sequential binding model which specifies the binding of n occurring before m did not provide a satisfactory fitting of the obtained

results. It should be mentioned that other possible models could not be excluded by this analysis. However, it is quite possible that the presence of calcium not only abolishes the stimulation of low level Hg^{2+} but also substantially decreases the inhibitory binding of Hg^{2+}. Presumably, Ca^{2+} can bind to the functional domain more easily than Hg^{2+}, or the acid phosphatase is more sensitive to Ca^{2+} binding.

B. BOVINE ISOCITRATE DEHYDROGENASE VARIATION WITH PRECURSOR

1. Overview

$NADP^+$-dependent isocitrate dehydrogenase [*threo*-D_S-isocitrate: $NADP^+$ oxidoreductase (decarboxylating) EC 1.1.1.42] can serve as source of NADPH for synthesis of metabolic end products in a variety of tissues (Colman, 1983; Greville, 1969); for example, in lactating ruminant mammary gland this enzyme may be a primary source of the NADPH required for fatty acid synthesis (Bauman and Davis, 1974). A survey of the distribution of Krebs cycle enzymes in mammary tissue showed that $NADP^+$: isocitrate dehydrogenase (IDH) is predominantly cytosolic (>90%) in nature, and that little or no NAD^+ : IDH activity is present (Farrell *et al.*, 1987). Since the latter enzyme is allosterically regulated by metabolites and is thought to control Krebs' cycle activity (Chen and Plaut, 1963; Gabriel and Plaut, 1984), the possible effects of metabolites on the kinetics of $NADP^+$: IDH could be studied. Effects of metal–citrate complexes on enzyme activity and activation were studied and analyzed using thermodynamic linkage to gain insight into possible mechanisms which may regulate this enzyme.

2. Experimental Procedures

All experiment procedures were described by Farrell (1980).

3. Data Analysis

Inhibition by Citrate. In the case of human heart $NADP^+$: IDH, a mitochondrial form of the enzyme, citrate has been shown to be a competitive inhibitor of DL-isocitrate (Seelig and Colman, 1978). As previously demonstrated (Farrell, 1980), metal–isocitrate is the true substrate and so metal–citrate could be the true inhibitor.

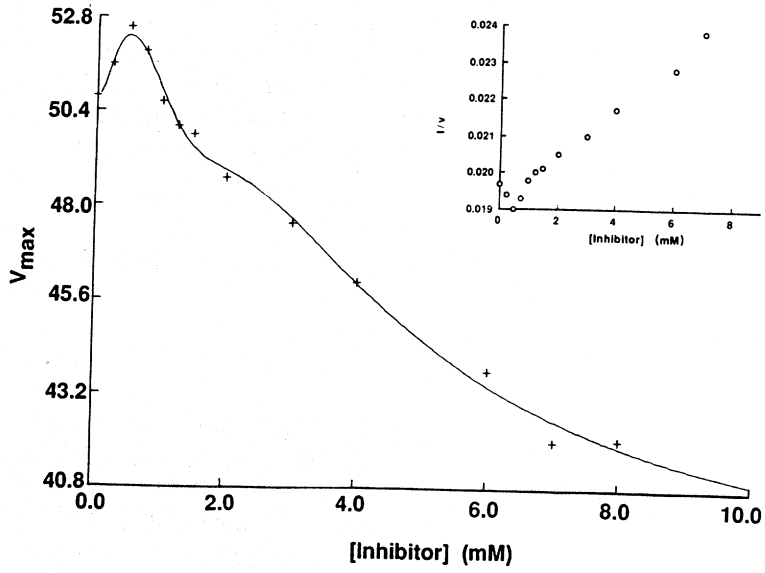

FIG. 20. Inset: Dixon plot of 1/velocity against millimolar concentration of Mn^{2+}–citrate. The main plot is of velocity at V_{max} conditions (μ mol/min/mg) against millimolar concentration of Mn^{2+}–citrate complex; the concentration of free Mn^{2+} was fixed at 80 μM and that of Mn^{2+}–isocitrate at 250 μM, variations of Mn^{2+}–citrate were then calculated. Data were fitted with Eq. (35) using the assumptions of thermodynamic linkage of velocity to binding of I (Mn^{2+}–citrate).

The traditional analysis of the Dixon plot ($1/v$ versus [I]) has the same shortcomings as pointed out by Cleland (1967) for double reciprocal analysis of v versus S; that is, such plots supress the sensitivity of the best data found at lowest [I]. By the use of nonlinear regression analysis, the data obtained can be directly fitted without the need for mathematical transformations or weighting factors. In addition, the data obtained at low inhibitor concentrations are not deemphasized. The Gauss–Newton procedure also provides a statistical evaluation of the constants and of the fit, which allows for comparison of various mathematical models (Meites, 1979). In an attempt to gain further insight into the meaning of this data, experiments were conducted at very low metal–citrate concentrations with free metal fixed at 80 μM and metal–isocitrate fixed at 250 μM (80 $\times$ K_m). The resulting plot (Fig. 20) shows the direct variance of v with [I]. Initial curvature upward is clearly seen followed by gradual decline with a shoulder between 2 and 4 mM. Assuming that changes in the observed velocity at constant enzyme, metal–substrate, and free metal concentrations are thermodynamically linked to concentration-dependent binding of

metal–citrate, [I], the data may then be analyzed by the linked-function theory of Wyman (1964) developed in our laboratory for study of metal ion-induced changes in protein solubilities (Farrell, 1988). Preliminary analysis with a variety of model isotherms suggested that the data contained three distinct regions of response to metal–citrate. Thus, it was assumed that the following equilibria exist in the steady-state experiments for the already activated enzyme:

$$\begin{array}{ccccc} \overset{(V_0)}{\mathrm{E}} + n\mathrm{I} & \overset{k_1}{\rightleftharpoons} & \overset{(V_1)}{\mathrm{EI}_n} + m\mathrm{I} & \overset{k_2}{\rightleftharpoons} & \overset{(V_2)}{\mathrm{EI}_m\mathrm{I}_n} \\ & & + & & + \\ & & q\mathrm{I} & & q\mathrm{I} \\ & & \Big\Vert\, k_3 & & \Big\Vert\, k_3 \\ & & \mathrm{EI}_n\mathrm{I}_q + m\mathrm{I} & \overset{k_2}{\rightleftharpoons} & \underset{(V_3)}{\mathrm{EI}_m\mathrm{I}_n\mathrm{I}_q} \end{array} \tag{28}$$

As noted above, preliminary analyses of Fig. 20 indicated three regions of response to metal–citrate. The simplest description of this observation is

$$V_{\mathrm{obs}} = V_0 f_{\mathrm{e}} + V_1(f_{\mathrm{EI}_n} - f_{\mathrm{EI}_n\mathrm{I}_m} - f_{\mathrm{EI}_n\mathrm{I}_m\mathrm{I}_q}) + V_2 f_{\mathrm{EI}_n\mathrm{I}_m} + V_3 f_{\mathrm{EI}_n\mathrm{I}_m\mathrm{I}_q} \tag{29}$$

where V_0 is the apparent $V_{\max}$ in the absence of concentration-dependent binding of an effector molecule (I) and V_1, V_2, and V_3 represent the velocity contributed by each state as modulated by the fraction of enzyme in each state and represented in stoichiometric Eq. (28). The analysis presupposes that $k_1 > k_2 \approx k_3$, and that k_1, k_2, and k_3 are independent sites. Other models were tested but the fits were poor and not justified statistically (Meites, 1979). Following the method of Wyman, thermodynamic linkage of the binding of I to change in velocity can be derived using binding nomenclature as previously described (Farrell *et al.*, 1988). For data following the behavior seen in Fig. 20, the equations are

$$\begin{aligned} V_{\mathrm{obs}} = {} & \frac{V_0}{1 + k_1^n\mathrm{I}^n} + V_1\left[\frac{k_1^n\mathrm{I}^n}{1 + k_1^n\mathrm{I}^n}\right. \\ & \left. - \frac{k_2^m\mathrm{I}^m}{(1 + k_2^m\mathrm{I}^m)(1 + k_3^q\mathrm{I}^q} - \frac{k_2^m\mathrm{I}^m k_3^q\mathrm{I}^q}{(1 + k_2^m\mathrm{I}^m)(1 + k_3^q\mathrm{I}^q)}\right] \\ & + \frac{(V_2)k_2^m\mathrm{I}^m}{(1 + k_2^m\mathrm{I}^m)(1 + k_3^q\mathrm{I}^q)} + \frac{(V_3)K_2^m\mathrm{I}^m k_3^q\mathrm{I}^q}{(1 + k_2^m\mathrm{I}^m)(1 + k_3^q\mathrm{I}^q} \end{aligned} \tag{30}$$

Here the association constants (k_i) and the terms n, m, and q have the

TABLE XVIII

PARAMETERS OBTAINED FOR LINKED-FUNCTION ANALYSIS OF THE VARIATION OF V_{max} WITH METAL–CITRATE[a]

Term	Coefficient (integer)	k (M^{-1})	$K_D \pm SE$[b] (mM)	V_{THE}[c] (%)
k_1	2	3790	0.246 ± 0.113	110
k_2	2	260	3.83 ± 0.032	−108
k_3	4	650	1.54 ± 0.004	−25

[a] Average values and error of coefficients for two complete runs, each point in triplicate; total error of the fits averaged 1%. Data of Fig. 20 were fitted with Eq. (30).

[b] Calculated dissociation constant ($1/k$).

[c] V_{THE} represents the predicted theoretical effect on V_{max} produced by the binding of each class of metal–citrate sites.

meanings expressed in the stoichiometric Eq. (28). Since Michaelis–Menten conditions are employed, [I] is taken to be the total concentration of metal–citrate complex fixed at the beginning of the experiment. The data were fitted by nonlinear regression analysis using integer values for n, m, and q; Eq. (30) implies no site–site interaction. In each case, the iterative analysis was carried out until a minimum value for the root-mean-square was found. The data were tested by F test for improved fit at each change in the integer values. This best analysis, given in Table XVIII, permits quantitation of the data. It has the benefit of using the best data (low [I], high v) for statistical fitting and provides a point of departure for discussion of the results. The analysis yields numbers for k_is that, when viewed in terms of dissociation constants, can be related to physiological conditions (and possibly to enzyme structure through n, m, and q) and allows assessment of the relative contributions of V_is to V_{obs}. Finally, there is an indication that metal–citrate may play a dual role in modulation of the enzyme.

4. *Interpretation*

The detailed analysis of v versus [I] (Fig. 20), using the assumptions of thermodynamic linkage, shows that metal–citrate can indeed stimulate activity, with a K_D of 0.25 mM; the maximum stimulation would be to 54.6, or an 8% increase (Table XVIII). In contrast, strongly inhibitory sites with K_D = 3.83 mM dramatically decrease activity with a predicted total repression of activity. At intermediate concentrations metal–citrate

$$+ \frac{(C_1 - C_2)\mathrm{P}_1 E_2^m}{\mathrm{P}_1 + \mathrm{P}_1 E_2^m} + \frac{C_3 \mathrm{P}_1 E_2^m E_3^q}{\mathrm{P}_1 + \mathrm{P}_1 E_2^m + P_1 E_3^q + P_1 E_2^n E_3^z}$$

Cancellation and collection of terms yields:

$$C_{\text{app}} = \frac{C_0}{1 + E_1^n} + \frac{(C_1)E_1^n}{1 + E_1^n} + \frac{(C_1 - C_2)E_2^m}{1 + E_2^m} + \frac{(C_3)E_2^m E_3^q}{(1 + E_2^m)(1 + E_3^q)} \quad (34)$$

In such experiments E would represent a concentration term. Indeed, Fox (1981) has shown that added plasmin, for example, increases the rate of disappearance of β-casein. But, as noted above, diffusion through the matrix must occur first; in ordinary enzyme kinetics the latter is neglected, in this instance it cannot be. According to Bull (1943),

$$D = \frac{dQ}{A\, dt\, (dC/dx)} \quad (35)$$

where D is the diffusion constant and dQ is the quantity of material (enzyme) which diffuses across a plane surface A in time dt under a concentration gradient dC/dx. If we assume that at the time of cheese manufacture the residual chymosin, plasmin, or other enzymes are uniformly distributed throughout the block, then there may be no concentration gradient and dC/dx would be a constant.
Therefore

$$dC/dx = \text{constant} = g/Vl \quad (36)$$

where C is replaced by g (the grams of enzyme present in volume V), and x by length l (the length of the sample). So, combining Eqs. (35) and (36), we get

$$dQ = (g/Vl)AD\, dt \quad (37)$$

Thus Q, the amount of enzyme diffusing through the matrix toward a fixed substrate at any time t, can be given by

$$Q = E = (gAD/Vl)t \quad (38)$$

If we consider gAD/Vl as a lumped diffusion constant for a given block of cheese, then

$$E = k_{\text{diffusion}}t \tag{39}$$

So far, we have considered only physical diffusion, but the observed conversion will also include factors for the rate constant k_{kinetic} so, in reality,

$$E = (k_{\text{diffusion}} \times k_{\text{kinetic}})t \tag{40}$$

Therefore, in our analysis, k_1 or k_2 in Eq. (31) represents the quantity in parenthesis in Eq. (40). The final equation used to analyze the data is then found by substituting Eq. (40) into Eq. (34) and using k_i:

$$C_{\text{app}} = \frac{C_0}{1 + k_1^n t^n} + \frac{C_1 k_1^n t^n}{1 + k_1^n t^n} + \frac{(C_1 - C_2)k_2^m t^m}{1 + k_2^m t^m} + \frac{C_3 k_2^m t^m k_3^q t^q}{(1 + k_2^m t^m)(1 + k_3^q t^q)} \tag{41}$$

It should be stressed here that the latter expression is valid only for sequential binding (reaction), i.e., $k_1 > k_2 > k_3$ and where n sites react prior to the m sites. Also, for n or m values greater than 1, k_1, k_2, and k_3 represent an average value for each of the n, m, or q sites.

The time-dependent profiles were directly analyzed using a Gauss–Newton nonlinear regression analysis program developed at this laboratory by Dr. William Damert. All profiles were analyzed by fixing the values of n and m and calculating the best least-squares fit for the optimum evaluated k_1 and k_2 values. The n and m values were then fixed to new values and the whole procedure repeated. The n and m values which yielded the minimum root-mean-square and lowest error values for k_1 and k_2 were then reported (Farrell and Kumosinski, 1988).

e. Protein Analysis. Protein in the supernatants obtained by the fractionation of cheese was determined by the Coomassie blue assay (Basch *et al.*, 1985).

3. *Data Analysis and Interpretation*

a. Extraction and Sodium Dodecyl Sulfate Gel Electrophoresis. Previous investigators have applied both SDS–PAGE and two-dimensional electrophoresis to the study of soft cheese ripening (Trieu-Cuot *et al.*, 1982), while Fox (1981) has studied changes in Cheddar cheese during

development using alkaline-urea PAGE. In preliminary experiments, both fat pellicles and pellets were observed after homogenization of cheese in protein solvent (reducing agent added). Both of these fractions were reextracted to ensure more complete recovery of protein as described in Section VI,A,2. The three supernatants (cs, fs, and ps) and the final pellet (pp) samples were electrophoresed and the gels were scanned. In this way, it was possible to visualize all of the proteins present in cheese.

Typically, electrophoretic patterns of cheese could illustrate as many as 24 protein bands. Electrophoretic separation of a standard total milk protein concentrate contains lactoferrin (MW 86,000), bovine serum albumin (67,000), immunoglobulin, heavy chain (~55,000), α_{s2}-casein (25,200), α_{s1}-casein (23,600), β-casein (24,000), κ-casein (19,000), γ_1-casein (20,600), β-lactoglobulin (18,400), α-lactalbumin (14,200), γ_2-casein (11,800), and γ_3-casein (11,600) (Eigel *et al.*, 1984). The caseins exhibit abnormal behavior in the SDS–PAGE (Basch, 1981). It is known that plasmin, a protease in milk, cleaves α_{s2}-, α_{s1}-, and β-caseins into smaller components which migrate faster than the parent caseins in the SDS–PAGE system (Eigel *et al.*, 1984). In a mature cheese, or to a lesser extent in a younger cheese, proteolytic changes can be seen (Basch *et al.*, 1989); cleavage of β-casein leads to formation of γ_1-, γ_2-, and γ_3-caseins and also proteose-peptone components 5, 8-fast, and 8-slow, which are at the front. Rennin hydrolyzes κ-casein into *para*-κ-casein and the macropeptides; in addition, microbial proteases may cause other changes (Fox, 1981). Since all the bands were too numerous for preliminary significant analysis, it was decided that the proteins of the cheese be grouped initially on the basis of protein classes. A typical densitometric scan of the SDS–PAGE of a cheese sample is shown in Fig. 21. Each peak is identified as indicated in the figure. Other unidentified peaks are the result of breakdown of several larger proteins by enzymes. The integrator of the densitometer measures the area under the curve and the percent of each peak in the total 100% of all the peaks in the scan is computed. Peaks 1–6 include all the protein bands which migrate in the gel slower than α_{s2}-casein. α_{s2}-, α_{s1}-, and β-caseins comprise peaks 7–9. Peaks 10–12 contain γ_1-casein and other proteins which migrate ahead of β-casein. Peaks 13–15 include the proteins which migrate between γ_1-casein and *para*-κ-casein. Several bands of low intensity migrating slower than *para*-κ-casein (peak 19) are included in peaks 16–18. Peaks 20–24, which migrate faster than *para*-κ-casein, may include γ_2- and γ_3-caseins, fragmentary products of β-casein.

Comparisons of four fractions (cs, fs, ps, and pp) of young Cheddar cheese (9 weeks) and similar data from aged Cheddar cheese (52 weeks) showed there are few significant differences among the major proteins in the four fractions. The Coomassie blue dye binding assay showed that the

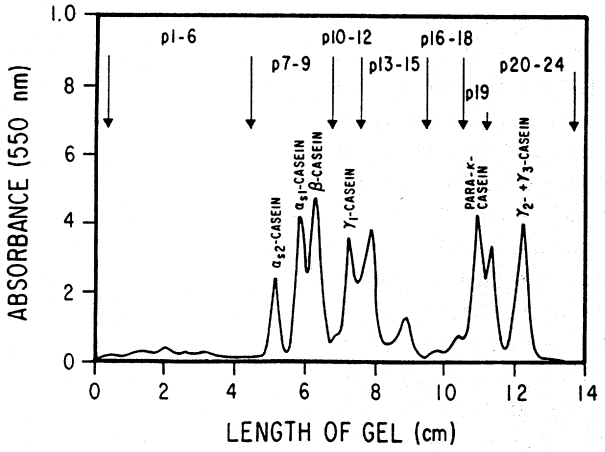

FIG. 21. Typical densitometric scan of the SDS–PAGE gel of stirred curd cheese. The peaks are identified; unidentified peaks are the result of breakdown of caseins by the enzymes.

cheese supernatants (cs) represent 89 ± 5% of the total extractable cheese protein. Therefore, during the rest of the study, the supernatant from the cheeses was used for data, graphical comparisons, and interpretations.

b. Summary of SDS–PAGE Analysis. Gel electrophoresis patterns of supernatants of traditional Cheddar cheese (PF) which had been ripened for 3, 9, 14, 20, 26, 39, and 52 weeks were examined (Basch *et al.*, 1989). Intact κ-casein is not observed in any of the cheese samples due to the addition of rennin along with the starter culture during its earliest stage of manufacture. It is likely that *para*-κ-casein is a normal constituent of cheese and not a product of storage since the amount of *para*-κ-casein detected is constant throughout the ripening ages of cheese as measured by the gel scans. This result agrees with Grappin *et al.* (1985), who reported that *para*-κ-casein, unlike other caseins from cheese, was not degraded during ripening. It is of interest that when the cheeses are young, the percent total casein (peaks 7–9) is high (~60%) and other protein groups are low. As the cheeses became older, the percent total casein decreases while other two groups (peaks 13–15 and 20–24) increase.

Of special note in the gel is the increase in number of protein bands and in their intensity in the regions between β-casein and *para*-κ-casein and that below *para*-κ-casein. These data indicate that, as the ripening age of cheese increases, there is breakdown of major caseins, i.e., β-casein into β_2- and β_3-caseins and also α_{s2}- and α_{s1}-caseins into large fragmentary proteins (Eigel *et al.*, 1984; Grappin *et al.*, 1985).

c. Effects of Ripening on SDS–PAGE Patterns. On first analysis, a plot of percent total protein versus ripening ages of traditional Cheddar cheese when data from before freezing ($n = 3$ for each point) appeared to show a gradual decrease in the percent of casein group (peaks 7–9). In contrast, plots of the degraded products (peaks 20–24) increase until about 39 weeks, then decline. The percentages of the rest of the protein groups, especially *para*-κ-casein (peak 19), were consistent over the time studied.

To estimate the rate of loss, a semilogarithmic plot of the disappearance curve of casein group (peaks 7–9) of Cheddar cheese before freezing was constructed and a linear regression performed. The correlation coefficient of the curve was 0.9323 with a confidence level of about 97%. Using the slope of the regression line, the decay constant λ was calculated and used for the half-life equation, $t_{1/2} = 0.693/\lambda$. It was that half-life, or time of half-disappearance, was 35.5 weeks for the casein groups.

d. Application of Nonlinear Regression Analysis. Since logarithmic forms of analysis can obscure subtle changes, it was decided to analyze the decay of the caseins directly using nonlinear regression analysis. Equations for this method have been presented in Section VI,A,2,d. Data for the disappearance of whole casein (Fig. 22A) and the appearance of γ_2- and γ_3-caseins (Fig. 22B) were analyzed by Eq. (41). From analysis of the whole-casein curve, four parameters are obtained: k_1, k_2, n, and m (results of all analyses are given in Table XIX). The parameters k_1 and k_2 represent the summed k of Eq. (40) and, while k_{kinetic} plays a role, $k_{\text{diffusion}}$ predominates. Hence, the bimodality of Fig. 22A argues for either two widely different enzymes with different diffusability or two very different enzyme concentrations, since $E(Q)$ of Eq. (38) contains the grams of enzyme present as well as the diffusion constant of the enzyme. Thus, for example, residual starter enzyme (chymosin) could be present at high initial concentrations and produce a rapid change (k_1 and n), while more dilute plasmin could produce the secondary effects (k_2 and m). In terms of cheese storage, it may be more effective to discuss these constants (k) in terms of their reciprocals, which can be thought of as the half-times for the transitions or the half-life of the casein components (see Table XIX). Whole casein decays in a bimodal form with inflections at 12 and 38 weeks, while γ_2- and γ_3-caseins appear with a half-time of 33 weeks. It thus appears that major changes in cheese composition occur early, with α_{s1}- (and possibly α_{s2}-) caseins decaying rapidly, followed by the breakdown of β-casein around 37 weeks.

In order to test this hypothesis, the whole casein group (peaks 7–9) was subdivided into α_{s1}-, α_{s2}-, and β-caseins and the gel data were replotted for disappearance of each casein. Data for changes in peaks 13–15 and

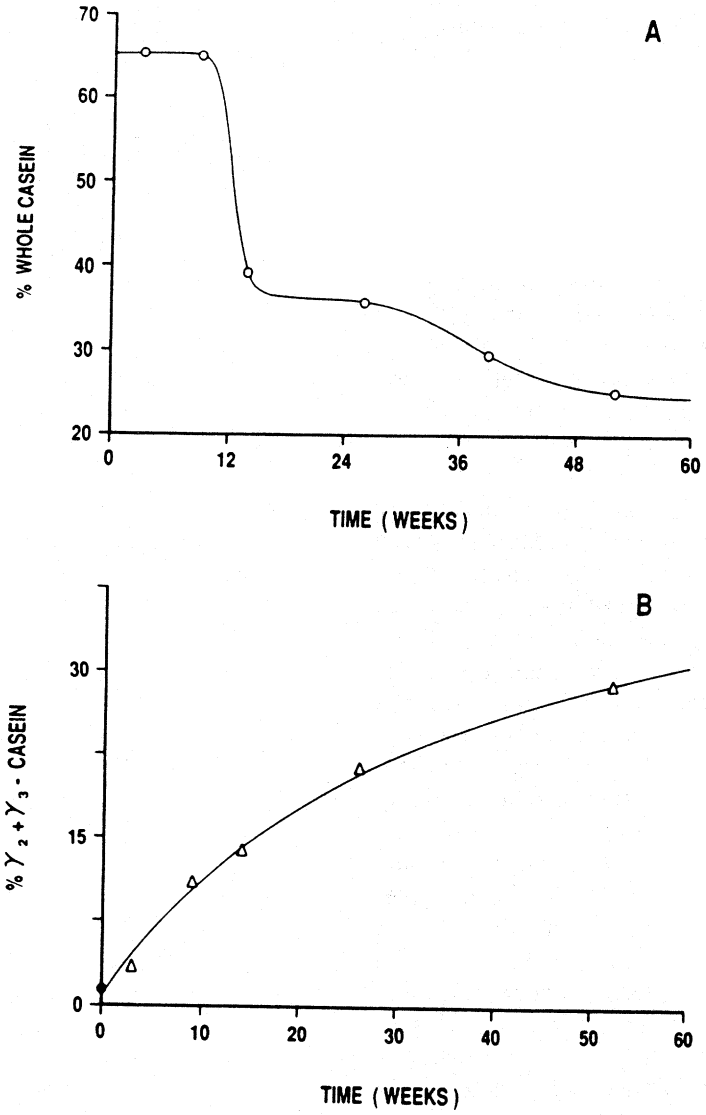

FIG. 22. Nonlinear regression plot of (A) the disappearance of whole casein (peaks 7–9) and (B) the appearance of degraded products (peaks 20–24 group, which contains γ_2- and γ_3-caseins) for Cheddar cheese. The filled circle (●) represents percent present in caseinate before cheesemaking. Data were analyzed by Eq. (41). Results are given in Table XIX.

TABLE XIX

NONLINEAR REGRESSION COEFFICIENTS FOR TIME-DEPENDENT CHANGES IN CASEIN COMPONENTS IN CHEDDAR CHEESE SUPERNATANT

Casein component	k subscript	k_{i-1} (weeks)	SE of k_i	Half-time in weeks $1/k_i$	Exponent	Nature of change
Casein peaks 7–9	k_1	0.0818	0.0002	12.2	16	Decrease
	k_2	0.0263	0.0002	38.0	8	Decrease
γ_2- + γ_3-	k_1	0.0270	0.0033	37.0	1	Increase
para-κ-	k_1	0.0140	0.0027	71.4	1	Decrease
α_{s2}-	k_1	0.0132	0.0032	75.2	1	Decrease
α_{s1}-	k_1	0.5124	0.0229	1.95	1	Decrease
Peaks 13–15	k_1	0.0613	0.0033	16.3	1	Increase
β-	k_1	0.0530	—	18.8	16	Increase
	k_2	0.0991	—	10.0	1	Decrease
	k_3	0.0265	—	37.7	12	Decrease
β- + β_0	k_1	0.0237	0.0033	36.6	8	Decrease

para-κ-casein were also plotted. In viewing the data for α_{s1}-casein (Fig. 23A) it became apparent that even at the earliest times (3 weeks) a substantial portion of this component, based on its normal relative distribution in milk (Davies and Law, 1983), was degraded. It was therefore decided to fix the zero time, y-axis, as the percent of the component present in acid caseins electrophoresed and scanned by the same method. The values for five acid caseinates, each scanned twice, were then used as the zero time data point for all the nonlinear regression analysis of casein component appearance or disappearance. The computer-fitted plots for these data are given in Figs. 23–25; results are in Table XIX.

Separation of the data showed interesting results. The most rapidly cleaved casein is α_{s1} which disappears with a half-life of 1.95 weeks based on extrapolation to α_{s1} in caseinate (Fig. 23A). The extrapolation to zero time may prejudice the data somewhat, but the implication is that this protein rapidly degrades (without extrapolation the half-life is still less than 8 weeks). It has long been suggested that curd formation may be related to α_{s1}-casein (Lawrence *et al.*, 1987). However, although α_{s1} is necessary for curd formation, its rapid degradation points to the fact that loss of structure may be necessary for proper cheese formation.

The larger proteolytic fragments (peaks 13–15) arise with a half-time of 16 weeks; the nature of these fragments is unknown but they may represent α_{s1} fragments (Fig. 23B).

Separation of the data produced a decay curve for α_{s2}-casein with a

TABLE XIX

NONLINEAR REGRESSION COEFFICIENTS FOR TIME-DEPENDENT CHANGES IN CASEIN COMPONENTS IN CHEDDAR CHEESE SUPERNATANT

Casein component	k subscript	k_{i-1} (weeks)	SE of k_i	Half-time in weeks $1/k_i$	Exponent	Nature of change
Casein peaks 7–9	k_1	0.0818	0.0002	12.2	16	Decrease
	k_2	0.0263	0.0002	38.0	8	Decrease
γ_2- + γ_3-	k_1	0.0270	0.0033	37.0	1	Increase
para-κ-	k_1	0.0140	0.0027	71.4	1	Decrease
α_{s2}-	k_1	0.0132	0.0032	75.2	1	Decrease
α_{s1}-	k_1	0.5124	0.0229	1.95	1	Decrease
Peaks 13–15	k_1	0.0613	0.0033	16.3	1	Increase
β-	k_1	0.0530	—	18.8	16	Increase
	k_2	0.0991	—	10.0	1	Decrease
	k_3	0.0265	—	37.7	12	Decrease
β- + β_0	k_1	0.0237	0.0033	36.6	8	Decrease

para-κ-casein were also plotted. In viewing the data for α_{s1}-casein (Fig. 23A) it became apparent that even at the earliest times (3 weeks) a substantial portion of this component, based on its normal relative distribution in milk (Davies and Law, 1983), was degraded. It was therefore decided to fix the zero time, y-axis, as the percent of the component present in acid caseins electrophoresed and scanned by the same method. The values for five acid caseinates, each scanned twice, were then used as the zero time data point for all the nonlinear regression analysis of casein component appearance or disappearance. The computer-fitted plots for these data are given in Figs. 23–25; results are in Table XIX.

Separation of the data showed interesting results. The most rapidly cleaved casein is α_{s1} which disappears with a half-life of 1.95 weeks based on extrapolation to α_{s1} in caseinate (Fig. 23A). The extrapolation to zero time may prejudice the data somewhat, but the implication is that this protein rapidly degrades (without extrapolation the half-life is still less than 8 weeks). It has long been suggested that curd formation may be related to α_{s1}-casein (Lawrence *et al.*, 1987). However, although α_{s1} is necessary for curd formation, its rapid degradation points to the fact that loss of structure may be necessary for proper cheese formation.

The larger proteolytic fragments (peaks 13–15) arise with a half-time of 16 weeks; the nature of these fragments is unknown but they may represent α_{s1} fragments (Fig. 23B).

Separation of the data produced a decay curve for α_{s2}-casein with a

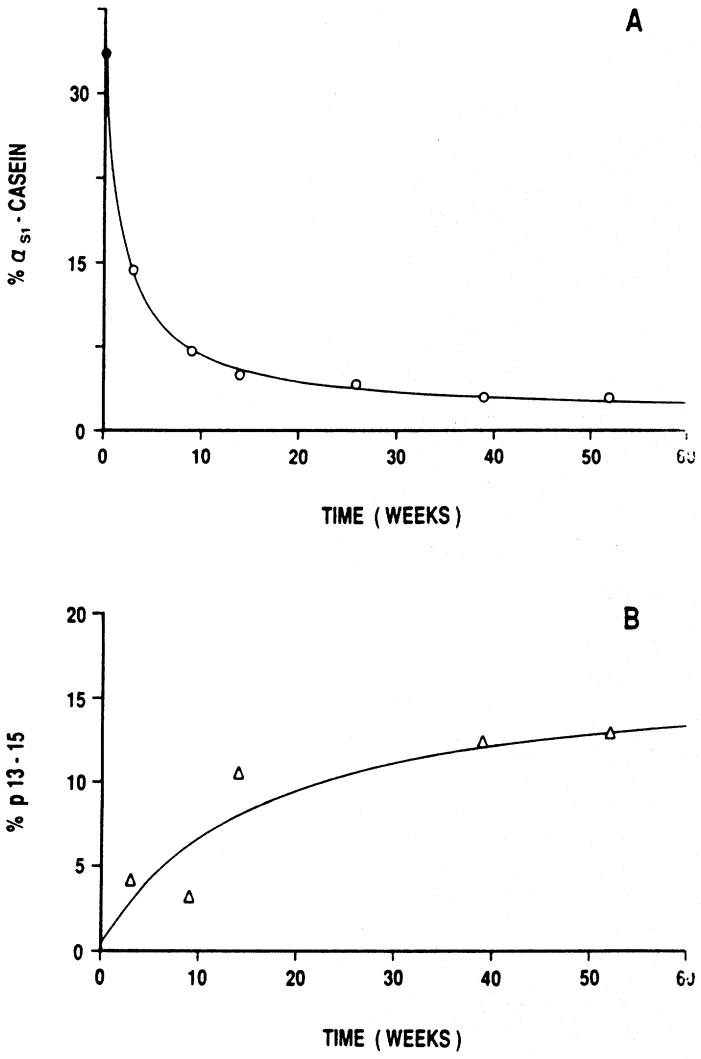

FIG. 23. Nonlinear regression plot of (A) the disappearance of α_{s1}-casein and (B) the appearance of degraded products (peaks 13–15) for Cheddar cheese. Filled circle represents percent present in caseinate before cheesemaking. Data were analyzed by Eq. (41). Results are given in Table XIX.

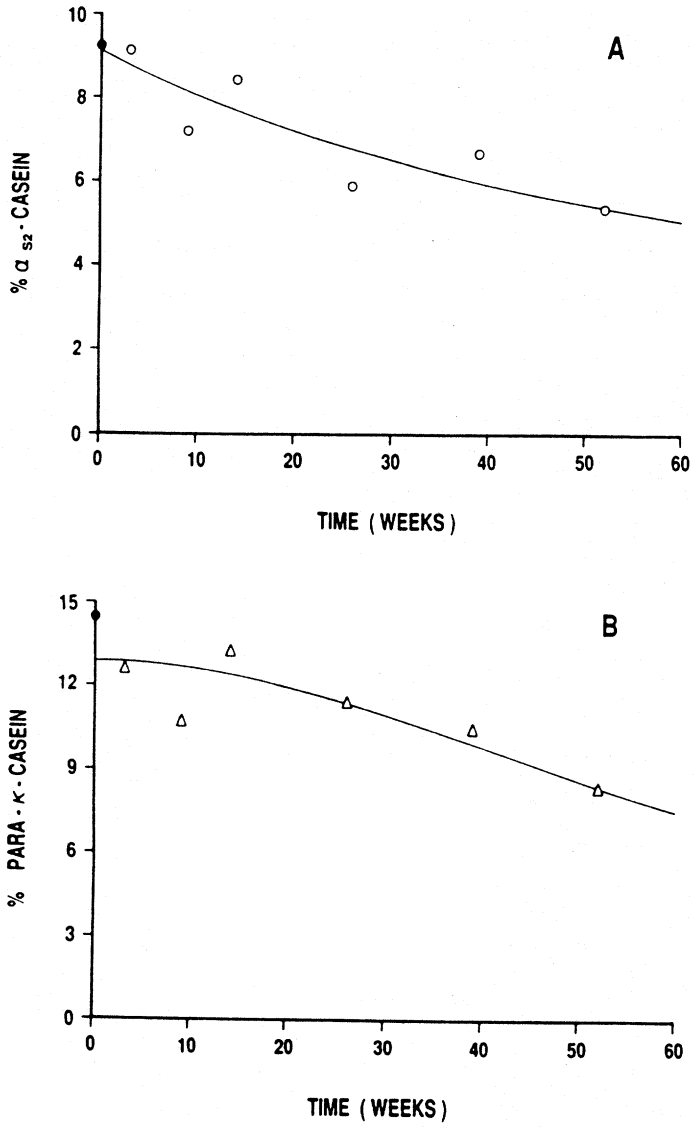

FIG. 24. Nonlinear regression plot of (A) the disappearance of α_{s2}-casein and (B) the disappearance of *para*-κ-casein for Cheddar cheese. Filled circle represents percent present in caseinate before cheesemaking. Data were analyzed by Eq. (41). Results are given in Table XIX.

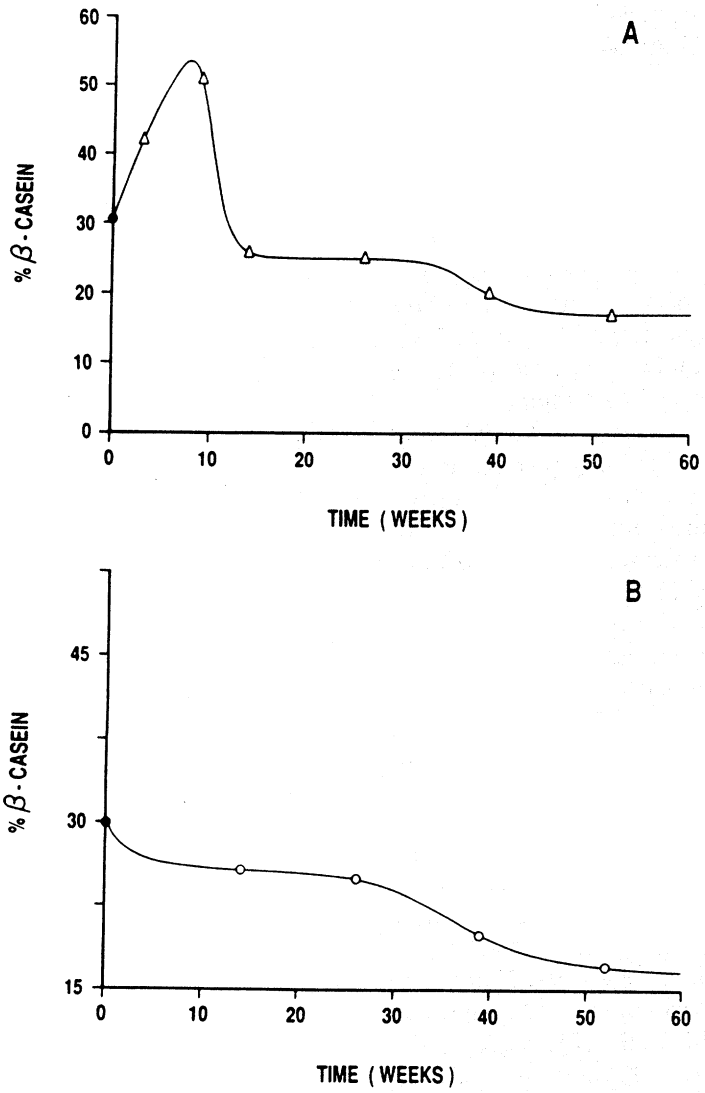

FIG. 25. Nonlinear regression plot of (A) the apparent disappearance of β-casein (peak 9); (B) replot subtracting theoretically skewed data due to α_{s1}-I. Filled circle represents percent present in caseinate before cheesemaking. Data were analyzd by Eq. (41). Results are given in Table XIX.

theoretical inflection of 75 weeks predicting an extremely long persistence of this protein as a major cheese component (Fig. 24A). Similar results were obtained for *para*-κ-casein with $1/k_1$ equal to 71 weeks (Fig. 24B). Here, to obtain a zero time estimate, the average κ-casein content of acid caseinate was used on the y-axis. These two cysteine- (or cystine) containing components persist for the longest periods of time, with predicted half-lives beyond the scope of most normal cheese storage.

Analysis of the changes in β-casein at first produced a curve (Fig. 25A) which mirrored that of whole casein (Fig. 22A). When the zero time value for β-casein was added to the y-axis, the data appear to have three inflections. Analysis by nonlinear regression gave these as 10.0, 18.8, and 37.7. The apparent increases in β-casein followed by a decrease are apparently due to the rapid conversion of α_{s1} to α_{s1}-I fragment.

It has been shown by several investigators (Lawrence *et al.*, 1987) that one of the first significant events in the cheese ripening process is the proteolytic breakdown of α_{s1}-casein to form the α_{s1}-I fragment. This cleavage is thought to be predominantly due to chymosin action. In the electrophoretic system employed in this work, α_{s1}-I comigrates with β-casein, as is the case for the SDS–PAGE system used by Trieu-Cuot *et al.* (1982). Conversion of the α_{s1} occurs predominantly in the first 7 to 14 day of ripening. Thus, at 3 weeks, the α_{s1} bands represent only 14% of the total caseinate while β-casein has "apparently" risen to nearly 50% at 9 weeks. As noted above, we have included the data from Table XVII for α_{s1}-caseinate at the zero time axis for ripening. Using these data as a starting point, we can calculate the half-lives of the α_{s1}- and α_{s2}-caseins and separate these transitions from that of β-casein. The half-life found for α_{s1} was 1.95 weeks, in excellent agreement with data reviewed by Lawrence *et al.* (1987). The rapid degradation of α_{s1} probably produces α_{s1}-I (and others, peaks 13–15). If one regraphs the β-casein without the data at 3 and 9 weeks, a single decay is observed (Fig. 25B) and the half-time for disappearance is 36.6 weeks, which corresponds nicely to the 37.0-week half-time for appearance of $\gamma_2 + \gamma_3$-caseins. Correspondingly, the optimal concentration for α_{s1}-I appears to be at about 10 weeks (Fig. 25A).

Finally, the exponential parameters n, m, and q need to be considered. In the study of binding isotherms (Farrell *et al.*, 1988) these generally reflect moles of ligand bound per mole of chelator. Here, the meaning is somewhat different since the substrate is in a fixed matrix and changes in molecular weight must be due to diffusion of the enzyme followed by an effective proteolytic cleavage. It could reflect the average number of cleavage sites on the protein or the number of collisions required to lead to effective degradation.

Thus, thermodynamic linkage through diffusion may be related by way of Eq. (34) to the relative concentration of the different species of enzymes,

and through Eq. (40) to kinetically effective collisions. In the case of k_1 for α_{s1} degradation, if k is only diffusion related, then from k_1 a diffusion constant of 8.47×10^{-7} cm^2/sec can be calculated. This value is quite close to the diffusion constant for proteins of MW 45,000 (Bull, 1943). All other ks are at least $10\times$ lower; thus, only this reaction approaches the correct value for diffusion in solution. All other conversions are much slower. In addition, interactions of the caseins in the solid matrix may play a role; e.g., it could be speculated that until γ_2 and γ_3 are formed, with resultant changes in cheese structure, few effective collisions of plasmin with α_{s2} can occur. Other speculations could be made; it must be remembered, however, that the thermodynamic linkage can only quantitate the changes; it cannot prove or disprove molecular mechanisms which share a common ΔG of reaction.

The quality of the natural cheese is of prime importance for the properties of the finished processed cheese. It has been suggested that the higher the relative casein content of the natural cheese, the better it is for the production of a stable processed cheese. The high content of intact casein results in process cheese with a long filamentous structure. This structure is extremely stable against chemical, thermal, or mechanical influences and is hydrophobic, absorbing water slowly and in limited quantities. Young rennet cheese has a relative casein content of 90–95% which decreases during ripening. The present study clearly shows that various caseins are degraded with different half-lives; α_{s1}-casein degrades first, while β-casein persists for a longer time, and α_{s2}- and para-κ-caseins exist for more than 70 weeks before degrading.

Processed cheese is produced from blends of cheeses of different ages. Generally, about 75% of the blend consists of 3-month (12 week) old cheeses with the remainder coming from 24 to 52-week-old cheeses. What appears to be important is a relatively high casein content (Thomas *et al.*, 1980). In the case of the immature, unripened Cheddar cheese these observations indicate that the presence of α_{s1}-I is of importance. Its half-time for disappearance is 10.0 weeks (Fig. 25A), thus at 12 weeks the majority of this protein (and of course α_{s1} itself) has been converted to lower-molecular-weight components. Additionally, for the more mature cheeses, ripening up to the half-life of β-casein (35 weeks) may be tolerated in mixtures; beyond this point poor processed products may result.

B. BACTERIAL GROWTH–TIME VARIATION

1. Overview

In the preceding section, the time variation of cheese ripening was modeled by a mechanism whereby enzymes can degrade the casein compo-

nents of cheese via a diffusion-controlled process. Here the concentration of enzymes attacking the casein suprastructure in cheese varied with time through the product of the diffusion coefficient of the enzymes, the rate constants of the enzymes, and time. Since such a heterogeneous system was successfully quantified, the possibility of modeling the time variation of other biological processes appears feasible. One possible process would be the variation of bacterial growth and product synthesis with time. Here, the rate-determining step would most likely not be the diffusion of nutrients of low molecular weight, but might be related to undefined steps in cell division of the bacteria. Moreover, quantitatively describing the time variation of growth and death of bacteria under a variety of conditions would allow investigators to find the optimum conditions for controlling bacterial growth and product synthesis. At this time, in this investigator's opinion, no such quantitative model exists. Even the usual exponential growth mechanism has not been successful. This lack of success is due to the fact that bacterial growth exhibits a lag before growth begins. This behavior cannot be quantitatively described by a simple exponential function. However, as seen in the Section VI,A, such time-dependent behavior can easily be described. In this section, the cheese-ripening equations are modified for bacterial growth and product production as well as tested on the growth of *Clostridium botulinum* type JDT-IV and toxin synthesis under several environmental conditions. The parameters (kinetic constants) will be thermodynamically linked to pH in order to obtain the optimum pH for toxin synthesis.

2. *Procedures*

a. Materials and Methods. All data were drawn from those of Bonventre and Kempe (1959a,b). These experiments were chosen since the strains used exhibit autolysis. The preparation of samples and experimental procedures are given in these references.

b. Theory. The stoichiometry and equation used were those given in Section VI,A,2,d [Eq. (41)]. Here k_1, k_2, and k_3 represent rate constants which include such factors as diffusion, kinetic processes, cell division, and product synthesis as the organisms respond to environmental changes, i.e., nutrient, pH, etc., added to the media. The C valves represent the bacterial growth (numbers) or toxin synthesis (concentration). In this study, bacterial growth or toxin synthesis is thermodynamically linked to time-dependent processes, which yield changes in the physiological state of the organisms.

TABLE XX

LINKAGE PARAMETERS FROM pH DEPENDENCE OF GROWTH OF *Clostridium botulinum* STRAIN JTD-IV

pH	k_1 (hr^{-1})	k_2 (hr^{-1})	n	m
5.5	0.118 ± 0.001	0.014 ± 0.001	4	4
6.5	0.026 ± 0.002	0.127 ± 0.007	4	4
7.0	0.032 ± 0.001	0.140 ± 0.002	4	4
8.3	0.152 ± 0.001	0.056 ± 0.001	4	4

3. *Analysis of Data*

The growth of *Clostridium botulinum* type JTD-IV as measured by optical density and toxin synthesis as a function of time from the results of Bonventre and Kempe (1959a) are shown in Fig. 26a,b. The growth curve (Fig. 26a) is biphasic (due to autolysis) with a corresponding growth and death behavior, whereas the toxin synthesis (Fig. 26b) is monophasic. Fitting the data to the modified linkage equations for cheese ripening [first three terms of Eq. (41)] using nonlinear regression analysis yields theoretical curves (solid lines in Fig. 26a,b) in excellent agreement with the experimental data with normal errors of 0.6 and 0.2 for Fig. 26a and b, respectively. The analysis yielded a growth rate of 0.126 ± 0.002 hr^{-1} with a death rate of 0.0235 ± 0.0005 hr^{-1} and n and m values of 4 and 4, respectively, for the growth of *Clostridium botulinum* in the presence of pyruvate or glycerol (Fig. 26a). The analysis of the toxin synthesis data (Fig. 26b) yielded only a k_1 value of 0.0246 ± 0.0001 hr^{-1} with a n value of 8. Here, the n and m values are parameters related to the lag time as the bacteria undergo physiological changes necessary to produce growth or toxin synthesis. The greater n or m, the longer the lag time. The death portion of the curve should be viewed as changes undergone prior to lysis. Here, it is assumed that either pyruvate and glycerol have been depleted from the media or that toxic products are built up. Hence, the time dependence of bacterial growth and toxin synthesis can be quantitatively modeled. When other carbon sources such as maltose, glucose, xylose, ribose, and galactose were used, n and m were constant (4, 4) while k_1 varied over a narrow range of 0.04 to 0.13 hr^{-1}. The parameters n and m thus may relate to organism-specific changes which occur in response to media changes. In fact, when no lag time is observed, $n = 1$. The other parameter (k_i) may represent the response of the organism's physiology to environment. Comparison of k_is could lead to the establishment of multifactorial optima for growth and possibly death. For example, the death rate from

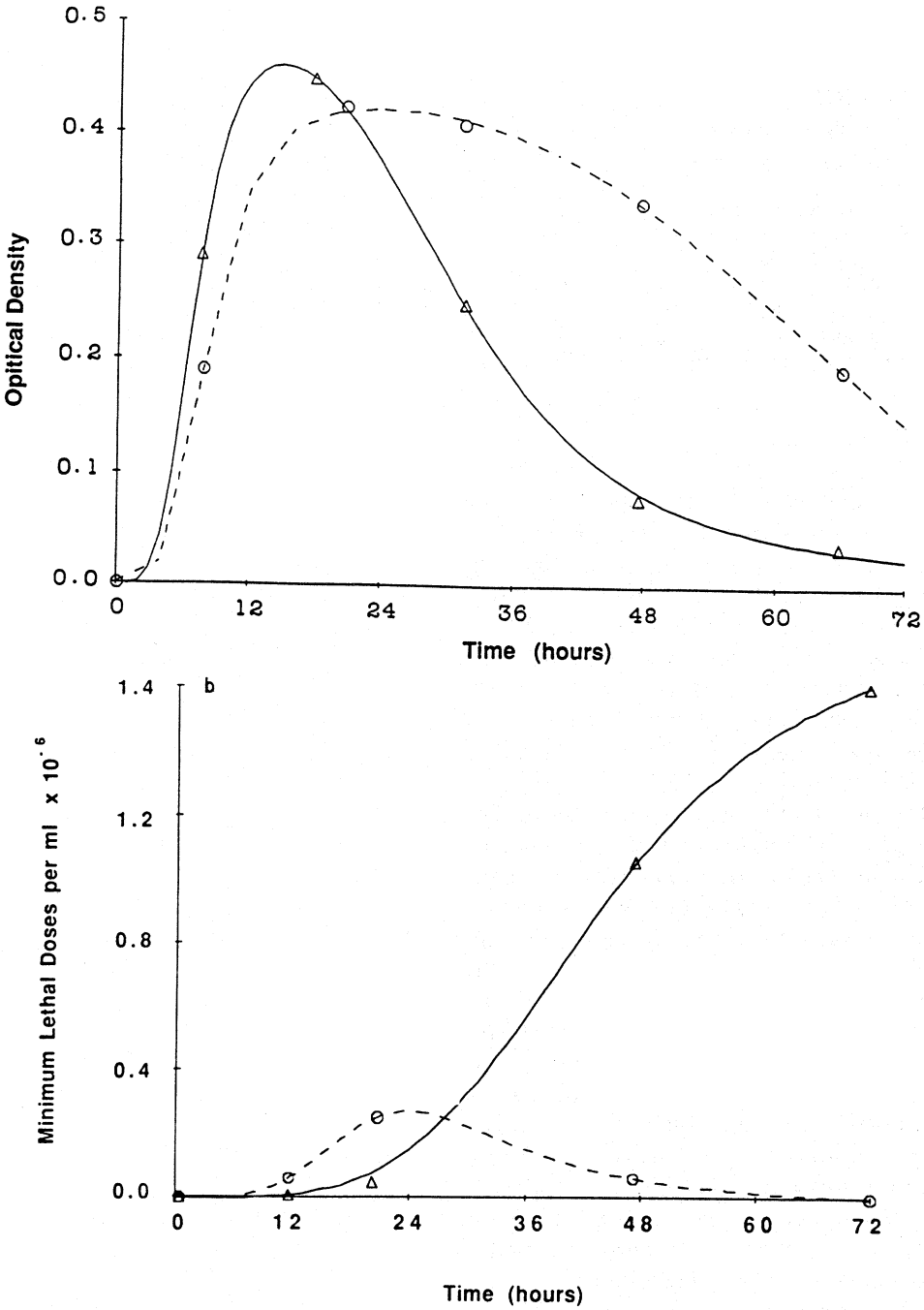

FIG. 27. (a) Effect of pH on growth of *Clostridium botulinum* strain JTD-IV. ○, pH 5.5 data; △, pH 7.0 data. Dashed and solid lines are best fit of data for pH 5.5 and 7.0, respectively, using first three terms of Eq. (41) and nonlinear regression analysis (see text). (b) Effect of pH on toxin synthesis by *Clostridium botulinum* strain JTD-IV. ○, pH 8.3 data; △, pH 6.5 data. Dashed and solid lines are best fits for pH 8.3 and 6.5 data, respectively, using Eq. (41) and nonlinear regression analysis (see text).

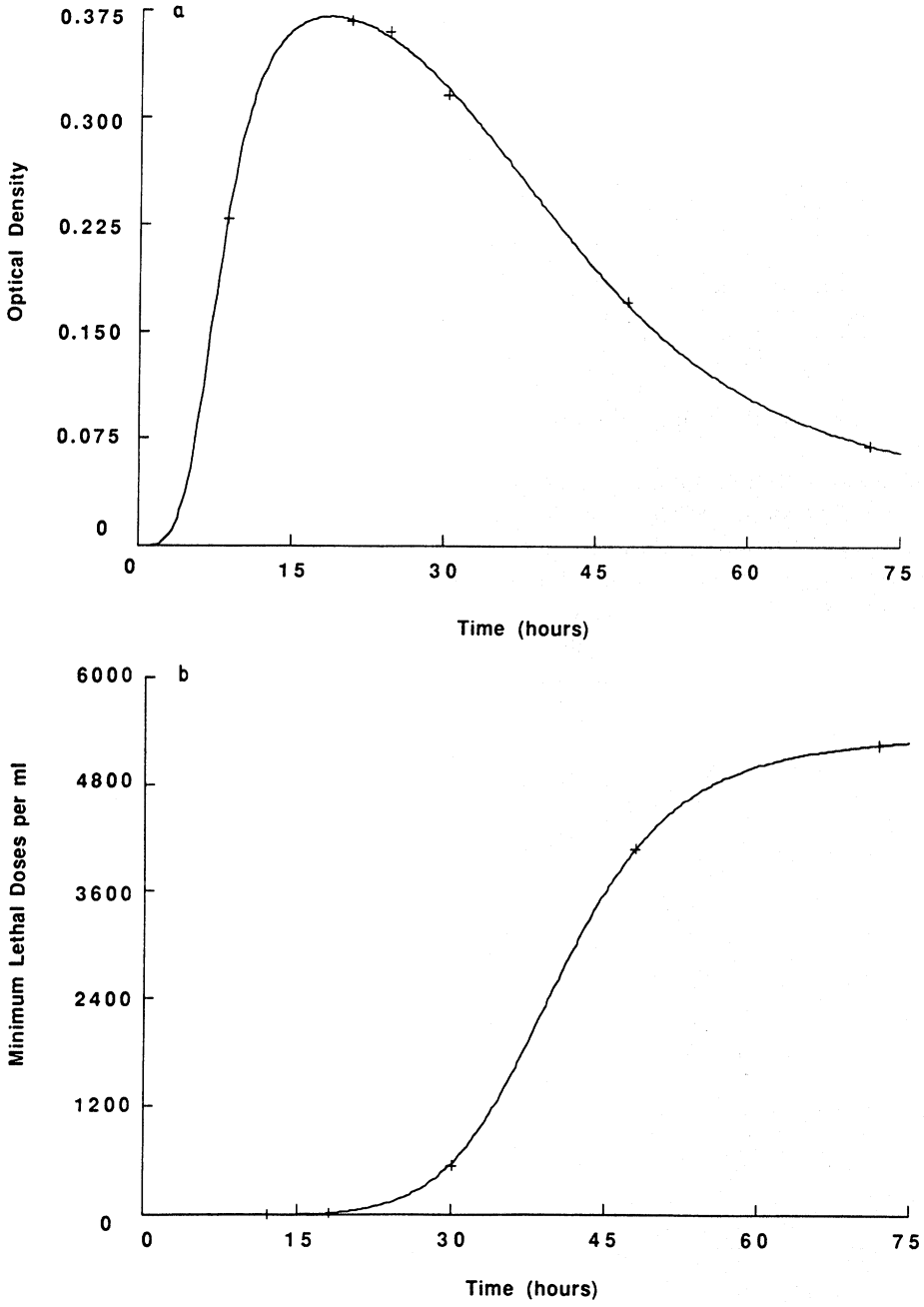

FIG. 26. (a) Effect of glycerol or pyruvate on growth of *Clostridium botulinum* strain JTD-IV. Solid line is best fit of data using Eq. (41) and nonlinear regression analysis (see text). (b) Effect of glycerol or pyruvate on toxin synthesis by *Clostridium botulinum* strain JTD-IV. Solid line is best fit of data using first three terms of Eq. (41) and nonlinear regression analysis (see text).

TABLE XXI

LINKAGE PARAMETERS FROM pH DEPENDENCE OF TOXIN SYNTHESIS FROM *Clostridium botulinum* STRAIN JTP-IV

pH	k_1 (hr^{-1})	k_2 (hr^{-1})	n	m
5.5	0.016 ± 0.0001		8	
6.5	0.0228 ± 0.0004		4	
7.0	0.0348 ± 0.0002	0.0089 ± 0.0001	8	12
8.3	0.0506 ± 0.00001	0.0339 ± 0.0001	4	4

Fig. 26a (0.0235 hr^{-1}) is nearly equivalent to the rate of toxin production (0.0246 hr^{-1}).

To test whether this methodology could describe the variation of such growth curves with environmental condition, the pH dependence of bacterial growth and toxin synthesis was tested using the results of Bonventre and Kempe (1959a). The results are presented in Fig. 27a and b for growth at pH 5.5 and 7 and toxin synthesis at pH 6.5 and 8.3, respectively. The fits to the data using this model are excellent, as represented by the dashed and solid lines in Fig. 27a and b. All normal errors were better than 1%. Thermodynamic kinetic constants for growth, k_1, or death, k_2, are given

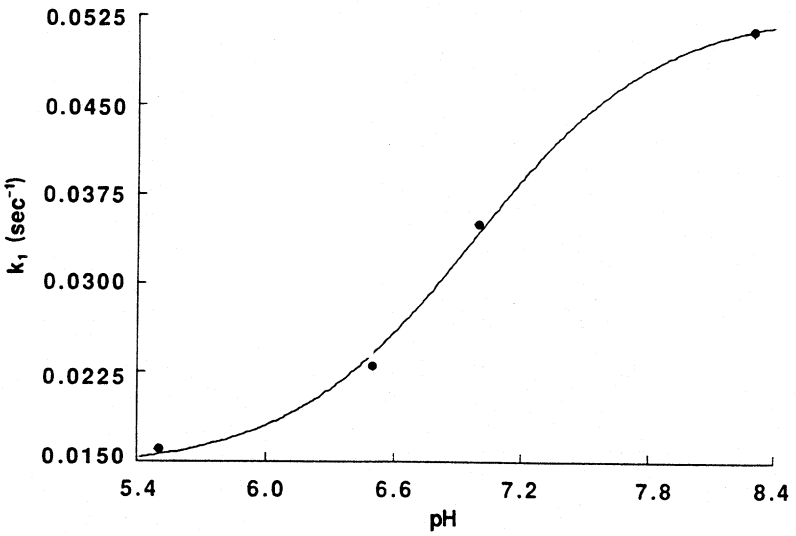

FIG. 28. Effect of pH on the k_1 parameter obtained from the nonlinear regression analysis of pH dependence of toxin synthesis of *Clostridium botulinum* strain JTD-IV (see Table XXI). Solid line is best fit using thermodynamic linkage and nonlinear regression analysis (see text).

in Table XX for the pH variation of bacterial growth. The k_1 values decrease and then increase as the pH is varied from 5.5 to 8.3. Since only four pH values were given and because of the biphasic nature of the k values in Table XX, it was no possible to link either of the k values thermodynamically to pH. However, in Table XXI, the k_1 values which were obtain from the toxin synthesis results did vary with pH in a monotonic fashion. Here, these results were linked to pH and the data and corresponding theoretical curve are shown in Fig. 28. Here, agreement between data and theoretical curve is excellent, with a error of less than 0.2%. The analysis yields a pK value of 7.0 ± 0.1 with a cooperative n value of 1. Thus, the analysis allows investigators to link the kinetic constants with pH. Although the k_is found here represent "lumped" constants, they are a first step toward collating and comparing growth curves in a quantitative fashion. Extension of these models to a variety of other environmental conditions could establish a new methodology for quantitating these interactions.

ACKNOWLEDGMENT

The author acknowledges a debt of gratitude to Mr. Chad Haggerty for his invaluable technical assistance in the preparation of this manuscript and to Drs. Harold M. Farrell, Jr., and Helmut Pessen for helpful discussions.

REFERENCES

Basch, J. J., Douglas, F. W., Jr., Procino, L. G., Holsinger, V. H., and Farrell, H. M., Jr. 1985. Quantitation of caseins and whey proteins of processed milks and whey protein concentrates, application of gel electrophoresis, and comparison with Harland–Ashworth procedure. *J. Dairy Sci.* **68,** 23.

Basch, J. J., Farrell, H. M., Jr., Walsh, R. A., Konstance, R. P., and Kumosinski, T. F. 1989. Development of a quantitative model for enzyme-catalyzed, time-dependent changes in protein composition during Cheddar cheese ripening. *J. Dairy Sci.* **72,** 591–603.

Bauman, D. E., and Davis, C. L. 1974. *In* "Biosynthesis of Milk Fat in Lactation" (B. L. Larson and V. E. Smith, eds.), Vol. II, pp. 31–75. Academic Press, New York.

Bieleski, R. L. 1974. Development of an externally-located alkaline phosphatase as a response to phosphorus deficiency. *Bull. R. Soc. N. Z.*, 165–170.

Bingham, E. W., Farrell, H. M., Jr., and Carroll, R. J. 1972. Properties of dephosphorylated α_{s1}-casein. Precipitation by calcium ions and micelle formation. *Biochemistry* **11,** 2450–2454.

Bingham, E. W., Farrell, H. M., Jr., and Dahl, K. J. 1976. Removal of phosphate groups from casein with potato acid phosphatase. *Biochim. Biophys. Acta* **429,** 448–460.

Bonventre, P. E., and Kempe, L. L. 1959a. Physiology of toxin production by *Clostridium botulinum* types A and B. II. Effect of carbohydrate source on growth, autolysis and toxin production. *Appl. Microbiol.* **7,** 372–374.

Bonventre, P. F. and Kempe, L.L. 1959b. Physiology of toxin production by *Clostridium botulinum* types A and B. III. Effect of pH and temperature during incubation on growth, autolysis and toxin production. *Appl. Microbiol.* **7,** 374–377.

Bringe, N. A., and Kinsella, J. E. 1986. Inhibition of chymosin and the coagulation of para-casein micelles by anions. *J. Dairy Sci.* **69,** 965–970.

Bull, H. B. 1943. "Diffusion in Physical Biochemistry," p. 272. Wiley, New York.

Bush, D. S., and McColl, J. G. 1987. Mass-action expressions of ion exchange applied to Ca^{2+}, H^+, K^+, and Mg^{2+} sorption on isolated cell walls of leaves from *Brassica oleracea*. *Plant Physiol.* **85,** 247–260.

Byler, D. M., Farrell, H. M., Jr., and Susi, H. 1988. Raman spectroscopy of caseins. *J. Dairy Sci.* **71,** 2622–2629.

Chang, C. W., and Bandurski, R. S. 1964. Exocellular enzymes of corn roots. *Plant Physiol.* **39,** 60–64.

Chen, R. F., and Plaut, G. W. E. 1963. Activation and inhibition of DPN-linked isocitrate dehydrogenase of heart by certain nucleotides. *Biochemistry* **2,** 1023–1032.

Cheung, W. Y. 1984. Calmodulin: Its potential role in cell proliferation and heavy metal toxicity. *Fed. Proc., Fed. Am. Soc. Exp. Biol.* **43,** 2995–2999.

Cleland, W. W. 1967. Enzyme kinetics. *Adv. Enzymol.* **29,**1–32.

Colman, R. F. 1983. Aspects of the structure and function of the isocitrate dehydrogenases. *In* "Peptide and Protein Reviews" (M. T. W. Hearn, ed.), Vol. 1, pp. 41–69. Dekker, New York.

Crasiner, M., and Giordani, R. 1985. Elution of acid phosphatase from sycamore cell walls. *Plant Sci.* **40,** 35–41.

Crasiner, M., Noat, G., and Ricard, J. 1980. Purification and molecular properties of acid phosphatase from sycamore cell walls. *Plant Cell Environ.* **3,** 217–224.

Crasiner, M., Moustacas, A.-M., and Ricard, J. 1985. Electrostatic effects and calcium ion concentration as modulators of acid phosphatase bound to plant cell walls. *Eur. J. Biochem.* **151,** 187–190.

Creamer, L. K., and Waugh, D. F. 1966. Calcium binding and precipitate solvation of casein. *J. Dairy Sci.* **49,** 706 (abstr.).

Creamer, L. K., Richardson, T., and Parry, D. A. D. 1981. Secondary structure of bovine α_{s1}- and β-caseins. *Arch. Biochem. Biophys.* **211,** 698–702.

Davies, D. T., and Law, A. J. R. 1983. Variation of the protein composition of bovine casein micelles and serum caseins in relation to micelle size. *J. Dairy Res.* **50,** 67.

DeMarty, M., Morvan, C., and Thellier, M. 1978. Exchange properties of isolated cell walls of *Lemma minor* L. *Plant Physiol.* **62,** 477–481.

Dickson, I. R., and Perkins, J. D. 1971. Studies on the interactions between purified bovine caseins and alkaline earth metal ions. *Biochem. J.* **124,** 235–240.

Eigel, W. N., Butler, J. E., Ernstrom, C. A., Farrell, H. M., Jr., Harwalkar, V. R., Jenness, R., and Whitney, R. M. 1984. Nomenclature of the proteins of milk: 5th Revision. *J. Dairy. Sci.* **67,** 1599–1631.

Farrell, H. M., Jr. 1980. Purification and properties of $NADP^+$: Isocitrate dehydrogenase from lactating bovine mammary gland. *Arch. Biochem. Biophys.* **204,** 551–559.

Farrell, H. M., Jr., and Kumosinski, T. F. 1988. Modeling of calcium-induced solubility profiles of casein for biotechnology: Influence of primary structure and post-translational modification. *J. Ind. Micro.* **3,** 61.

Farrell, H. M., Jr., and Thompson, M. P. 1988. The caseins of milk as calcium binding proteins. *In* "Calcium Binding Proteins" (M. P. Thompson, ed.). CRC Press, Boca Raton, Florida.

Farrell, H. M., Jr., Deeney, J. T., Tubbs, K., and Walsh, R. A. 1987. Role of the isocitrate dehydrogenases and other Krebs cycle enzymes in lactating bovine mammary gland. *J. Dairy Sci.* **70,** 781–788.

Farrell, H. M., Jr., Kumosinski, T. F., Pulaski, P., and Thompson, M. P. 1988. Calcium-induced associations of the caseins: A thermodynamic linkage approach to precipitation and resolubilization. *Arch. Biochem. Biophys.* **265,** 146–155.

Faulkner, A., and Peaker, M. 1982. Secretion of citrate into milk. *J. Dairy Res.* **49,** 159–169.

Fox, P. F. 1981. Proteinases in dairy technology. *Neth. Milk Dairy J.* **35,** 233.

Frieden, C. 1979. Hysteretic enzymes. *Annu. Rev. Biochem.* **48,** 471–489.

Fry, S. C. 1979. Phenolic components of primary cell wall and their possible role in the hormonal regulation of growth. *Planta* **146,** 343–351.

Gabriel, J. L., and Plaut, G. W. E. 1984. Citrate activation of NAD^+-specific isocitrate dehydrogenase from bovine heart. *J. Biol. Chem.* **259,** 1622–1628.

Grappin, R., Rank, T. C., and Olson, N. F. 1985. Primary proteolysis of cheese proteins during ripening. A review. *J. Dairy Sci.* **68,** 531.

Greville, G. D. 1969. *In* "Citric Acid Cycle: Control and Compartmentation" (J. M. Lowenstein, ed.), pp. 1–136. Dekker, New York.

Laemmli, U. K. 1970. Cleavage of structural proteins during the assembly of the head of bacteriophage T4. *Nature (London)* **227,** 680.

Lamport, D. T. A. 1970. Cell wall metabolism. *Annu. Rev. Plant Physiol.* **21,** 235–270.

Lamport, D. T. A., and Catt, J. W. 1981. Glycoproteins and enzymes of cell wall. *Encycl. Plant Physiol., New Ser.* **13B,** 133–165.

Lawrence, R. C., Creamer, L. K., and Gilles, J. 1987. Texture development during cheese ripening. *J. Dairy Sci.* **70,** 1748.

Linde, A. 1982. Calcium metabolism in dentinogenesis. *In* "The Role of Calcium in Biological Systems" (L. J. Anghileri and A. M. Tuffet-Anghileri, eds.), Vol. III. CRC Press, Boca Raton, Florida.

Linderstrom-Lang. 1929. On the heterogeneity of bovine casein. *C. R. Trav. Lab. Carlsberg* **17,** 1–116.

McNeil, M., Darvill, A. G., and Albersheim, P. 1979. The structural polymers of the primary cell walls of dicots. *Prog. Chem. Org. Nat. Prod.* **37,** 191–196.

Melander, W., and Horvath, C. 1977a. Salt effects on hydrophobic interactions in precipitation and chromatography of proteins. *Arch. Biochem. Biophys.* **183,** 200.

Melander, W., and Horvath, C. 1977b. Effect of neutral salts on the formation and dissociation of protein aggregates. *J. Solid-Phase Biochem.* **2,** 141.

Nagahashi, G., and Seibles, T. S. 1986. Purification of plant cell walls: Isoelectric focusing of $CaCl_2$ extracted enzymes. *Protoplasma* **134,** 102–110.

Neet, K. E., and Ainslie, G. R., Jr. 1980. Hysteretic enzymes. *In* "Methods in Enzymology" (D. L. Purich, ed.), Vol. 64, pp. 192–224. Academic Press, New York.

Noat, G., Crasiner, M., and Ricard, J. 1980. Ionic control of acid phosphatase activity in plant cell wall. *Plant Cell Environ.* **3,** 225–229.

Noble, R. W., and Waugh, D. F. 1965. Casein micelles, formation and structure I. *J. Am. Chem. Soc.* **87,** 2236–2245.

O'Neill, M. A., and Roberts, K. 1981. Methylation analysis of cell wall glycoproteins and glycopeptides from Chlamydomonas reinhardii. *Phytochemistry* **20,** 25–28.

Oppenheim, F. G., Offner, G. D., and Troxler, R. F. 1982. Phosphoproteins in parotid saliva from the subhuman primate *M. fascicularis*. *J. Biol. Chem.* **257,** 9271–9282.

Pepper, L., and Farrell, H. M., Jr. 1982. Interactions leading to the formation of casein submicelles. *J. Dairy Sci.* **65,** 2259–2266.

Pitman, M., Lüttge, U., Kramer, D., and Ball, K. 1974. Free space characteristics of barley leaf slices. *Aust. J. Plant Physiol.* **1,** 65–75.

Plaut, G. W. E., Cook, M., and Aogaichi, T. 1983. The subcellular location of isozymes of NADP-isocitrate dehydrogenase in tissues from pig, ox and rat. *Biochim. Biophys. Acta* **760,** 300–308.

Schmidt, D. G. 1984. Association of caseins and casein micelle structure. *In* "Developments in Dairy Chemistry" (P. F. Fox, ed.). Appl. Sci. Publ., London.

Schmidt, R. H., Illingworth, B. L., and Ahmed, E. M. 1978. Heat-induced gelation of peanut-protein/whey-protein blends. *J. Food Sci.* **43,** 615–621.

Seelig, E. G., and Colman, R. F. 1978. *Arch. Biochem. Biophys.* **188,** 394–409.

Sentenac, H., and Grignon, C. 1981. A model predicting ionic equilibrium concentrations in cell walls. *Plant Physiol.* **68,** 415–419.

Shen, J. L. 1981. *ACS Symp. Ser.* **147,** 89.

Shone, M. G. T. 1966. The initial uptake of ions by barley roots. *J. Exp. Bot.* **17,** 89–95.

Steinhardt, J., and Reynolds, J. A. 1969. *In* "Multiple Equilibria in Proteins," p. 325. Academic Press, New York.

Sugawara, S., Inamoto, Y., and Ushijima, M. 1981. Resolution and some properties of acid phosphatase isoenzymes bound to the cell wall of potato tubers. *Agric. Biol. Chem.* **45,** 1767–1773.

Tanford, C. 1961. *In* "Physical Chemistry of Macromolecules," p. 624. Wiley, New York.

Thomas, M. A., Newell, G., and Abad, G. 1980. Effects of freezing on the objective and subjective properties of processed cheese. *J. Food Technol.* **15,** 599.

Thompson, M. P. 1966. Phenotyping of caseins of cows' milk. *J. Dairy. Sci.* **49,** 792–794.

Thompson, M. P., Gordon, W. G., Boswell, R. T., and Farrell, H. M., Jr. 1969. Solubility solvation and stabilization of α_{s1}- and β-caseins. *J. Dairy Sci.* **52,** 1166–1173.

Trieu-Cuot, P., Archieri-Haze, M. J., and Gripon, J.-C. 1982. Effect of aspartyl proteinases of *P. caseicolum* and *P. roqueforti* on caseins. *J. Dairy Res.* **49,** 487.

Tu, S.-I., and Brouillette, J. N. 1987. Metal ion inhibition of corn root plasma membrane ATPase. *Phytochemistry* **26,** 65–69.

Wagman, D. D. 1968. *NBS Tech. Note (U.S.)* **270.**

Waugh, D. F., and Noble, R. W. 1965. Casein micelles, formation and structure II. *J. Am. Chem. Soc.* **84,** 2246–2257.

Waugh, D. F., Slattery, C. W., and Creamer, L. K. 1971. Binding of calcium to caseins. *Biochemistry* **10,** 817–823.

Wyman, G., Jr. 1964. Linked functions and reciprocal effects in hemoglobin: A second look. *Adv. Protein Chem.* **19,** 223–286.